Development and Field Test of a Two-Dimensional Vertically Scanning Ozone Lidar

FINAL REPORT

Contract Number: 93-330

Prepared for:

California Air Resources Board and
the California Environmental Protection Agency

Submitted by:

Department of Commerce
National Oceanic and Atmospheric Administration
Environmental Research Laboratories
Environmental Technology Laboratory
Atmospheric Lidar Division
325 Broadway, Boulder, CO 80303

Prepared by:

Yanzeng Zhao and R. Michael Hardesty
principal investigators

June 1997

Disclaimer

The statements and conclusions in this report are those of the NOAA/ERL/ETL and not necessarily those of the California Air Resources Board. The mention of commercial products, their source, and their use in connection with material reported herein is not to be construed as actual or implied endorsement of such products.

The purpose of this project was to develop and test the two-dimensional scanning capability of the lidar. The data collected are experimental and will not become part of the official aerometric data base maintained by the Air Resources Board. With additional validation, these data can be useful for analysis of the atmospheric processes influencing the transport of pollutants near Victorville.

Apology

The contract manager (Leon Dolislager) apologizes to Drs. Hardesty and Zhao of NOAA for the delay in releasing their report. Two other contractors associated with the Mojave Desert Ozone Study of 1995 compared some of their ozone data with data collected by NOAA's lidar. Because the conclusions differed with some of the conclusions in NOAA's report, Mr. Dolislager promised the Research Screening Committee of the Air Resources Board to conduct additional analyses before releasing the report. Although the bulk of the analyses were completed a few years ago, the results were never summarized into an appendix to this report as originally planned. Mr. Dolislager is particularly grateful to Dr. Zhao for her patience and understanding during this long delay in releasing the report. A brief summary of the supplemental analyses is provided in Appendix D.

Acknowledgments

Mr. Richard Cupp, contracting lidar engineer, redesigned the optical supporting system and the detector package, and reassembled the whole system. The modified system is improved significantly in stability and background noise reduction. Mr. Cupp also sketched the basic design for the scanning system. Mr. Richard Marchbanks, optical engineer, carried out the engineering design of the scanner, assembled and installed it on top of the lidar, and wrote programs to control the movement of the scanner. He also participated in modifications of the sea-container, and miscellaneous hardware preparation. During the 1995 Victorville Experiment Mr. Marchbanks was responsible for packing, shipping, and setting up the ozone lidar at the site, and assisted in troubleshooting, realignment, and operation of the lidar. Ms. Ann M. Weickmann, computer analyst, improved the data-taking program to include a pre-triggering mode (that significantly improved the subtraction of the background noise) and scanner control commands, and modified the data averaging program. Ann was also one of the crew during the first week in the field. Ms. Joanne George, computer analyst, improved the lidar data analysis programs to include graphics display for intermediate results which is valuable for speeding data processing, and subroutines for reading meteorological data from wind profiler/RASS and surface data. She also developed programs for ozone advection flux calculations. Ms. Kathleen Healy, computer analyst, modified the original program written in IDL language to display ozone time-height variations, and developed new IDL programs to display ozone distribution in a two-dimensional scanning mode, ozone flux time-height variations in a barb format, and ozone flux components in a contour format. Mr. Dan Shell, student assistant, helped in various parts of hardware preparation, lidar shipping and setting up, and participated in the field experiment. He also carried out data tape copying and most of the raw data averaging. Mr. Scott Sandberg, electronic engineer, participated in the field experiment during the third week to help operation of the ozone lidar and a UV radiometer. Mr. Hutch Johnson, meteorologist, processed the surface ozone data that were only recorded on a strip chart recorder in the first week of the experiment.

Meteorological data analyzed and provided by Mr. Dan Wolfe, meteorologist, contributed greatly to the signal processing of the ozone lidar data and the calculations of ozone advection flux.

Dr. Wynn Eberhard, physicist, discussed important issues with the lidar team on data interpretation and intercomparison, and contributed significantly in preparing this final report.

The valuable contributions of the technical team mentioned above are gratefully acknowledged.

This report was submitted in fulfillment of Contract #93-330 entitled "Development and Field Test of a Two-Dimensional Vertically Scanning Ozone Lidar " by the National Oceanic and Atmospheric Administration's Environmental Technology Laboratory under the partial sponsorship of the California Air Resources Board. Special thanks are given to Mr. Leon Dolislager for his valuable help in preparing this final report; his critical review of the manuscript and many helpful suggestions. Work was completed as of June 1997.

(This page intentionally left blank.)

TABLE OF CONTENTS

(This page intentionally left blank.)

LIST OF FIGURES

(This page intentionally left blank.)

LIST OF APPENDICES

(This page intentionally left blank.)

ABSTRACT

The ETL ground-based ozone lidar was deployed in August 1995 near one of the major ozone transport corridors from the Los Angles Air Basin to the Mojave Desert. A newly developed two-dimensional scanning system was added to the modified and ruggedized lidar system. The scanning system provides the capability of showing horizontal inhomogeneity. Scanning data also serve as strong internal check of the lidar system itself, and that is a great advantage. The afternoon data on most days show a layer of higher ozone concentrations in the lower boundary layer, and another layer aloft. The two layers merge in mid afternoon but separate again later. Advection ozone fluxes are calculated using lidar profiles and wind profiler data. The results show more ozone is transported aloft, although higher ozone concentrations may exist in the lower altitude.

(This page intentionally left blank.)

EXECUTIVE SUMMARY

This report describes the ozone lidar experiments conducted by NOAA's Environmental Technology Laboratory (ETL) in Victorville, California during August 1995, sponsored by the California Air Resources Board. The main objectives of the experiment were (1) to test the newly-developed two-dimensional scanning system of the ETL ozone lidar, and (2) to collect ozone concentration and wind profiles close to Cajon Pass (a major ozone transport corridor from the Los Angeles urban area to the Mojave Desert) to obtain first-hand information about temporal and spatial variations of ozone concentration and advection flux profiles in this region.

The scanning system operated well. One of the advantages of the scanning system is that the scanning data provide an internal check of the reliability of the lidar system. They revealed engineering problems in the mirror mount that induced errors in ozone concentrations measured in the morning. These have been solved in a new design.

Measurements in the afternoon were successful. Data analysis shows one layer of high ozone concentrations in the lower boundary layer, and another aloft on most days during this experiment. The two layers usually merged in a time period from 1400 to 1600 PDT, but sometimes the merging took place at a much later time. Ozone advection fluxes are calculated using lidar and wind profiler data together. Measurements in the experiment show that in most cases more ozone is transported aloft, despite higher concentrations of ozone in the boundary layer. The ozone advection flux measurement has been the first one ever done in the United States using lidar and wind profiler data.

(This page intentionally left blank.)

I. INTRODUCTION

The NOAA/ETL's ground-based ozone lidar[1] was employed in two field experiments in California in 1993, sponsored by the California Air Resources Board (CARB). The results obtained in these experiments demonstrated that this lidar is capable of continuously measuring ozone profiles with good accuracy, and has a range coverage from near the surface to about 2 to 3 km in a very polluted area. Thus, it has good capability for addressing air quality issues, especially in Southern California, where the ozone problem continues to be the worst in the United States despite significant progress in reducing emissions of organic gases and nitrogen oxides.

The potential inhomogeneity of ozone distributions in a heavily polluted area with complicated terrain and meteorological conditions led to the development of a two-dimensional scanning system for the ozone lidar. The scanning capability was desired for both monitoring and modeling studies (assessment of variability within a grid cell). Sponsored by CARB and NOAA, a preliminary elevational scanning system was developed for the ETL ozone lidar in 1995. In addition, various modifications were carried out during late 1994 to early 1995 to improve the mechanical and thermal stability of the lidar, to increase the signal-to-noise ratio in lidar signals, and to make the system complete eye-safe. The newly-modified system was deployed in August 1995 in Victorville, CA, which is close to Cajon Pass, a major ozone transport corridor from LA urban area to the Mojave Desert Air Basin. Field tests were carried out to observe the vertical profiles and two-dimensional distributions of the ozone concentrations in a vertical plane. An UV ozone analyzer was installed in the lidar to measure surface ozone. A 449-MHz wind profiler/RASS[2] system was deployed by the System Demonstration and Integration Division of ETL at the same site (few tens of meters away from the lidar), providing both wind and temperature profiles for ozone mixing ratio and ozone advection flux calculations.

The Mojave Desert in summer provided us a very harsh and extreme environment to test the new system. On July 30, shortly after we finished aligning the lidar, we experienced a wind storm (with tornadic force winds) that uprooted trees, broke power lines, and blew sand into our lidar container through seals on the scanner that opened slightly in the extremely hot temperature. We waited for 18 hours to have the power back, and spent two hours to clean up the lidar, and another day for realignment. The chiller for the laser cooling water stopped working three times during the early days of testing because of overheating protection. The crew finally solved the problem by a temporary remedy. The large temperature variation caused much trouble in the scanning system, but it also revealed problems in the mirror mount design more clearly.

Despite all the problems we had, we successfully obtained data for at least part of each of eight days. Data analysis showed interesting features in ozone profiles in this ozone transport corridor in the afternoons. And this was the first reported vertical profiles of ozone advection fluxes measured by a lidar system and a wind profiler, which should be very useful for ozone transport studies.

II. THE ETL OZONE LIDAR

A detailed description of the ETL ozone lidar and the methodology of a differential absorption lidar (DIAL) system can be found in Reference 1. The following sections will describe what are new in the system.

2.1 Hardware improvements to the ETL ozone lidar

During the end of 1994 and early 1995, we made several significant improvements in hardware and signal processing techniques of the ozone lidar to solve the problems found during the experiments in 1993.

- A rugged invar optical table was purchased to replace the first optical table which was poor both in mechanical and thermal quality. A well-designed supporting system of the table replaced the old one. The reassembled system has shown superb mechanical and thermal stability (beam deviation on the order of less than 10 μrad, 100 times smaller than the lidar's field of view).

- The detector package was redesigned to shorten the optical paths of the 266-nm and 289-nm channels, to improve the optical seals, and to add an additional filter to decrease the noise level (see Fig. 1). These improvements reduced the background radiation noises in both 266 and 289-nm channels to almost zero, while in the 1993 experiments the background noise had been 1000 times higher.

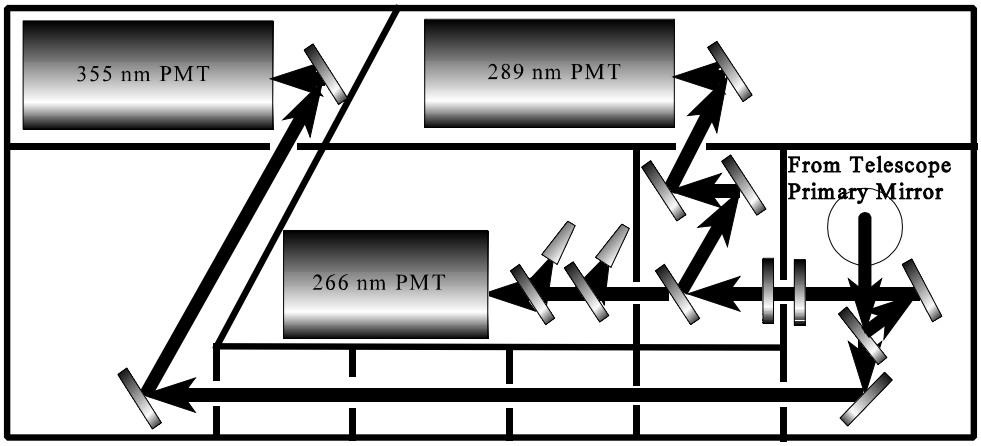

Fig. 1 Optical Layout of the Modified Detector Package

- Double-shielded cables were purchased to replace the single-shield cables for signal channels. This reduced the electro-magnetically induced (EMI) noises by a factor of 10 compared to the 1993 EMI noise data.

- Laser energy at wavelengths 532 and 1064 nm (these were used in the 1993 experiments and were not eye safe) are converted to 355 nm through a third harmonic generator (THG), and the residual energy at the visible and infrared wavelengths were blocked by dichroic mirrors. Thus, all the wavelengths of the ETL ozone lidar are in the UV region, and eye-safe for airplane pilots and passengers. A detailed calculation of eye-safety is in Appendix A.

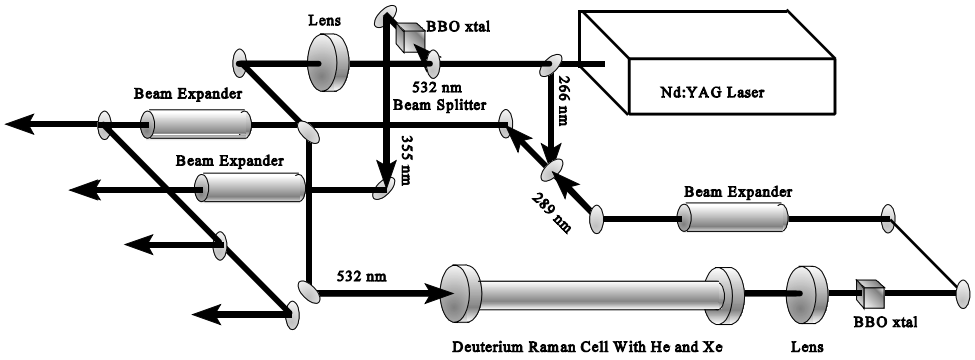

Fig. 2 Optical Layout of the Modified Transmitter

- A new barium borate (BBO) crystal set for converting 532 and 632.5 nm to 289 nm was purchased which has a sealed housing to prevent the crystal surfaces from degradation by water vapor. Windows of the housing and the crystal are sol-gel coated. These anti-reflection coatings increased the laser energy throughput, and endured much higher laser intensities. The crystal is longer than the previous one. All these factors made the new set with higher conversion efficiency (about twice as much as that of the old one) at 289 nm, higher damage threshold, and more humidity-proof.

- New laser experiments provided more insight into the physics of the Raman shift and laser beam pointing, resulting in Raman threshold reduction and much higher pointing stability of the 266/289 wavelength pair, which is crucial to the accuracy of ozone concentration measurement.

- When the background noise was reduced to almost zero, we were able to discover a problem involving internal interference within the photomultiplier tube (PMT). Because the interference starts near the end of the lidar signals when the amplitudes are low, we

were unable to see it before the background noise was eliminated. Although signal-induced noise caused by the residual gas in the PMT has been known for years, this was the first time that a theory of ion-related fluorescence was postulated. Based on theoretical considerations and lidar data taken from horizontal measurements on Table Mountain, in Boulder, CO, during October to November 1995, a model was developed and software was written for removing the fluorescence from the tail of the signal. The model's predictions agreed well with the lidar signals. Removing fluorescence interference significantly improved the accuracy of ozone concentration calculation beyond 2 km.

2.2 Lidar scanning system

Based on a request by the California Air Resources Board, a two-dimensional scanning system was developed. The schematic optical layout is shown in Fig. 3. M_1, 61×34×5.5 cm (24×13.5×2"), is a steering mirror, and has an angle of -37.5E to the vertical direction. M_2, 61×53×5.5 cm (24×21×2"), is a scanning mirror, which changes the elevation angle of the outgoing laser beams and incoming backscattered radiations in a range from 30E to 150E. Both mirrors have UV-enhanced aluminum coatings. Fig. 3a shows the elevation angle limit (30E) on the left side, while Fig. 3b shows the elevation angle limit on the right side (150E). A rectangular hole in the supporting frame below M_1 is used for horizontal measurements and calibrations, as shown in Fig. 3c. The whole scanning system was installed on a rack which was fastened on six poles welded to the top of the sea-container. A computer-controlled electronic scanner instructs the movement of a motor that drives mirror M_2, and the program of the scanner is integrated in the data-taking program of the data-acquisition system. All parameters of scanning, e.g., range of angle to be scanned, increment of angle, and number of laser shots per angle, are set up before data-taking.

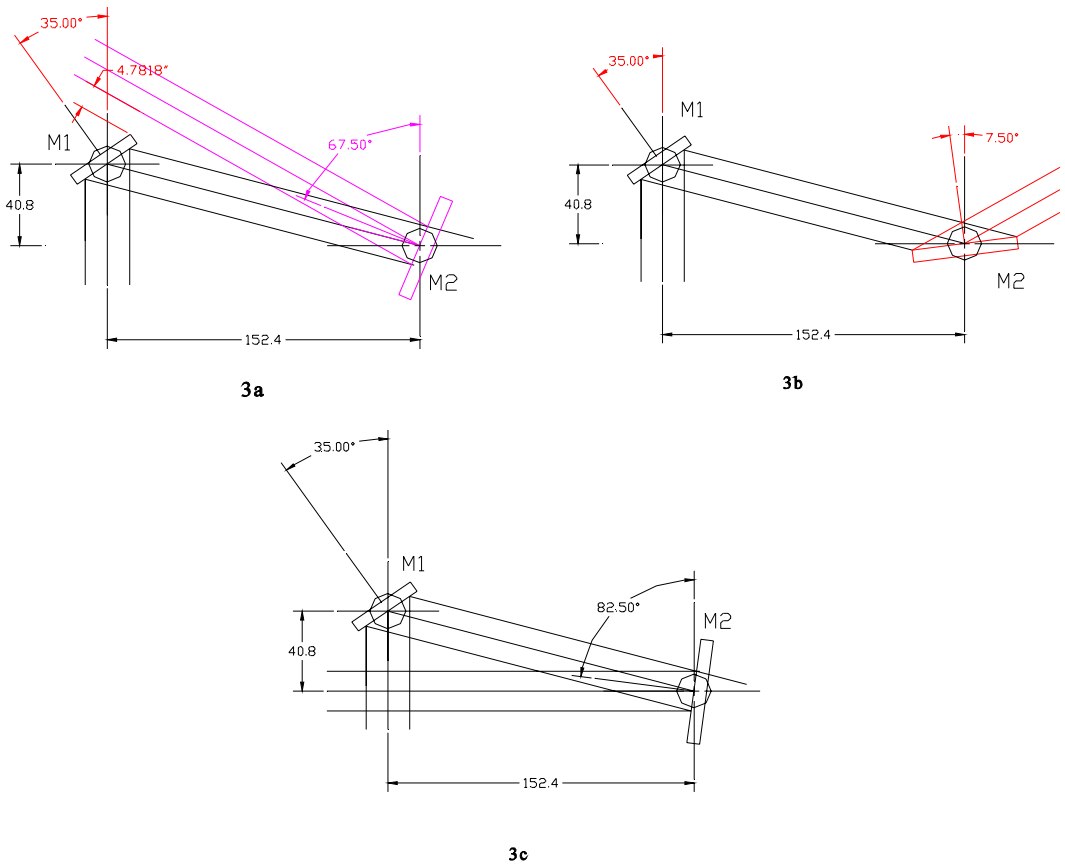

Fig. 3 Optical Layout of the Two-Dimensional Scanning System

2.3 Evaluation of the scanning system in the field experiment

The scanning system worked well in terms of mechanical and electrical scanning operation and software control of the system. The experiment also showed an unexpected advantage of adding the scanner. Data analysis showed that the scanning data provided an excellent internal check of the system itself. We also can see interesting features of the two-dimensional distribution of ozone concentrations when the wind was strong and westerly. Thus, the first phase of development confirmed the benefits of the scanner.

The field test also revealed some problems in the scanner. A thorough test of the scanner and its components were not possible before the Victorville experiment because of late delivery and errors by the manufacturer of the mirrors. The scanning system was not assembled, installed on the lidar, and moved to the local testing site until ten days before we shipped the lidar to Victorville. During the days at the testing site other software and hardware also needed some debugging, leaving very short time to only a preliminary test of the scanning system. However, the extremely large diurnal variations of temperature and the intense sunshine in the Mojave

Desert in summer time provided severe test that helped us to discern some of the engineering problems and component deficiencies in the scanner. Much was learned in this experiment about optical quality of these aluminum mirror-coatings, thermal and mechanical distortions of mirror mounts, spikes caused by scattering from the scanning mirrors, how those problems affect the overlap functions of the lidar and thus the accuracy of the ozone concentration retrieval, and what would be the good ways to solve the problems. Field-testing the scanning system for future improvements was one of our major objectives of this experiment, and that goal was achieved. A modified scanning system with more sophisticated design has since been completed. Laboratory and field tests show that the system is essentially free from these problems. Moreover, we now have an operational strategy that will provide more frequent and better system calibrations for future experiments.

The engineering problems we found in the scanning system are as follows:

- *Mirror scattering*

  The first problem we found was the extremely high spikes at the beginning of the signals. The spikes were caused by the scattering of the laser beam from the mirrors, especially M_2. Despite several simple efforts to baffle the scattering before and during early days of the experiment, the amplitudes of the spikes were not reduced sufficiently. We were forced to cover the first beam, because it was the beam closest to the receiver and contributed most to the scattering. However, even without the first beam, the spike at 266 nm was still very large. It might have affected the ozone retrievals out to a range of as much as 75 m.

  Without the first beam, ozone concentration measurements below ~300 m were less accurate because the values of the near-range overlap functions were very low. Moreover, the relative changes of the overlap function (this is the ratio of the backscattered radiation received by the detector to the total backscattered radiation striking on the telescope, before the laser beams fully enter the field of view) at about 600-800 m (where the central part of the second beam starts to enter the field of view) were sensitive to transmitter-receiver alignment changes induced by distortions of the scanning mirrors .

- *Mirror coating damage*

  After a few tests of data taking on August 2, we found mirror M_2 was seriously damaged, because the manufacturer failed to meet specifications. We had this mirror re-coated on an emergency basis by another vender. The new coating endured the laser beams throughout the rest of the experiment, although, at the strongest beam, a slightly foggy spot appeared after several days of intensive operation.

- *Mirror distortion*

Data analysis surprisingly revealed that the mirrors were distorted in the morning. The mirrors were expected to maintain their flatness because they were 2" thick. However, data show that the mirror mount design was not sufficient to overcome thermal distortions. Early morning scanning data that show adjacent arcs of extremely high and low ozone with same radius (see APPENDIX B, Fig. a) are strong evidence that the errors were caused by shifted overlap functions. The errors decreased quickly during the warming up period (see APPENDIX B, Fig. b based on data taken one hour later than Fig. a). The errors were much less in the afternoon when the temperature changes were slower, and the time of day and conditions were close to those of the calibrations (see APPENDIX B, Fig. c - e). Vertical profiles of the early morning observations from 7:41 to 8:58 are shown in Fig. f. The artificial peak at about 700 m reduces rapidly, whereas the dip at about 950 m increases. During this period, the ambient air temperature increased about 8E C (14.4E F). With exposure to direct sun light, the mirror sets very likely experienced even higher temperature increases.

Comparing the correction functions [$\ln(\eta_{289}/\eta_{266})$] taken at 18:42-18:58 PDT on 8/08/95 (with two mirrors) and at 08:41-09:00 PDT on 8/13/95 (with only one mirror) (see Fig. g in APPENDIX B), the approximate equivalent error in ozone concentration due to the change in overlap function is shown in Fig. h in APPENDIX B. Positive errors occur in the range of 700 to 810 m with a peak of 30 ppb at 790 m, and negative errors occur in the range of 830 to 1100 with a dip of -70 ppb at 920 m, which are qualitatively in good agreement with what we see in the morning profiles. Beyond 1050 m, no significant errors in ozone concentration are shown, which are expected, because the range is near and/or beyond the full-overlap range. Below 600 m, it is not appropriate to compare the two because both the mirror warping effect and the scattering contributions in the near range are different in one-mirror and two-mirror settings.

2.4 Modifications of the scanning system

- *Mirror mount redesign*: A new supporting system has replaced the old one. This makes the mirror surface flatness independent of the mounts. Laboratory tests have shown that the surface of the mirrors remain flat even with a substantial differential heating on the mirror mount.

- *A new baffling system* has reduced the spikes in the signal to almost zero.

- *Mirror recoating*: The scanning mirror M_2 has been recoated by the best UV coating company. Damage threshold tests have been performed on a witness sample with the highest laser intensity to be used in the field. No damage has been found.

- *Scanning encoder*: An encoder has been added to the rotating axis of the scanning mirror mount. This eliminates the effect of backlash during scanning, and enables us to precisely steer the system to carry out horizontal calibrations.

- *New beam expander*: The new beam expander has a magnification of 5× to replace the old 3× one, reducing the laser fluence by a factor of 3 to help prevent mirror coating damage.

- *Improvement of the overlap functions*: The distances of the three beams at the 266-289 nm pair to the receiver have been re-arranged to avoid having range intervals where the accuracy of ozone concentrations are overly-sensitive to system alignment.

In addition to the hardware improvements of the scanning system, we are testing the lidar before deploying it to the field. More frequent horizontal calibrations will also be carried out in future field experiments. With the help of the modified scanning system, we can do this once every hour, or even once in every scan.

III. OPERATIONAL NOTES

- August 3 and 4, 1995

During these two days, the scanning system was under repair due to the coating damage. All measurements were vertical without scanning mirrors, and all three beams of the 266-289 nm pair were working. It was very hot and the sky was clear. In the late afternoon to the evening of August 4, we saw steady increase in surface ozone concentrations (measured by the UV ozone analyzer) until 8:30 pm, with a peak concentration of 155 ppb. This was the highest surface ozone concentration observed during this experiment.

Unfortunately, without a steering mirror calibrations in the horizontal direction could not be performed. To avoid a total loss of the interesting data taken in these two days, we borrowed the overlap function partly from the calibration on August 8 for the second and third beams, and partly from a later calibration performed at Table Mountain site in Boulder for the first beam. The mirror which we used at Table Mountain was the same mirror (M_1) in the same mount, and the mirror distortion might give us different overlap functions in the calibration. With this approximation, we might have quite large errors in calculating ozone concentration in altitudes lower than 300 m.

- August 7-13, 1995

It was sunny and hot on the first three days (Aug. 7-9). On Aug. 10 there was a low pressure system moving in. We had partly cloudy days from Aug. 10-12. In most cases the clouds were altocumulus or cirrus higher than 3.5 km (agl).

During these six and half days, the scanning system was back in operation, and only beams #2 and #3 were used in the ozone channel, as we mentioned in Section 2.3. The spikes affected down-stream signals to a range of 75 m, the mirrors warped differently in the diurnal cycle, and we only had one valid calibration in late afternoon - all these problems gave us a lot of trouble in data processing. In the afternoons, when the mounts were hotter and looser, the mirrors apparently had less stress on them, and with the data-taking time being closer to the time of calibration, the relative differences in overlap functions were much smaller. This can be seen clearly in the scanning data in the afternoon which showed ozone concentration distributions more or less horizontally stratified with convective patches embedded. The pictures were much more reasonable and convincing, although there still might have been some residual systematic errors lower than 1000 m due to unknown mirror warping.

IV. INTERCOMPARISONS WITH QUARTZITE MOUNTAIN DATA

Three elevated surface ozone stations close to the lidar site (872 m MSL) were Quartzite Mountain (1366 m MSL), Baldy Mesa (1295 m MSL), and Shadow Mountain (SM) (1256 m MSL), among which Quartzite Mountain (QM) is the closest (a map of the region is shown in APPENDIX C). Both QM and SM sites are isolated peaks above desert floor. QM site is 461 m higher than the lidar site, and is 3.33' north and 5.95' east of the lidar at approximately 34E 35.3' N and 117E 23.3' W. Thus the direction from the lidar to QM is 245E. Interstate Highway 15 lies from SW to NE to the QM site. The closest range from Interstate 15 to QM is about 3 km SE of QM. If wind blows from the south (this was often the case), the distance from Interstate 15 to QM is about 6 km. With a wind speed of 3 m/s and 10 m/s, this translates into a 30 min and 10 min time lapse from Interstate 15 to QM, respectively. Meteorological data taken during the experiment showed that the wind at QM was almost always strong southerly. This wind may carry the pollutant emissions from the Interstate 15 and the Victorville area up the mountain to the ozone monitoring site.

Although deposition of ozone to the surface undoubtedly occurs, the amount of deposition is probably small compared to other settings (e.g., forested ridge) because QM is an isolated peak in a desert. More importantly, photochemical destruction of ozone by NO emissions from the Victorville urban area to the south of QM can reduce ozone concentrations on the mountain by a few tens of parts per billion during appropriate meteorological conditions (e.g., southerly, upslope flow). When comparing the lidar ozone measurements at 465 m, $O_{3,l}$, with those measured at QM, $O_{3,QM}$, and defining ΔO_3 as $O_{3,l} - O_{3,QM}$, we can see the following interesting phenomena:

1. Lidar-measured ozone concentrations have a similar diurnal trend as the surface ozone measured at QM, with a peak generally between 15-17 PDT, but lidar-measured ozone concentrations in most cases are higher, i.e. $\Delta O_3 > 0$.

2. When surface ozone concentrations measured at the three monitoring stations in the region show good horizontal homogeneity, such as in the afternoon of August 9 [see Fig. 4e], lidar-measured ozone concentrations were similar to those at QM, especially when the wind was more westerly.

3. When wind at the lidar site (461 m agl) had a strong westerly component, ΔO_3 were at a minimum, on the average of ~10 ppb. This can be seen in Fig. 4c and 4f, during the days of August 7 (from 17 to 19 PDT) and August 10 (from 14 to 21 PDT, except at around 18 PDT, when plumes of ozone arrived at the lidar site, which are clearly shown on the surface record). It is worth noting the comparison on August 4 (see Fig. 4b). From 8 to 18 PDT when the wind was from south, ΔO_3 were 20 to 30 ppb. However, when wind turned from southerly to WSW from 19 to 20 PDT, ΔO_3 dropped to 10-15 ppb.

4. When winds at the lidar site were slow and from north or northeast, e.g., August 8 (see Fig. 4d), from 12 to 15 PDT, lidar-measured ozone concentrations were very close to and

a little less than the surface QM ozone measurement. ΔO_3 were from ~0 to -10 ppb on the average. After 15 PDT when the wind direction changed suddenly from northeastly to southerly throughout the layer from surface to 1000 m, and wind speed increased, ΔO_3 also increased suddenly, approximately from 0 to 30 ppb.

5. When winds were from the south, ΔO_3 was much greater and more variable (see Fig. 4a, 4b, 4d, and 4g). It seems that when the surface ozone mixing ratios at QM and Baldy Mesa sites were similar and wind speeds light, ΔO_3 was relatively small [compare data on Aug. 4 and Aug. 11, to those on Aug. 3 and Aug. 8 (from 15-19 PDT)].

The above results indicate that $\hat{I} O_3$ is more variable and often larger when winds are from the south; this association between the ozone measurements on QM and at the same altitude by lidar during southerly air flow is consistent with the frequent transport of polluted air from the greater Los Angeles region and with the ozone near ground level being modified as it passes over the Victorville urban area and on occasion rises up the slope of QM.

Figure 4a

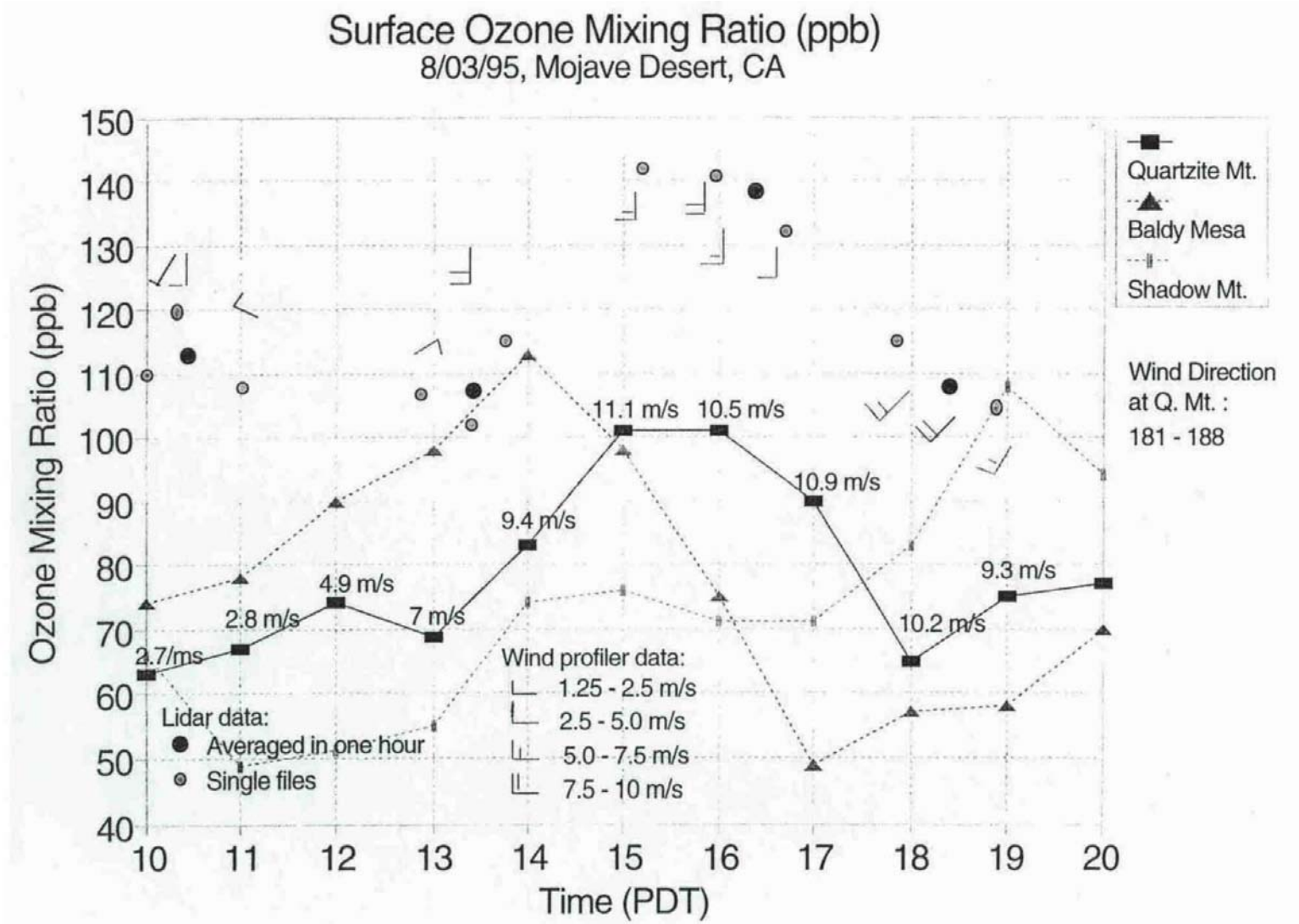
Surface Ozone Mixing Ratio (ppb)
8/03/95, Mojave Desert, CA
Ozone Mixing Ratio (ppb)
Time (PDT)
Quartzite Mt.
Baldy Mesa
Shadow Mt.
Wind Direction at Q. Mt. : 181 - 188
2.7/ms
2.8 m/s
4.9 m/s
7 m/s
9.4 m/s
11.1 m/s
10.5 m/s
10.9 m/s
10.2 m/s
9.3 m/s
Lidar data:
Averaged in one hour
Single files
Wind profiler data:
1.25 - 2.5 m/s
2.5 - 5.0 m/s
5.0 - 7.5 m/s
7.5 - 10 m/s

Figure 4b

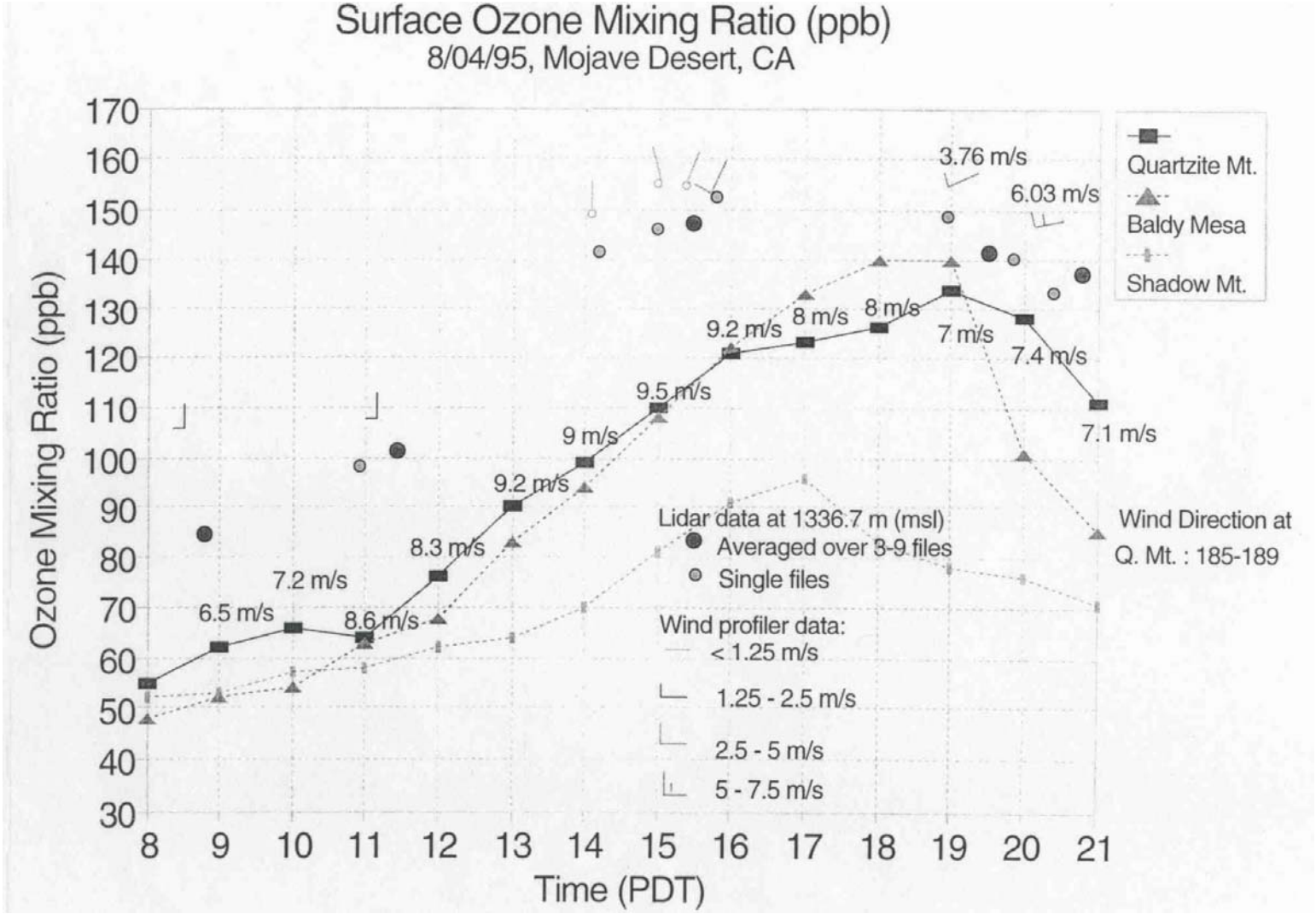
Surface Ozone Mixing Ratio (ppb)
8/04/95, Mojave Desert, CA
Ozone Mixing Ratio (ppb)
Time (PDT)
Quartzite Mt.
Baldy Mesa
Shadow Mt.
Lidar data at 1336.7 m (msl)
Averaged over 3-9 files
Single files
Wind profiler data:
< 1.25 m/s
1.25 - 2.5 m/s
2.5 - 5 m/s
5 - 7.5 m/s
Wind Direction at
Q. Mt. : 185-189
6.5 m/s
7.2 m/s
8.6 m/s
8.3 m/s
9.2 m/s
9 m/s
9.5 m/s
9.2 m/s
8 m/s
8 m/s
7 m/s
3.76 m/s
6.03 m/s
7.4 m/s
7.1 m/s

Figure 4c

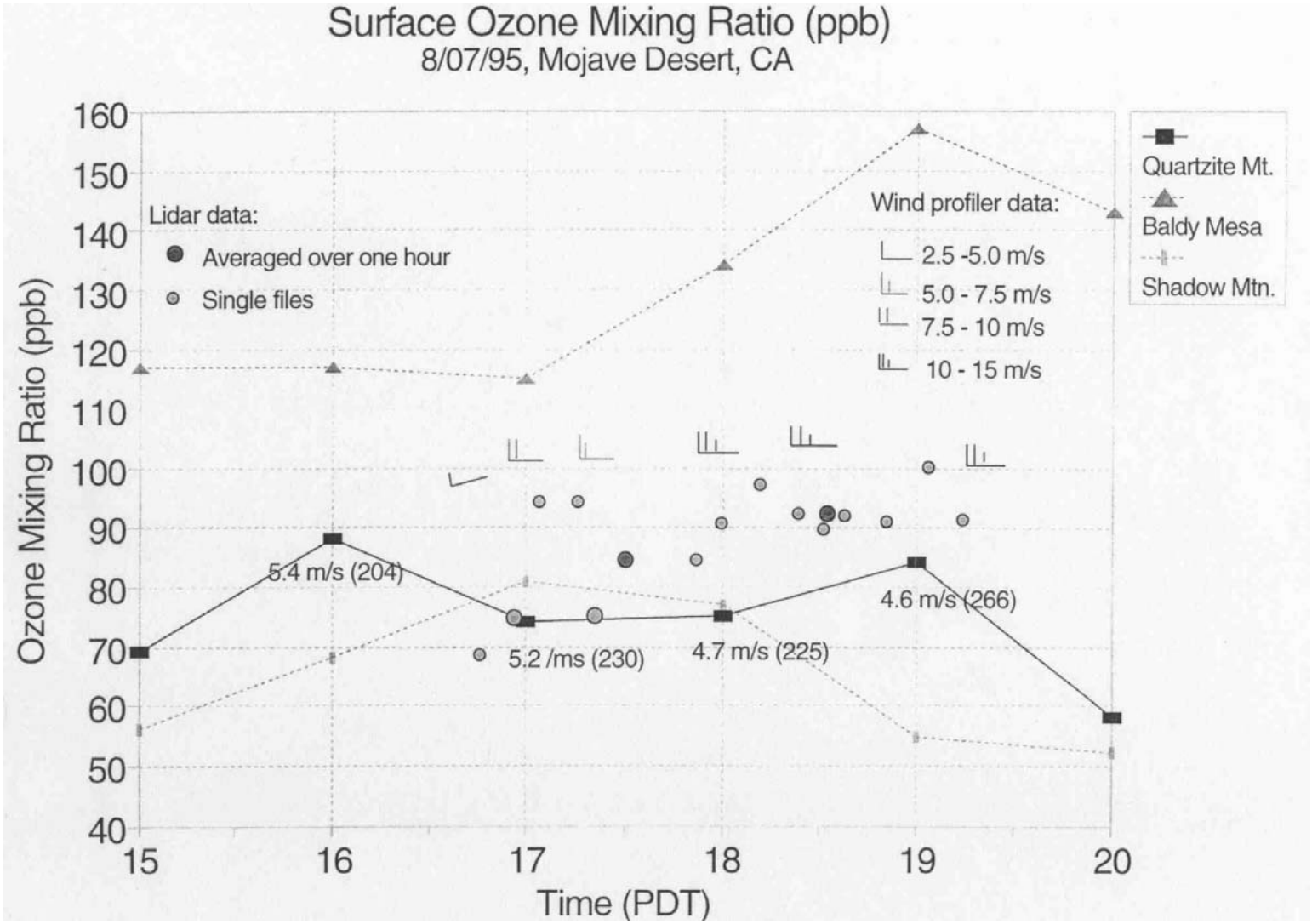
Surface Ozone Mixing Ratio (ppb)
8/07/95, Mojave Desert, CA
Ozone Mixing Ratio (ppb)
160
150
140
130
120
110
100
90
80
70
60
50
40
15
16
17
18
19
20
Time (PDT)
Lidar data:
Averaged over one hour
Single files
Wind profiler data:
2.5 -5.0 m/s
5.0 - 7.5 m/s
7.5 - 10 m/s
10 - 15 m/s
Quartzite Mt.
Baldy Mesa
Shadow Mtn.
5.4 m/s (204)
5.2 /ms (230)
4.7 m/s (225)
4.6 m/s (266)

Figure 4d

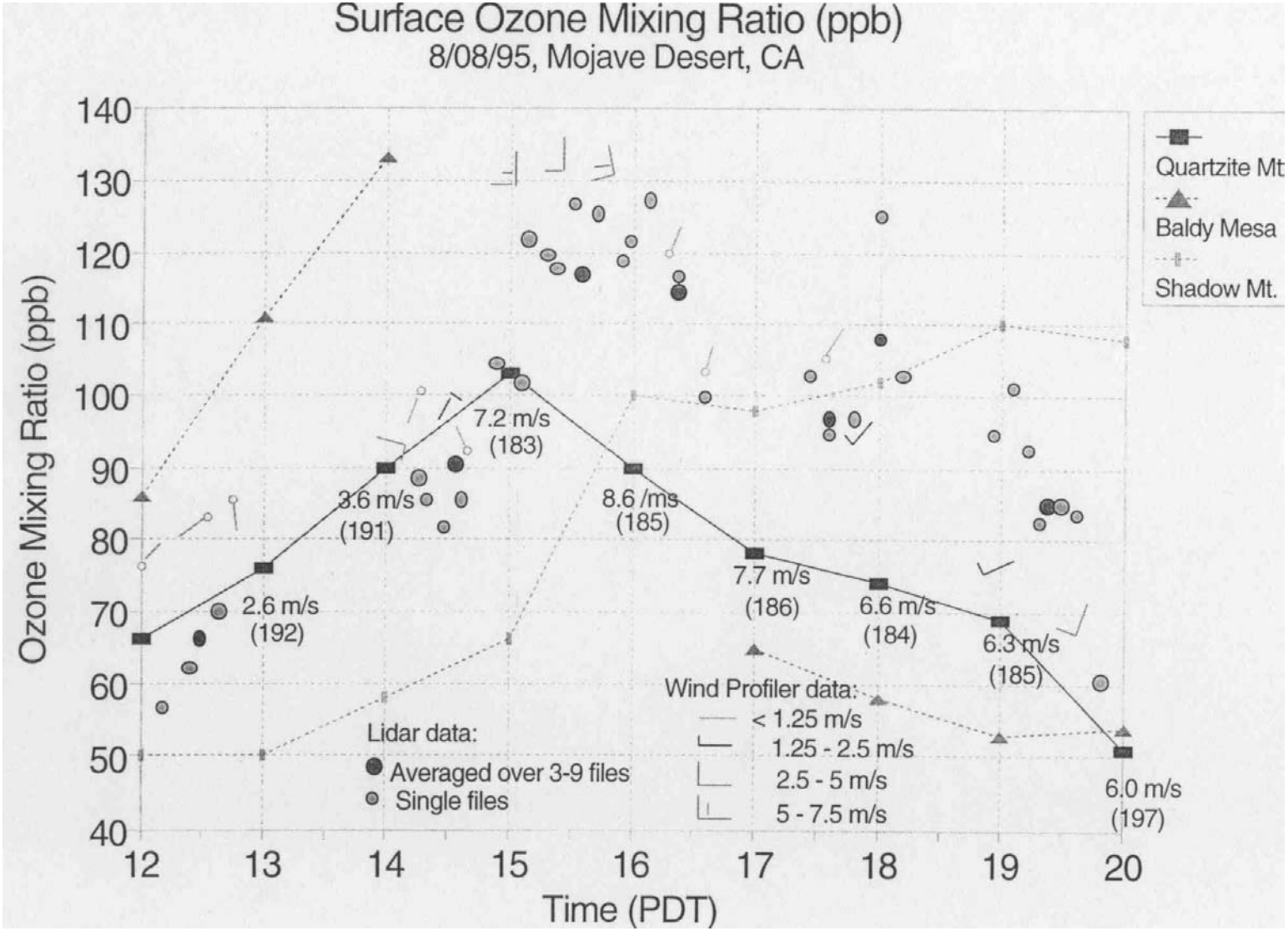
Surface Ozone Mixing Ratio (ppb)
8/08/95, Mojave Desert, CA
Ozone Mixing Ratio (ppb)
Time (PDT)
140
130
120
110
100
90
80
70
60
50
40
12
13
14
15
16
17
18
19
20
Quartzite Mt.
Baldy Mesa
Shadow Mt.
2.6 m/s
(192)
3.6 m/s
(191)
7.2 m/s
(183)
8.6 /ms
(185)
7.7 m/s
(186)
6.6 m/s
(184)
6.3 m/s
(185)
6.0 m/s
(197)
Lidar data:
Averaged over 3-9 files
Single files
Wind Profiler data:
< 1.25 m/s
1.25 - 2.5 m/s
2.5 - 5 m/s
5 - 7.5 m/s

Figure 4e

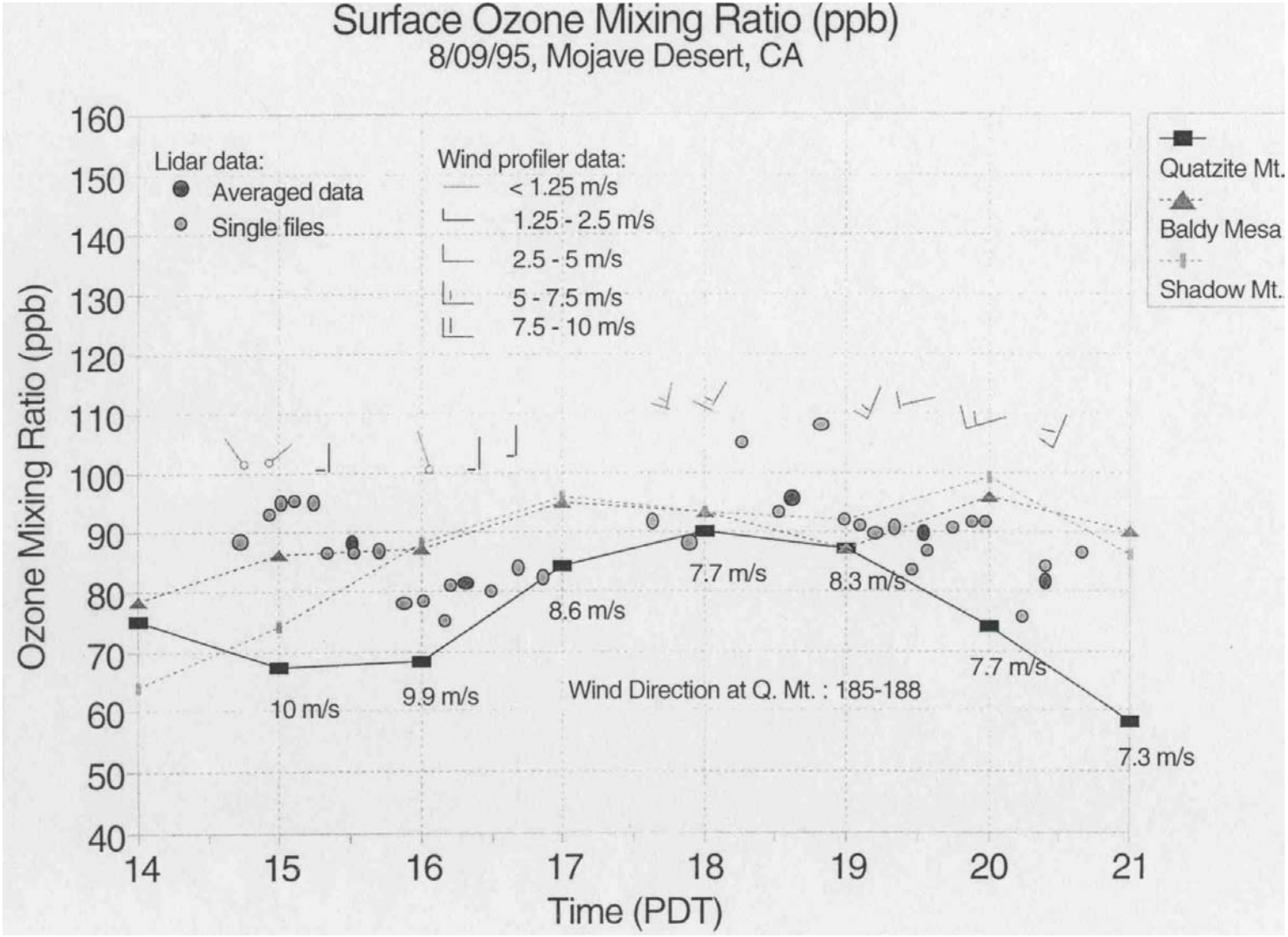
Surface Ozone Mixing Ratio (ppb)
8/09/95, Mojave Desert, CA
Lidar data:
Averaged data
Single files
Wind profiler data:
< 1.25 m/s
1.25 - 2.5 m/s
2.5 - 5 m/s
5 - 7.5 m/s
7.5 - 10 m/s
Quatzite Mt.
Baldy Mesa
Shadow Mt.
Ozone Mixing Ratio (ppb)
160
150
140
130
120
110
100
90
80
70
60
50
40
14
15
16
17
18
19
20
21
Time (PDT)
10 m/s
9.9 m/s
8.6 m/s
7.7 m/s
8.3 m/s
7.7 m/s
7.3 m/s
Wind Direction at Q. Mt. : 185-188

Figure 4f

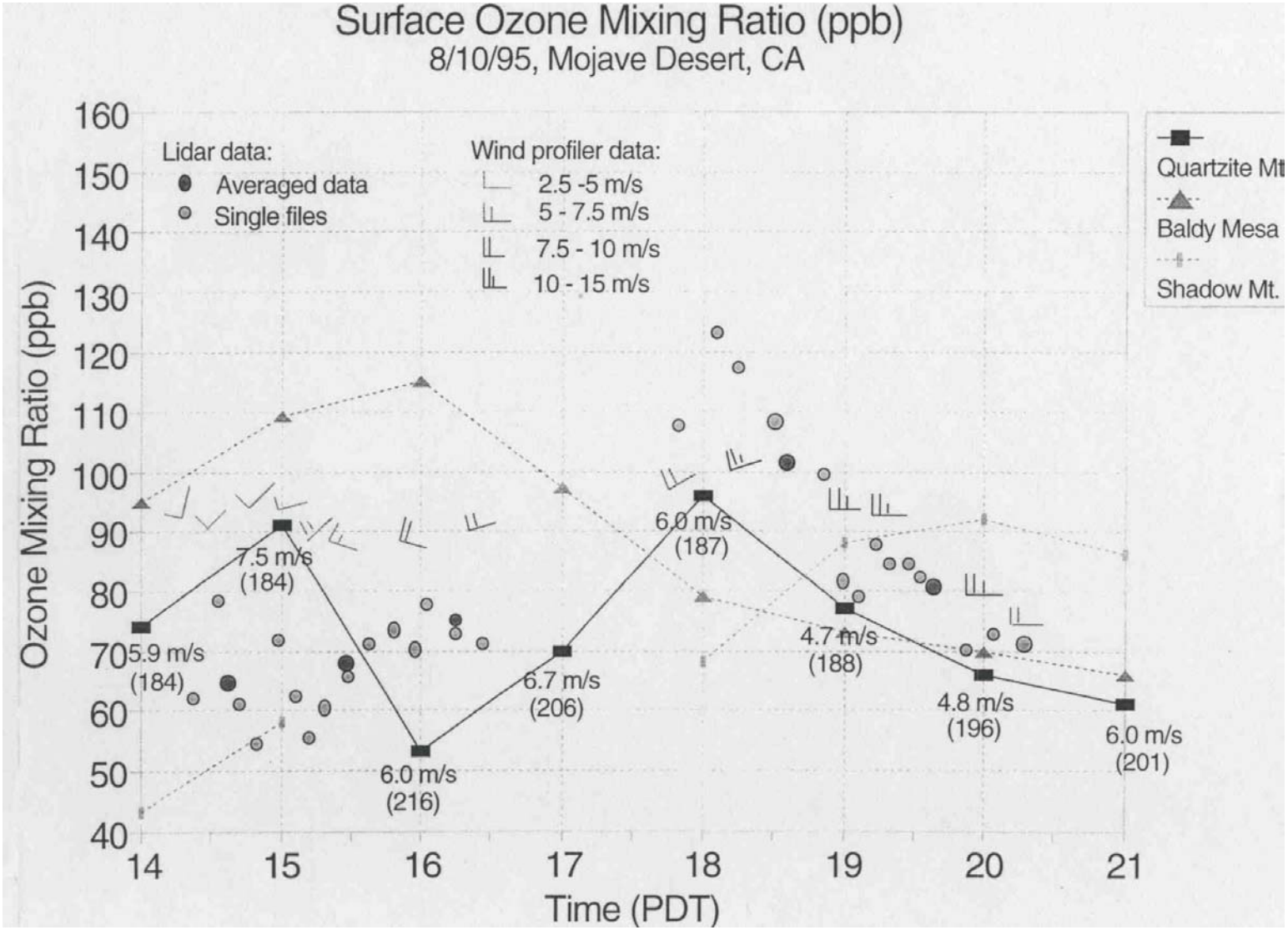
Surface Ozone Mixing Ratio (ppb)
8/10/95, Mojave Desert, CA
Lidar data:
Averaged data
Single files
Wind profiler data:
2.5 -5 m/s
5 - 7.5 m/s
7.5 - 10 m/s
10 - 15 m/s
Quartzite Mt
Baldy Mesa
Shadow Mt.
Ozone Mixing Ratio (ppb)
160
150
140
130
120
110
100
90
80
70
60
50
40
14
15
16
17
18
19
20
21
Time (PDT)
5.9 m/s
(184)
7.5 m/s
(184)
6.0 m/s
(216)
6.7 m/s
(206)
6.0 m/s
(187)
4.7 m/s
(188)
4.8 m/s
(196)
6.0 m/s
(201)

Figure 4g

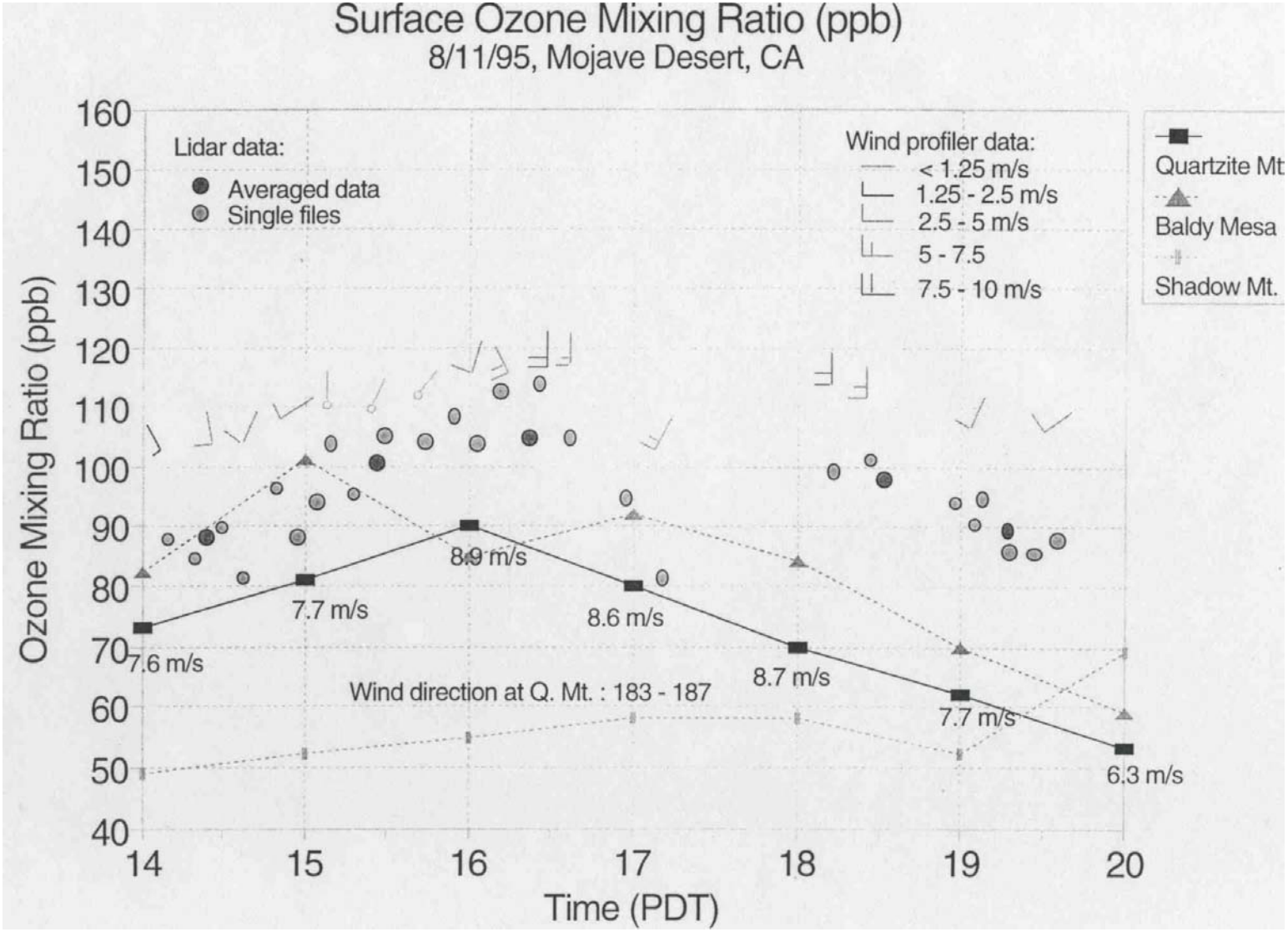
Surface Ozone Mixing Ratio (ppb)
8/11/95, Mojave Desert, CA
Ozone Mixing Ratio (ppb)
Time (PDT)
Lidar data:
Averaged data
Single files
Wind profiler data:
< 1.25 m/s
1.25 - 2.5 m/s
2.5 - 5 m/s
5 - 7.5
7.5 - 10 m/s
Quartzite Mt.
Baldy Mesa
Shadow Mt.
7.6 m/s
7.7 m/s
8.9 m/s
8.6 m/s
8.7 m/s
7.7 m/s
6.3 m/s
Wind direction at Q. Mt. : 183 - 187

V. INTERCOMPARISONS WITH AIRBORNE OZONE DATA

In a previous intercomparison between lidar and airborne DASIBI in Davis, CA, during July 1993, the results were satisfactory, and the agreement between the ozone lidar and the airplane measurements were better than 10 ppb in most cases. However, in the 1995 Victorville experiment the lidar data and the airplane data did not agree well. In the morning, apparently the lidar scanning mirrors had distortions, as mentioned in Section 2.3. But during the afternoon when the mirror distortion was at a minimum as shown in the scanning display, lidar and airplane measurements still disagreed. These discrepancies may have been caused by spatial, temporal variations in the area with a very complex terrain and meteorological conditions. Methodological differences in measurement may also contribute to the differences in results as well.

The ozone profiles measured by the airplane (J. J. Carroll and A. J. Dixon[3]) during the up-spirals and down-spirals were significantly different from each other by 10-50 ppb most of time, and the ozone profiles in down-spirals were almost always higher than the corresponding profiles in up-spirals. The pair of loop-shaped upward and downward profiles look like hysteresis. We did not see that discrepancy in airplane data taken during the intercomparison experiment in Davis. It is difficult to explain this up-and-down bias with either temporal or spatial ozone variations. If the differences were caused by temporal variations, then the lidar profiles grouped together closely (each about 7.5 min) should exhibit large variations over one-hour measurements, the approximation for the up- and down-profiles in airplane measurements. If spatial variations were to blame, then it is also hard to imagine that ozone concentrations closer to the lidar site (downward spirals are tighter) at different altitudes are always higher than those in the surroundings. Therefore, we have strong reservations about using these particular airplane data as a reference standard for evaluating the accuracy of the lidar measurements.

Airborne ozone concentration measurements were also conducted in July 1981 in the Mojave Desert by MRI (T. B. Smith et al, April 1983[4]). Vertical profiles of ozone concentrations at Victorville and Hesperia (12 miles south of Victorville) on different days and at different times varied significantly, although some of the airplane measured ozone concentration profiles in the late afternoon showed a dip at about 1500 m msl, and a peak at about 2300 m msl, similar to those observed by the lidar. The complexity of ozone vertical distributions in this area may contribute considerably to the uncertainties in lidar-airplane comparisons.

Because of the spatial, temporal, and methodological differences, comparison of the lidar-derived data with in-situ data (from aircraft or mountain peak) by necessity is more qualitative than quantitative in nature in this area. At this point, we think evaluation of the internal consistency of the lidar data (Level 1a data validation) is the best method for assessing the reliability of the lidar data. As noted earlier, the 2-D scanning feature of the lidar provides a good internal check of the lidar data. If the scanning data show an arc structure, that is a strong indication of artificial effects due to things like scanning mirror distortion. On the other hand, if the scanning data do not show such artificial structure, but a more or less horizontally stratified

ozone concentrations, then we believe that the ozone profiles are reliable. The ozone profiles that we believe are reliable, without significant systematic errors that can mask the temporal and spatial trend, are those taken in the afternoon, roughly from 14-15 PDT to early evening. Additional analysis of the lidar data in conjunction with meteorological and other air quality data (Level 1b validation) should lead to better insights and perhaps more refined assessments.

VI. VERTICAL DISTRIBUTION OF OZONE CONCENTRATIONS AS MEASURED BY LIDAR

1. **8/03/95** and **8/04/95**

The scanning mirrors were not available on these two days, and thus no "diurnal variations" due to the mirror warping effect are expected. Furthermore, without a steering mirror the beam could not be directed horizontally for calibrations of the lidar system. The overlap functions used to process the data taken on these two days were borrowed from the calibration on 8/08 for the outside two beams with two scanning mirrors and the calibration on 10/21/95 in an experiment at Table Mountain site in Boulder, CO, for the nearest first beam with one steering mirror. Although there might be some systematic errors in lower altitudes with substitute calibrations, the ozone profiles should not be affected by overlap functions of the first beam above 500 m because it is beyond the full overlap range of the beam and the field of view. Even for ozone data below 500 m, we have no evidence to say that the low level peaks at 100 - 200 m and 400-500 m are artifacts just because we do not feel convinced. If the low-level peaks are derived from the approximation of overlap functions, they should be constant and linearly superimposed on the ozone profiles. But the ozone profiles on 8/03 and 8/04 do change significantly, especially in the evening of 8/4 after 1800 PDT the profiles do not show peaks at ~500 m. Explanations can be found in the variation of atmospheric conditions.

The lower peak at 100-200 m in 8/03 and 8/04 can often be seen during 8/08-8/11. It is reasonable to assume that there would be a positive gradient of ozone mixing ratio in the surface friction layer when the pollutants are being transported to the site. Vertical mixing can reduce the gradient, but may not completely because there are ozone sinks near ground level. Nitrogen oxide emissions from Victorville could suppress the ground level ozone concentrations. Furthermore, the lidar site is on the northeast corner of the former George Air Force Base, where a large area south of the lidar are covered by trees and lawns well watered every day. This would have high deposition rate of ozone. In the Los Angeles Free Radical Study in Claremont, CA, during September in 1993, a peak of ozone mixing ratio at 150-200 m was often detected by the lidar (see Reference 1).

Because scanning mirrors were not involved and the ozone profiles are reasonable compared with historical data taken by both airplane in the general area and by lidar during the 1993 Claremont experiment, ozone profiles observed in these two days can serve as a check to the lidar measurements with the scanner.

Time-height plots of ozone mixing ratios on 8/03 and 8/04 are shown in Fig. 5a and 5b, respectively. In Fig. 5a, a layer of high ozone concentrations in the lower boundary layer from 50 to 500 m AGL (~920-1400 m MSL) lasts from 10 to 1800 PDT. A higher ozone layer aloft at ~1000-1400 m AGL (~1900-2300 m MSL) starts to develop at ~1400 PDT, and lasts until 1700 PDT. A layer of low ozone concentration exists at about 700 m AGL (~1600 m MSL) in between the two high ozone layers. The two layers with high ozone merge from 1430 to 1600 PDT, and separate again after 1630 PDT. RASS data show a stable layer below 630 m most of

the day time. Sometimes the lapse rate is higher or close to adiabatic: e.g, at 1400 PDT from 510 m to 870 m (this closely correlated with the merge of the two ozone layers), and at 1500 PDT from 150 to 270 m. In the surface layer from 0 to 150 m, the lapse rate in the afternoon before 1600 PDT is super-adiabatic, and less than neutral afterwards.

On August 4, transport of ozone started very early. As we mentioned before, this was a special case during this experiment. There was a steady growth of surface ozone from 0900 PDT to 2030, the peak reached 155 ppb at 20:30 PDT, then suddenly tapered off. The altitude of the top of the lower layer kept increasing after 0900 PDT until it merged with the ozone aloft. The ozone layer aloft started to develop about 1400 PDT. The two ozone layers shown in Fig. 5b merged from 1530 PDT until ~2000 PDT when the higher layer disappeared. RASS data from 0900 to 1300 PDT are not available. In the late afternoon during 1400 to 1900 PDT, the lapse rate was super-adiabatic from ground level to 150 m. Lapse rate from 150-510 m PDT was less than neutral, but it was higher above 510 m during 1900-2000 PDT, which was correlated with a sudden wind change from southwesterly to westerly above 400 m after 1800 PDT.

2. 8/07/95

Because the chiller failed, the afternoon data are available only between 1645 and 19:20. Fig. 5c shows a higher ozone layer of 120-130 ppb aloft at about 1100 to 1500 m but no high ozone layer below 1000 m, with the exception of occasional short-term high ozone plumes very close to the ground.

3. 8/08/95

Shown in Fig. 5d, the general trend of ozone temporal and spatial variation is similar to that of 8/03/95, but the lower layer started at a later time, about 1400 PDT, and the top of the layer was higher. The layer aloft at 1200-1500 m AGL started to develop after 1300 PDT. This was the layer aloft with the highest ozone concentrations we observed during this experiment. The peak reached 160 ppb at 1250 m. The two ozone layers merged from 1530 to ~1700 PDT (correlating with wind changes), with short periods of lower ozone at 800 m in between. Ozone mixing ratios from the surface to 1.5 km were more or less uniform. The higher layer persisted to evening with a lower altitude of ~1000-1200 m.

The 355 nm channel detected two aerosol layers in late afternoon and evening: one from the surface to ~600 m, and the second from 1000 to 4000 m, with a low aerosol extinction at ~800 m. In the second layer aerosol extinction coefficient dropped suddenly above 4000 m.

4. 8/09/95

Fig. 5e shows a low-level ozone layer that was shallow and confined below 400 m. There was still a layer aloft but appeared late and descended to a lower height after 1900 PDT. The two layers never merged. A dip of ozone at 650 to 800 m was observed throughout 1600-2000 PDT. RASS data showed a stable thermal structure in the lower altitudes.

5. 8/10/95

A low pressure system moved in with strong westerly wind. The sky was sunny in the morning and became partly cloudy in the afternoon. In Fig. 5f no high ozone layer aloft was observed before 1700 PDT. For a short period, high ozone concentrations were transported to the site around 1800 PDT. Spikes of high ozone mixing ratio can also be seen on the record of surface ozone concentrations. The two layers of ozone briefly merged at ~1800 PDT. A short time later at 1830 PDT, the high ozone layer aloft subsidized and an layer of near background ozone concentrations developed at 600 m.

6. 8/11/95

This day was cloudy (mostly altocumulus and cirrus). The lower-altitude ozone layer developed after 1400 PDT, and lasted until 1830 PDT. The high ozone layer only existed a short time, from 1530 to 1700 PDT. The two merged for only about half hour at ~1630 PDT. This correlates very closely with the wind profiles.

According to the above day-to-day analysis of lidar data, ozone concentrations do show a two layer structure in the afternoon, one in the lower boundary layer, and another aloft. The two layers usually merge in mid afternoon, and separate again later.

The two-dimensional (2D) ozone data usually show more or less horizontal homogeneity within 2 km. One exception is seen in the late afternoon from 17:48 to 18:19 PDT on August 10 when a ozone plume arrived the site (see Fig. 5f). The wind was strong westerly. In an adjacent scanning display, we can see ozone being transported from the west to east (see Fig. 6a-c).

Figure 5a

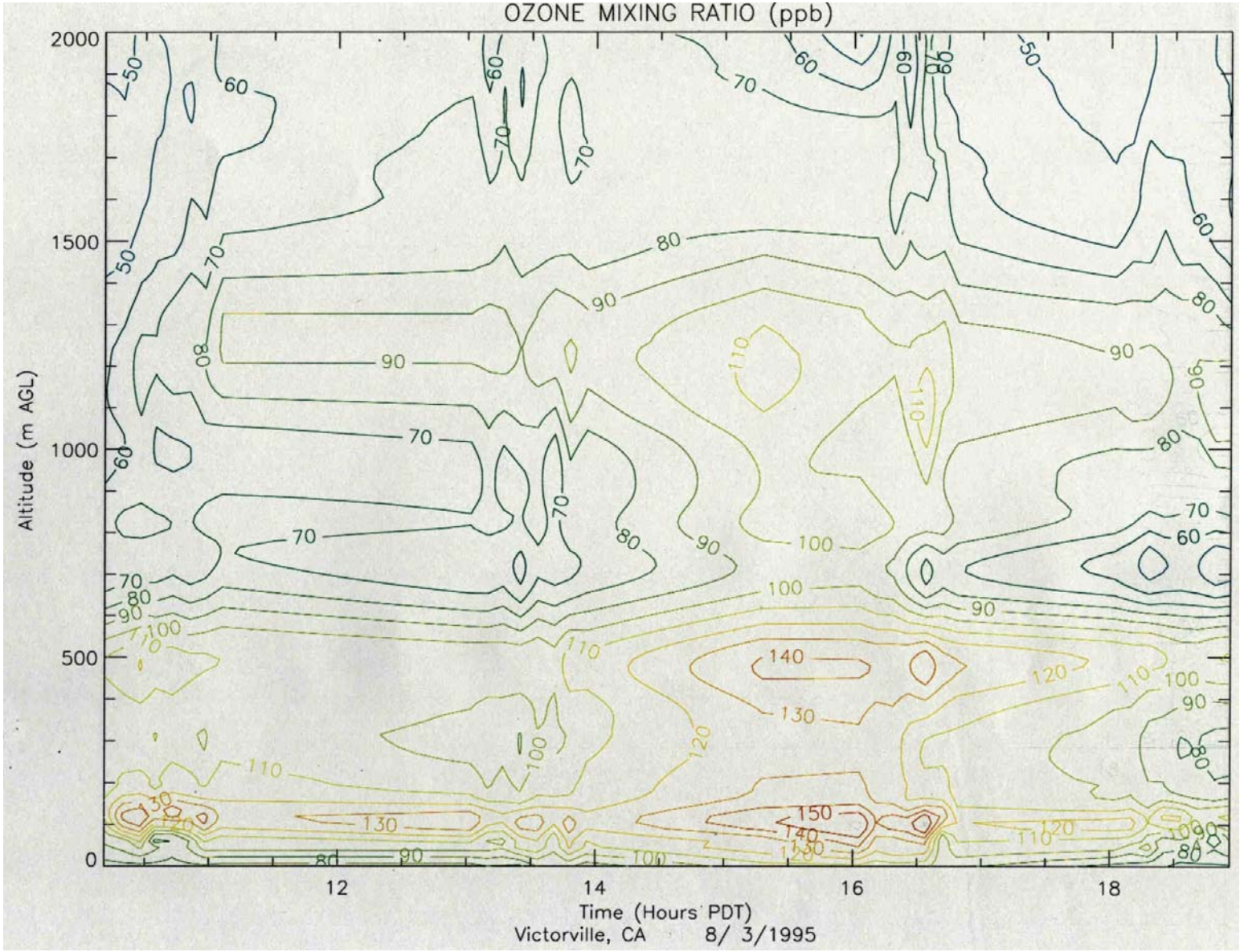
OZONE MIXING RATIO (ppb)
Altitude (m AGL)
2000
1500
1000
500
0
12
14
16
18
Time (Hours PDT)
Victorville, CA 8/ 3/1995

Figure 5b

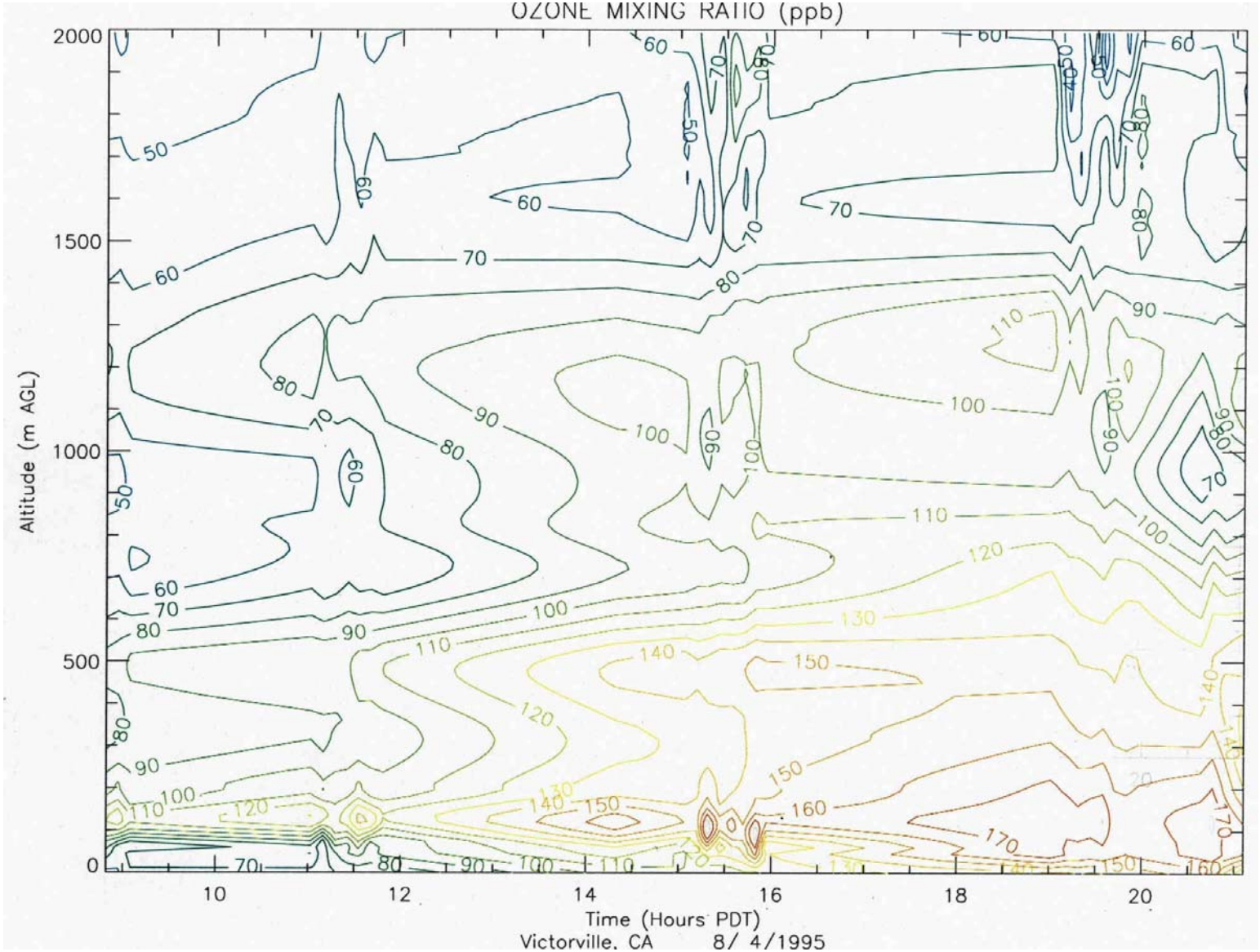
OZONE MIXING RATIO (ppb)
Altitude (m AGL)
2000
1500
1000
500
0
10
12
14
16
18
20
Time (Hours PDT)
Victorville, CA 8/ 4/1995

Figure 5c

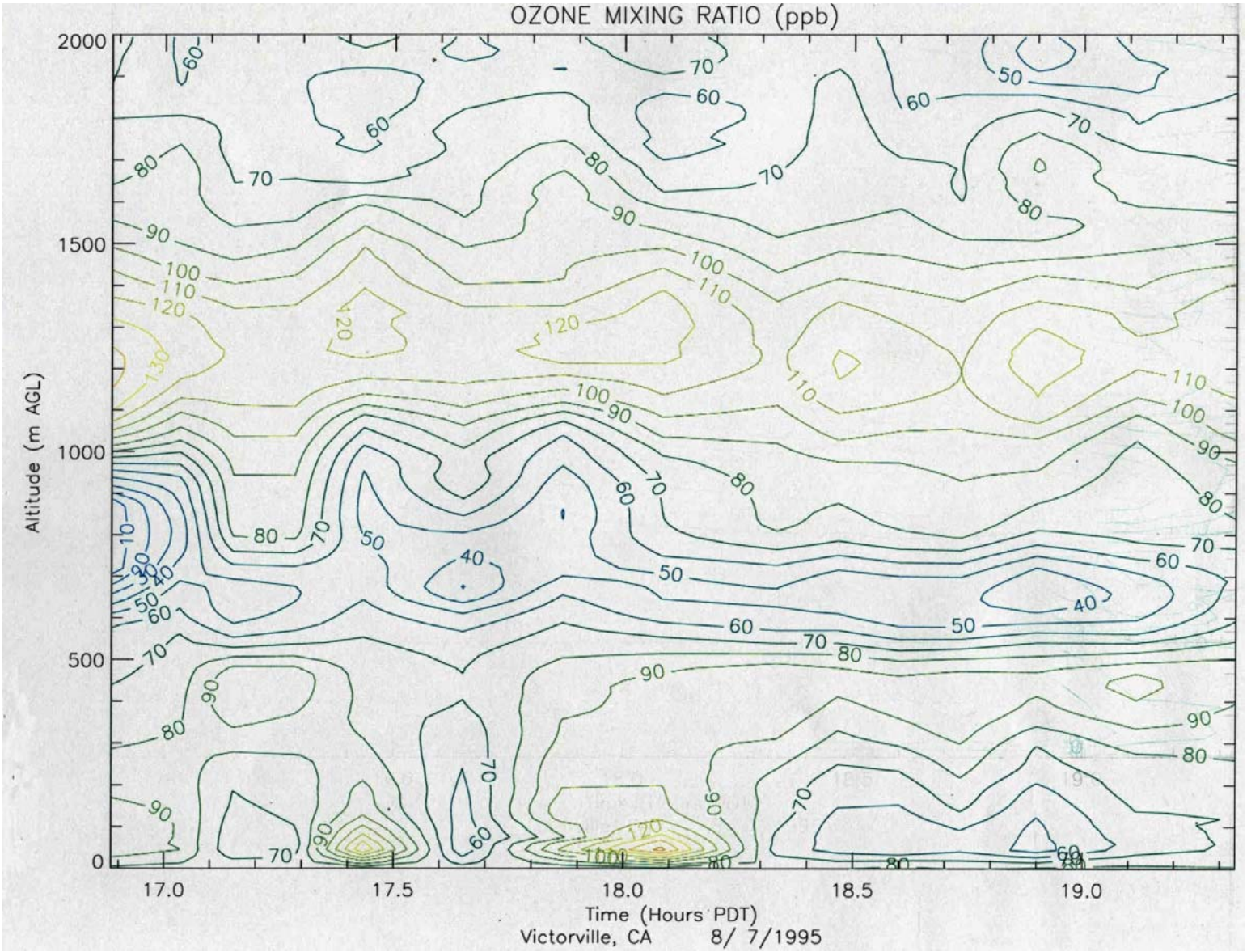
OZONE MIXING RATIO (ppb)
Altitude (m AGL)
2000
1500
1000
500
0
17.0
17.5
18.0
18.5
19.0
Time (Hours PDT)
Victorville, CA 8/ 7/1995

Figure 5d

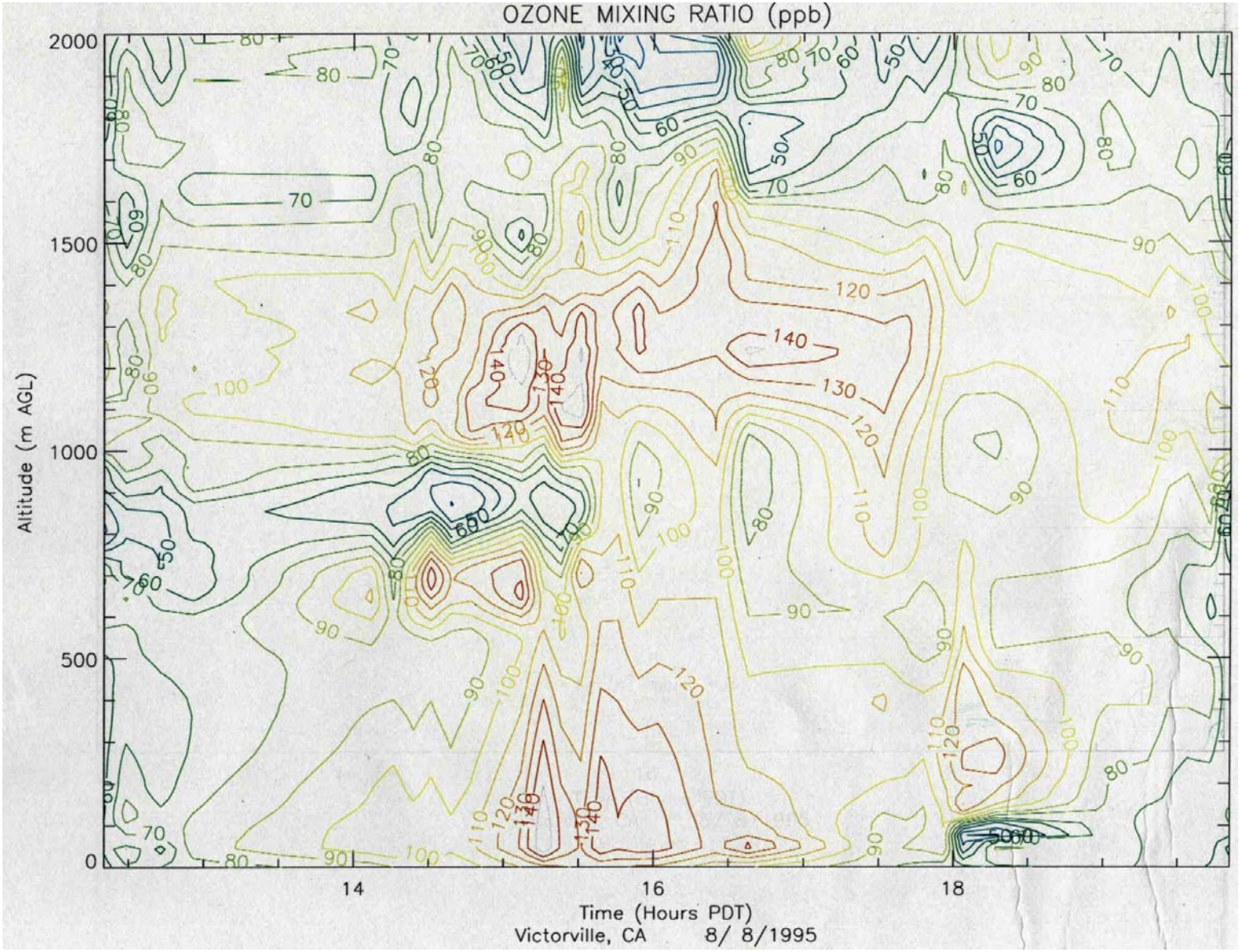
OZONE MIXING RATIO (ppb)
Altitude (m AGL)
2000
1500
1000
500
0
14
16
18
Time (Hours PDT)
Victorville, CA 8/ 8/1995

Figure 5e

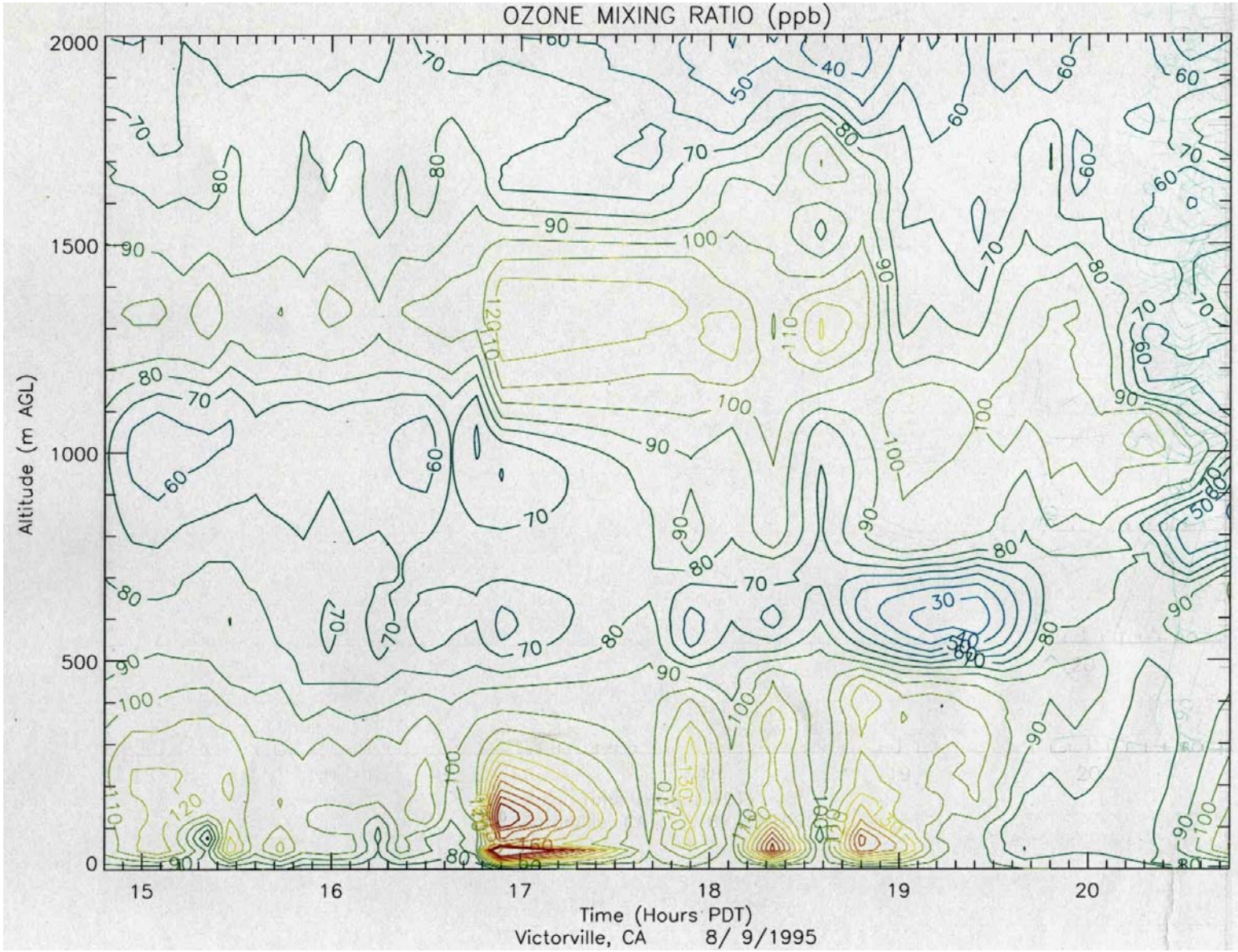
OZONE MIXING RATIO (ppb)
Altitude (m AGL)
2000
1500
1000
500
0
15
16
17
18
19
20
Time (Hours PDT)
Victorville, CA 8/ 9/1995

Figure 5f

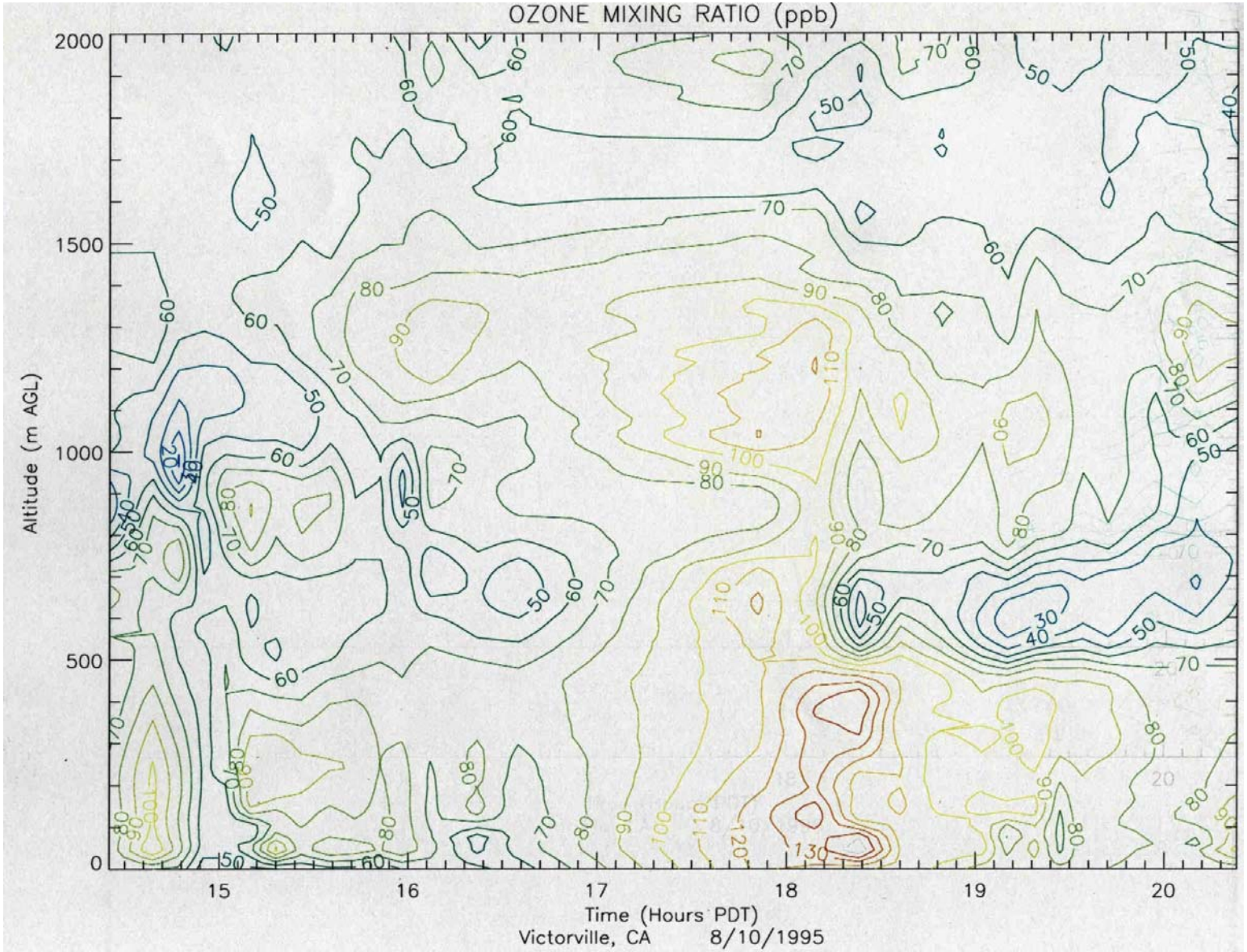
OZONE MIXING RATIO (ppb)
Altitude (m AGL)
2000
1500
1000
500
0
15
16
17
18
19
20
Time (Hours PDT)
Victorville, CA 8/10/1995

Figure 5g

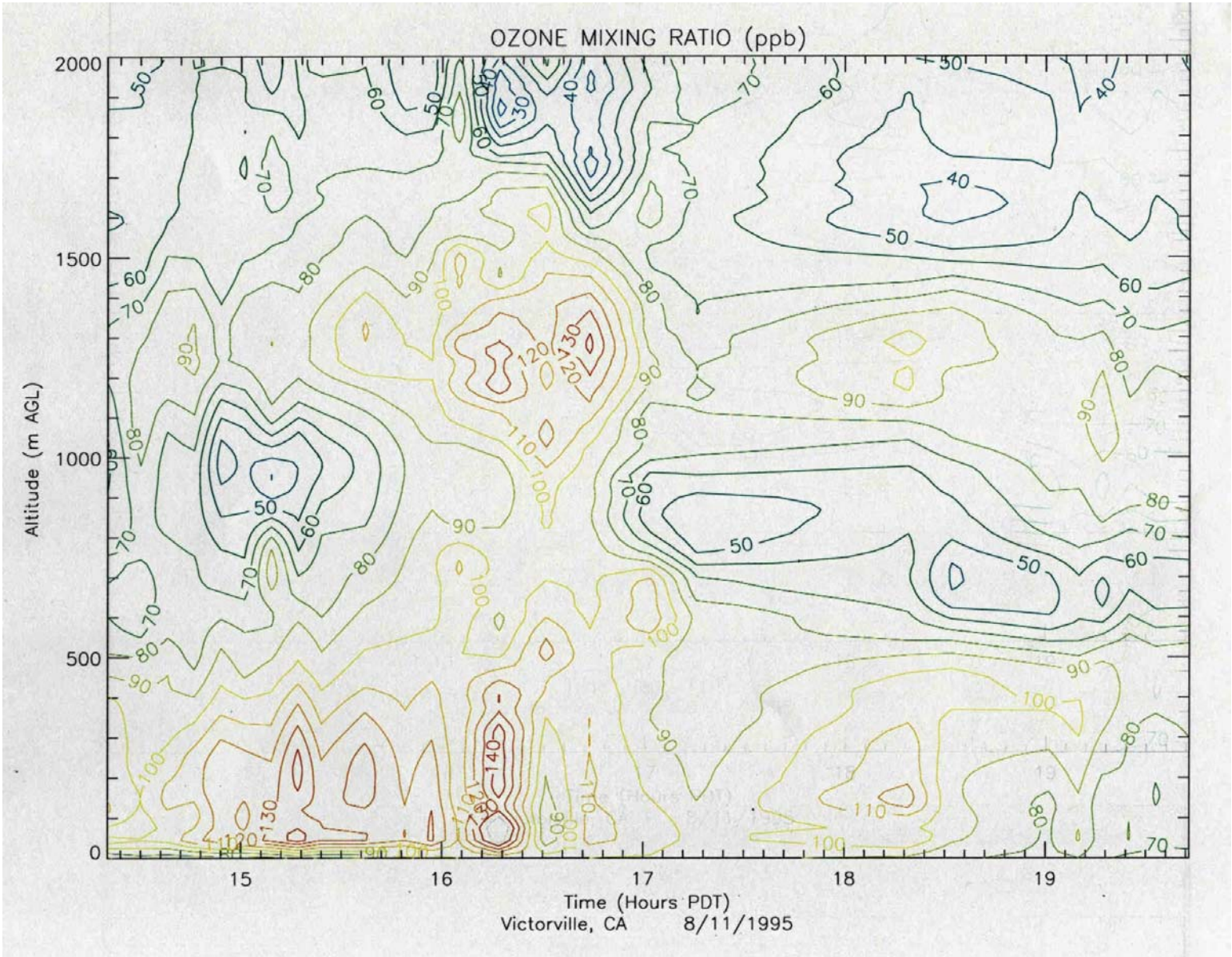
OZONE MIXING RATIO (ppb)
Altitude (m AGL)
2000
1500
1000
500
0
15
16
17
18
19
Time (Hours PDT)
Victorville, CA 8/11/1995

Figure 6a

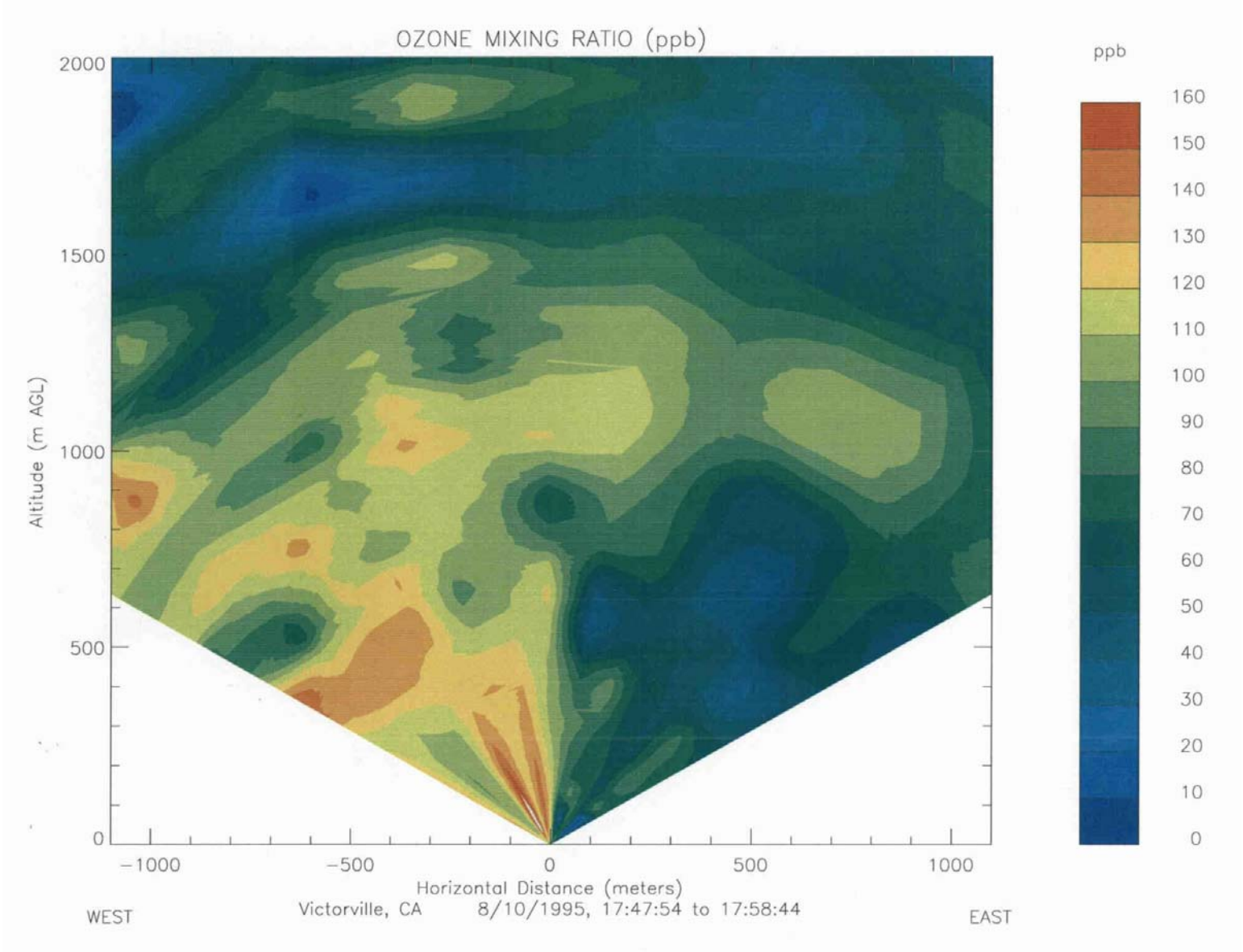
OZONE MIXING RATIO (ppb)
ppb
160
150
140
130
120
110
100
90
80
70
60
50
40
30
20
10
0
2000
1500
1000
500
0
Altitude (m AGL)
−1000
−500
0
500
1000
Horizontal Distance (meters)
WEST
Victorville, CA 8/10/1995, 17:47:54 to 17:58:44
EAST

Figure 6b

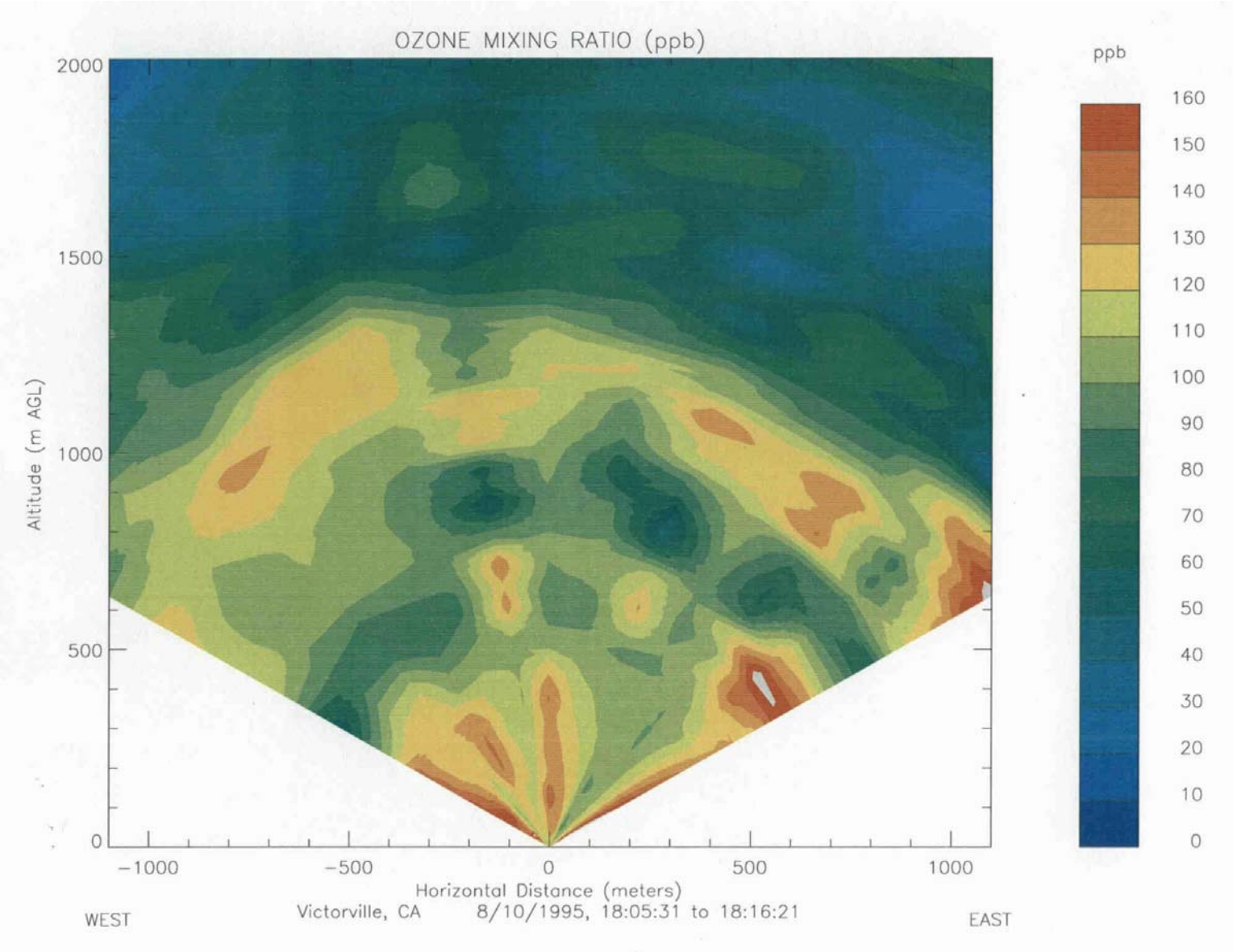
OZONE MIXING RATIO (ppb)
ppb
160
150
140
130
120
110
100
90
80
70
60
50
40
30
20
10
0
2000
1500
1000
500
0
Altitude (m AGL)
−1000
−500
0
500
1000
Horizontal Distance (meters)
WEST
Victorville, CA 8/10/1995, 18:05:31 to 18:16:21
EAST

Figure 6c

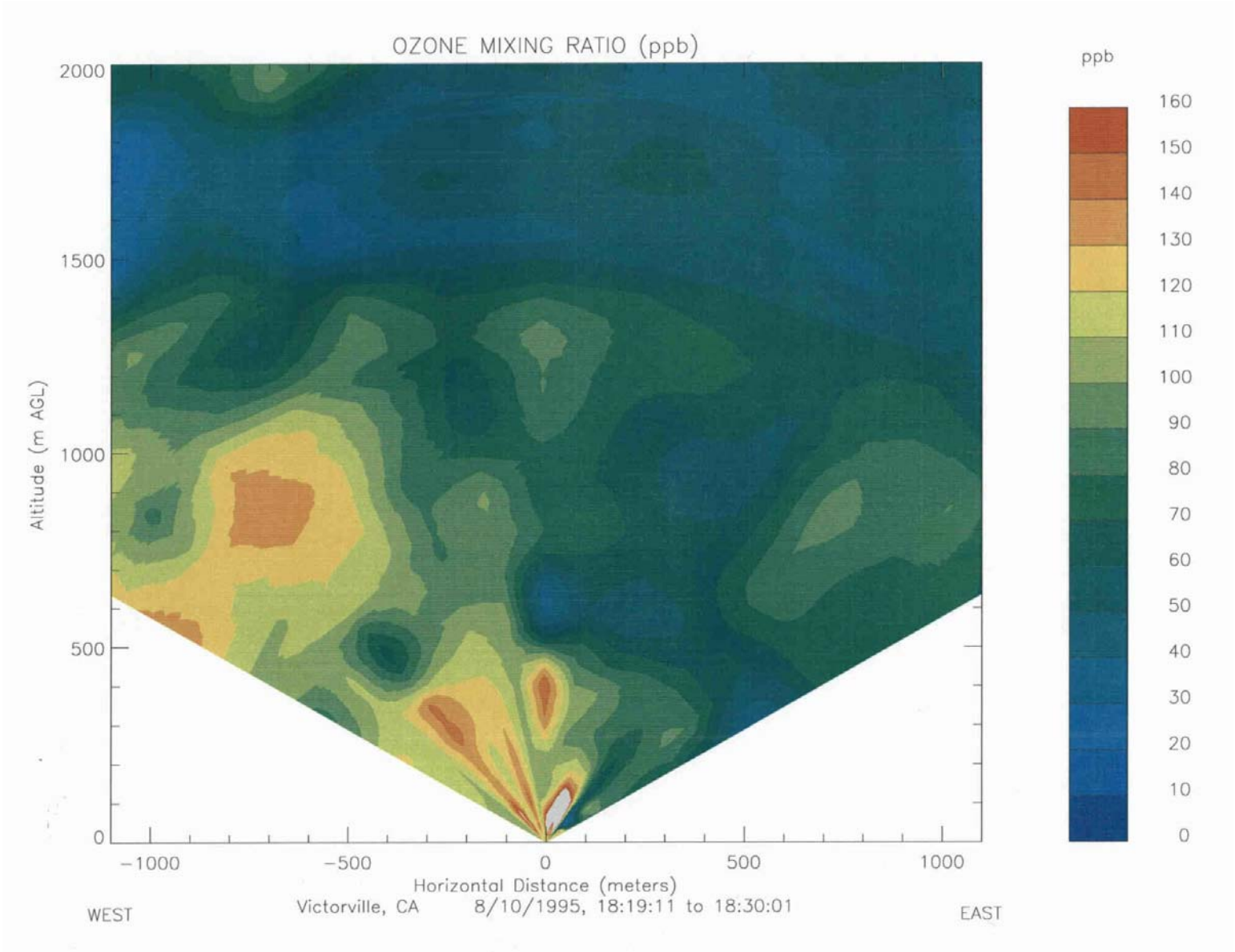
OZONE MIXING RATIO (ppb)
ppb
160
150
140
130
120
110
100
90
80
70
60
50
40
30
20
10
0
2000
1500
1000
500
0
Altitude (m AGL)
−1000
−500
0
500
1000
Horizontal Distance (meters)
WEST
Victorville, CA 8/10/1995, 18:19:11 to 18:30:01
EAST

VII. OZONE ADVECTION FLUXES

Profiles of ozone advection fluxes were calculated as the product of the ozone profiles and wind profiles (in ppb m/s). These profiles showed that ozone flux in the layer aloft usually was higher than that near ground level due to the fact that winds were stronger aloft. Except for a short time period when convection was active, the ozone flux from surface to 2 km was more or less uniform. The flux direction is determined by wind direction. Ozone flux in the lower boundary layer was dominantly southerly, while the layer aloft was westerly or southwesterly in most cases. In addition, a low-level layer of higher ozone flux was almost always associated with westerly wind.

The above results indicate that advection transport of ozone from South Coast Air Basin to the Mojave Desert Air Basin can occur both at low-levels and aloft, but ozone flux is higher above 1000 m. These high ozone fluxes aloft may transfer ozone to remote sites where air quality problems can occur when vertical mixing process takes place.

Figure 7a

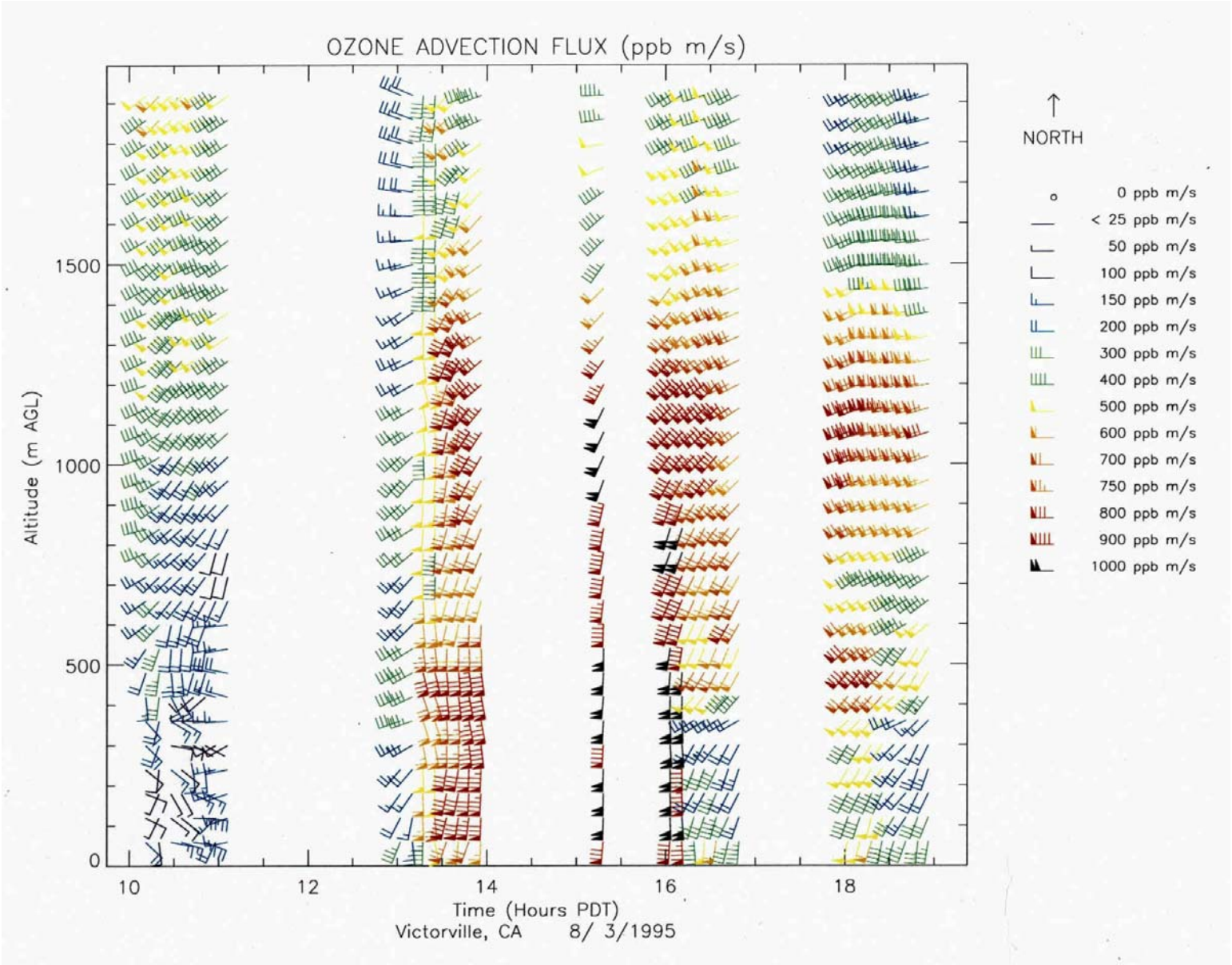
OZONE ADVECTION FLUX (ppb m/s)
Altitude (m AGL)
0
500
1000
1500
10
12
14
16
18
Time (Hours PDT)
Victorville, CA 8/ 3/1995
NORTH
0 ppb m/s
< 25 ppb m/s
50 ppb m/s
100 ppb m/s
150 ppb m/s
200 ppb m/s
300 ppb m/s
400 ppb m/s
500 ppb m/s
600 ppb m/s
700 ppb m/s
750 ppb m/s
800 ppb m/s
900 ppb m/s
1000 ppb m/s

Figure 7b

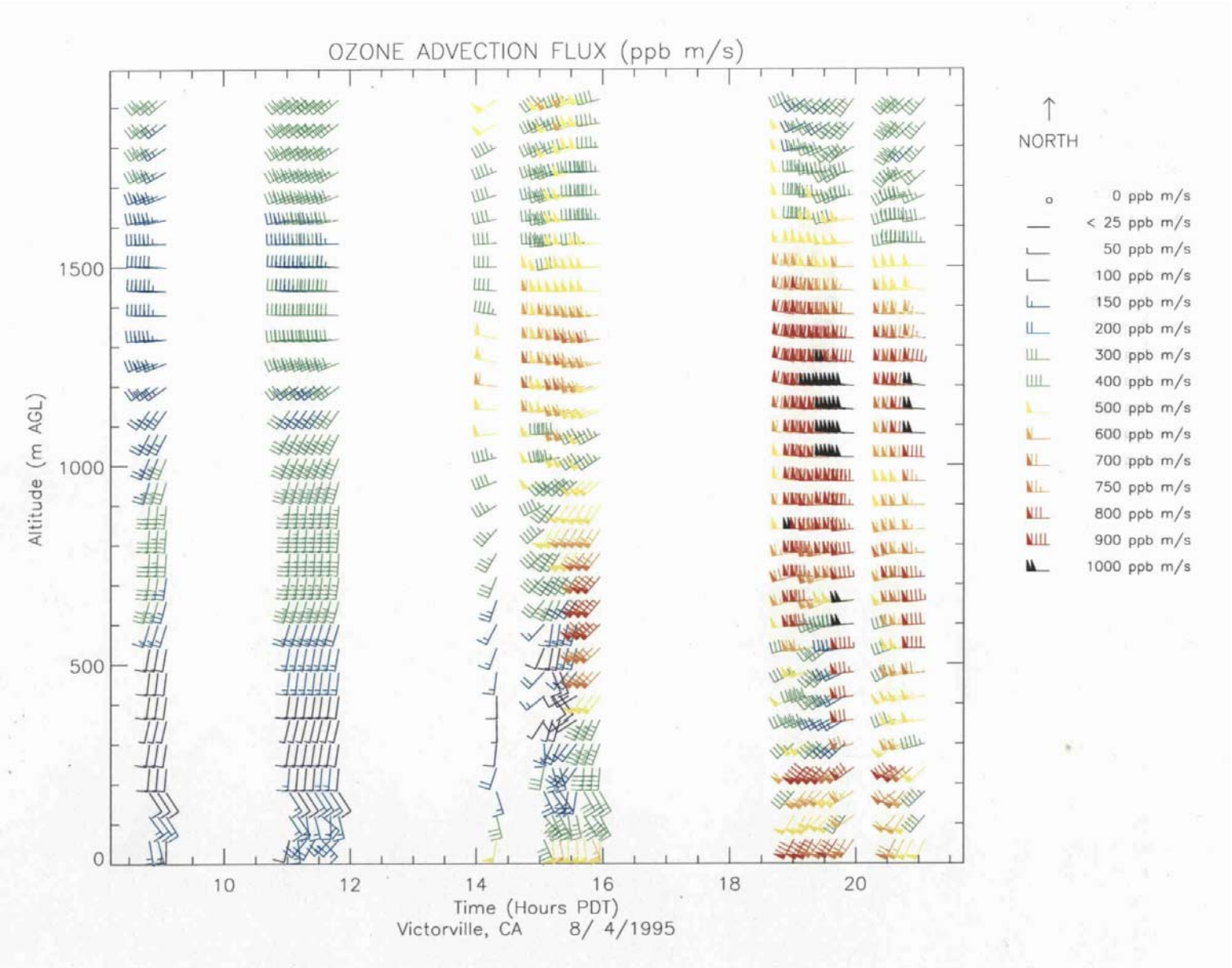
OZONE ADVECTION FLUX (ppb m/s)
Altitude (m AGL)
0
500
1000
1500
10
12
14
16
18
20
Time (Hours PDT)
Victorville, CA 8/ 4/1995
NORTH
0 ppb m/s
< 25 ppb m/s
50 ppb m/s
100 ppb m/s
150 ppb m/s
200 ppb m/s
300 ppb m/s
400 ppb m/s
500 ppb m/s
600 ppb m/s
700 ppb m/s
750 ppb m/s
800 ppb m/s
900 ppb m/s
1000 ppb m/s

Figure 7c

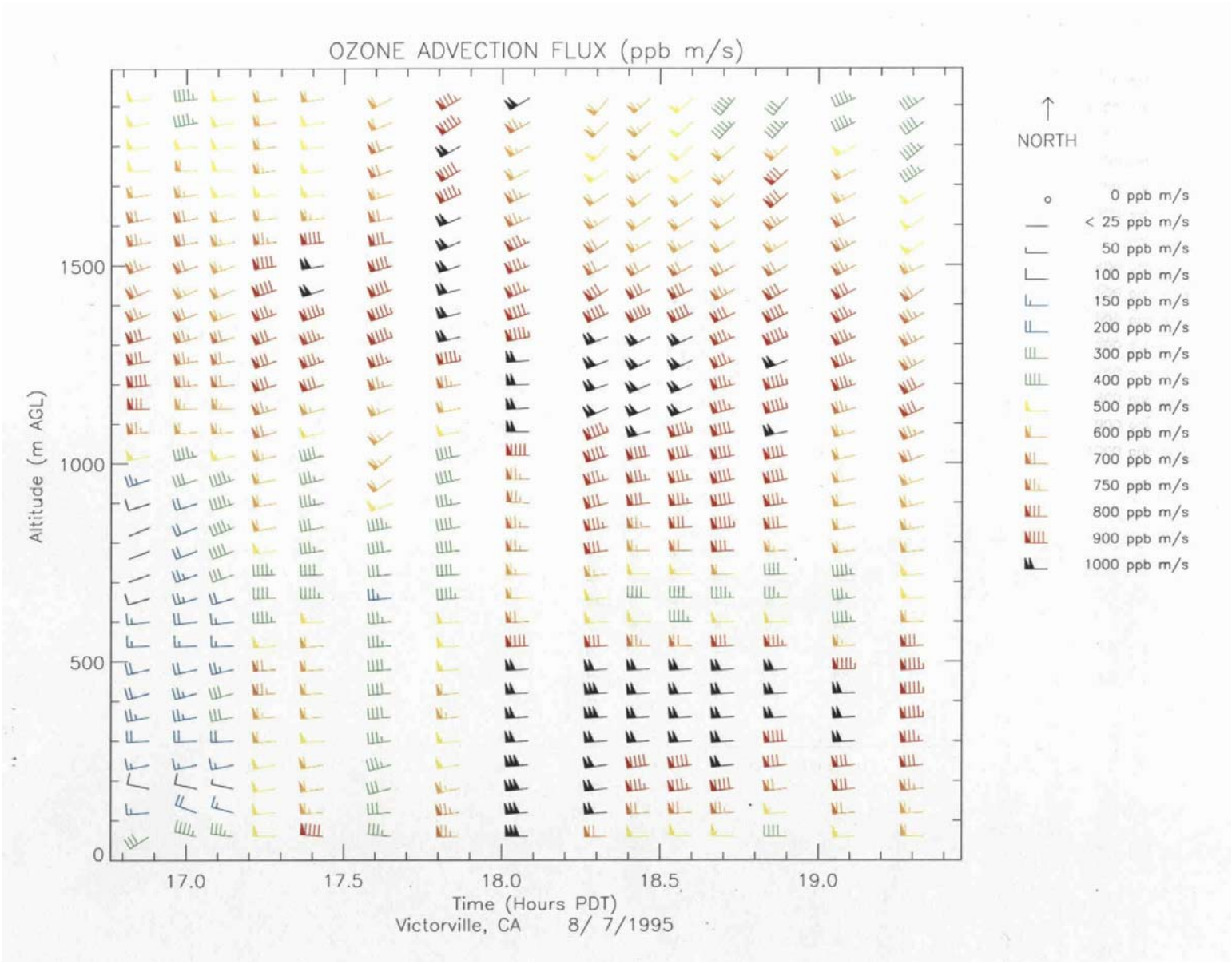
OZONE ADVECTION FLUX (ppb m/s)
NORTH
0 ppb m/s
< 25 ppb m/s
50 ppb m/s
100 ppb m/s
150 ppb m/s
200 ppb m/s
300 ppb m/s
400 ppb m/s
500 ppb m/s
600 ppb m/s
700 ppb m/s
750 ppb m/s
800 ppb m/s
900 ppb m/s
1000 ppb m/s
Altitude (m AGL)
0
500
1000
1500
17.0
17.5
18.0
18.5
19.0
Time (Hours PDT)
Victorville, CA 8/ 7/1995

Figure 7d

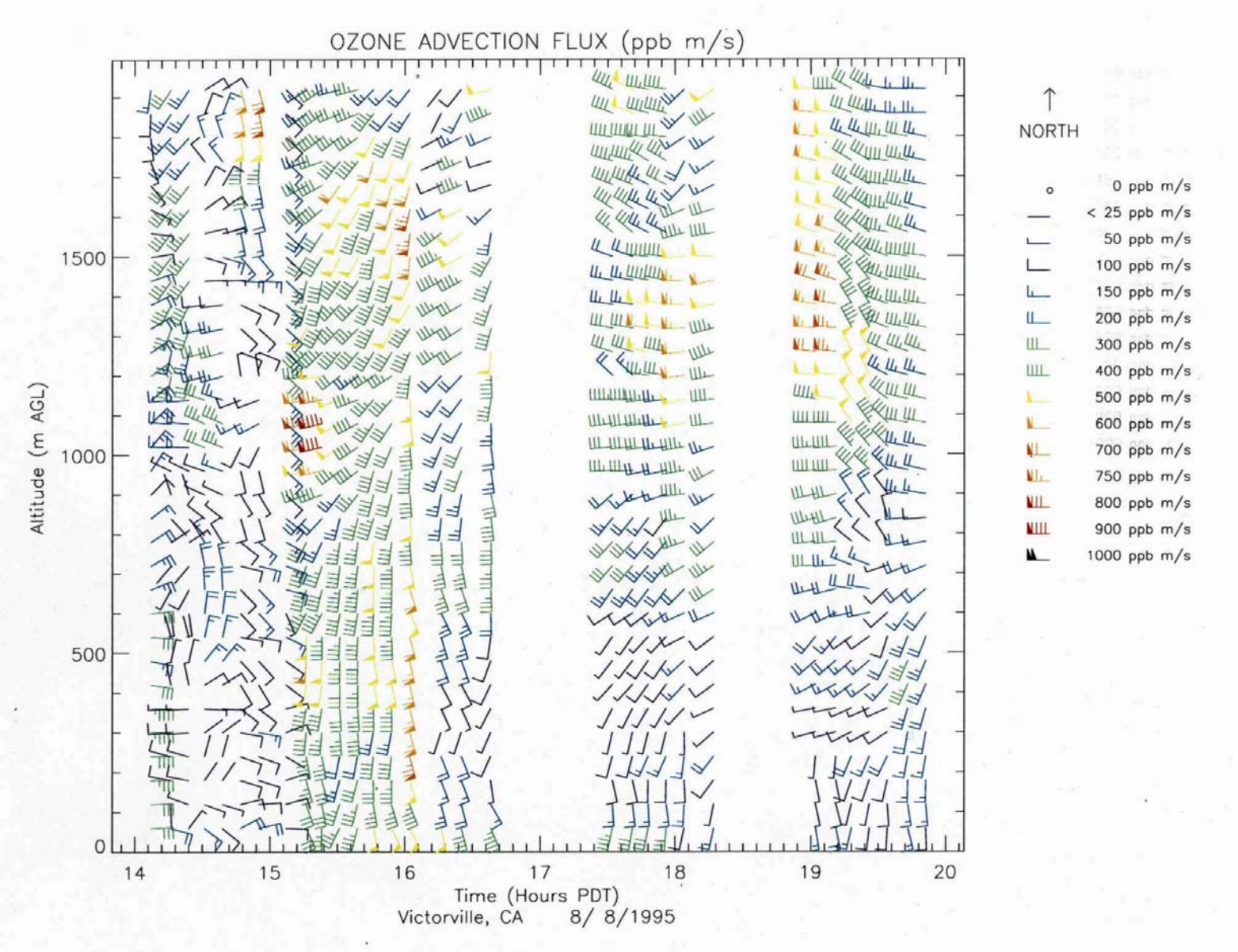
OZONE ADVECTION FLUX (ppb m/s)
Altitude (m AGL)
0
500
1000
1500
14
15
16
17
18
19
20
Time (Hours PDT)
Victorville, CA 8/ 8/1995
NORTH
0 ppb m/s
< 25 ppb m/s
50 ppb m/s
100 ppb m/s
150 ppb m/s
200 ppb m/s
300 ppb m/s
400 ppb m/s
500 ppb m/s
600 ppb m/s
700 ppb m/s
750 ppb m/s
800 ppb m/s
900 ppb m/s
1000 ppb m/s

Figure 7e

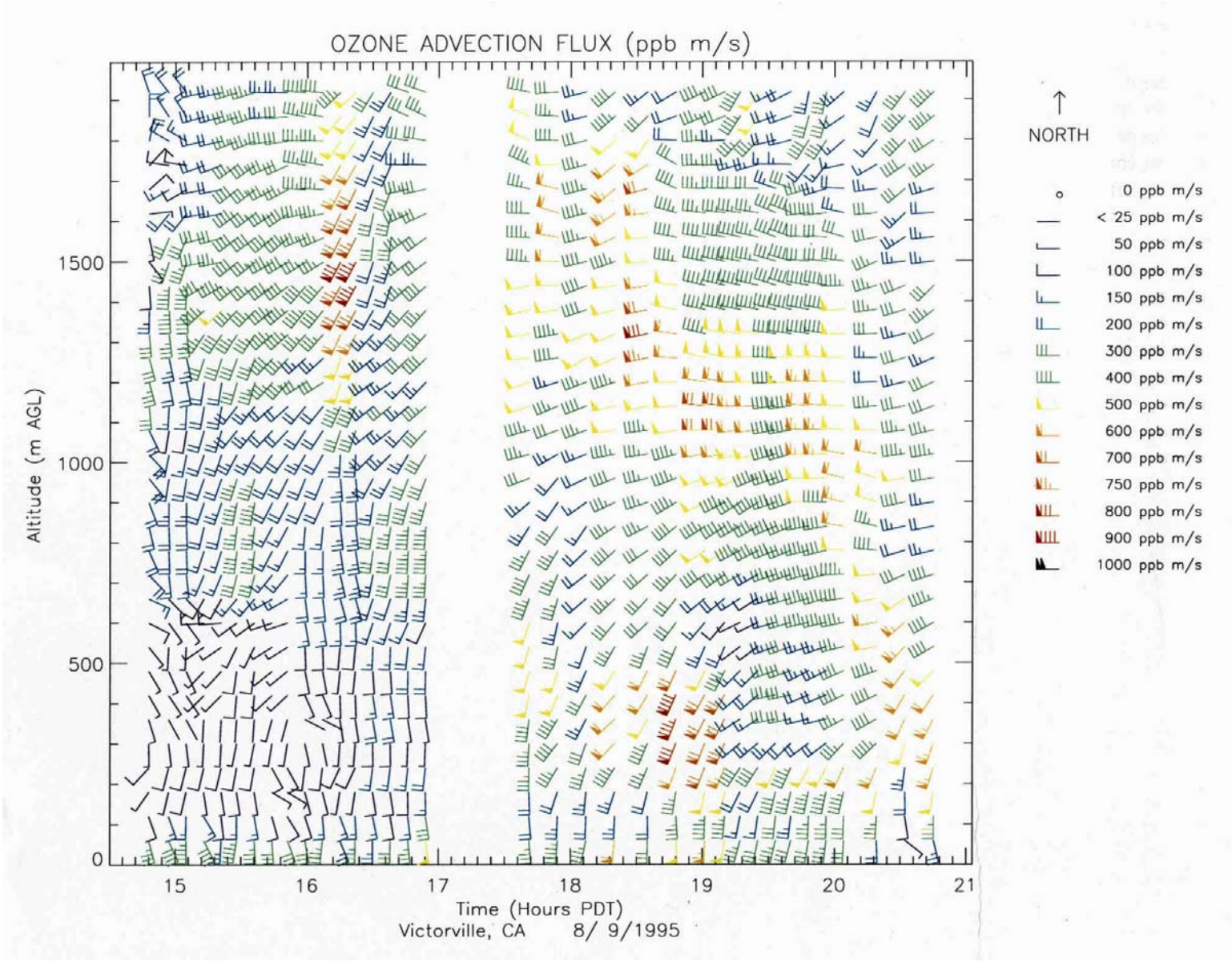
OZONE ADVECTION FLUX (ppb m/s)
Altitude (m AGL)
0
500
1000
1500
15
16
17
18
19
20
21
Time (Hours PDT)
Victorville, CA 8/ 9/1995
NORTH
0 ppb m/s
< 25 ppb m/s
50 ppb m/s
100 ppb m/s
150 ppb m/s
200 ppb m/s
300 ppb m/s
400 ppb m/s
500 ppb m/s
600 ppb m/s
700 ppb m/s
750 ppb m/s
800 ppb m/s
900 ppb m/s
1000 ppb m/s

Figure 7f

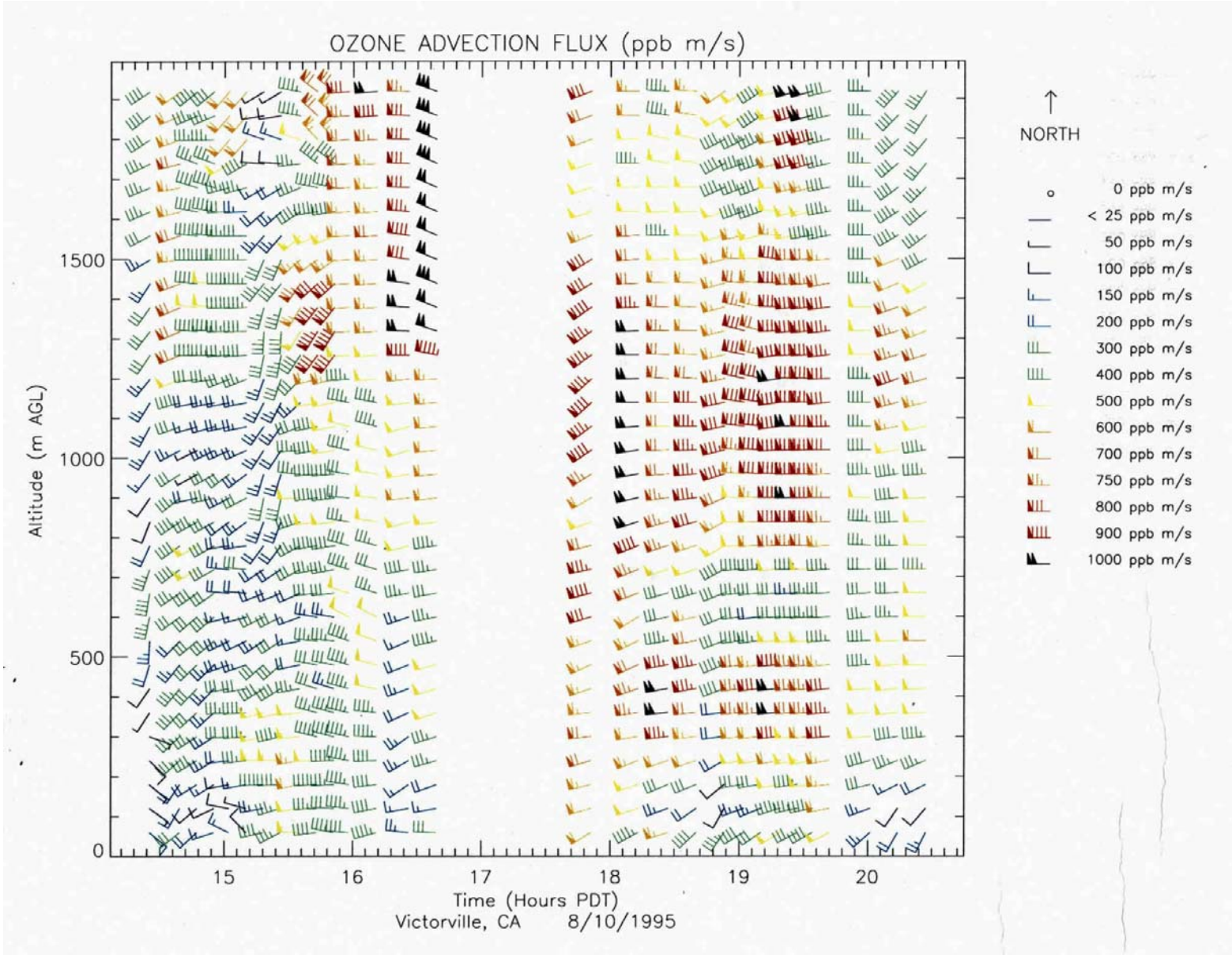
OZONE ADVECTION FLUX (ppb m/s)
NORTH
0 ppb m/s
< 25 ppb m/s
50 ppb m/s
100 ppb m/s
150 ppb m/s
200 ppb m/s
300 ppb m/s
400 ppb m/s
500 ppb m/s
600 ppb m/s
700 ppb m/s
750 ppb m/s
800 ppb m/s
900 ppb m/s
1000 ppb m/s
Altitude (m AGL)
0
500
1000
1500
15
16
17
18
19
20
Time (Hours PDT)
Victorville, CA 8/10/1995

Figure 7g

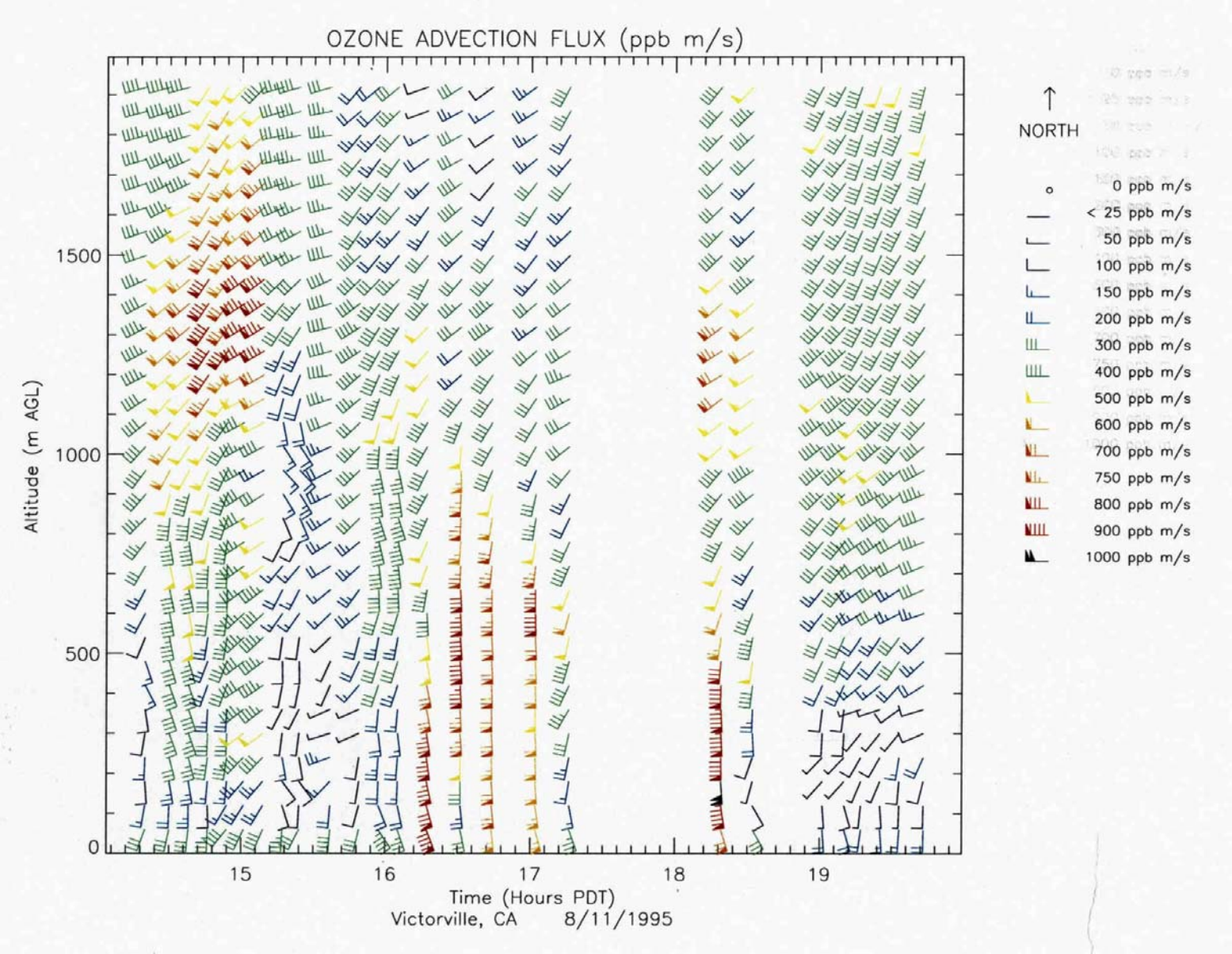
OZONE ADVECTION FLUX (ppb m/s)
Altitude (m AGL)
0
500
1000
1500
15
16
17
18
19
Time (Hours PDT)
Victorville, CA 8/11/1995
NORTH
0 ppb m/s
< 25 ppb m/s
50 ppb m/s
100 ppb m/s
150 ppb m/s
200 ppb m/s
300 ppb m/s
400 ppb m/s
500 ppb m/s
600 ppb m/s
700 ppb m/s
750 ppb m/s
800 ppb m/s
900 ppb m/s
1000 ppb m/s

VIII. SUMMARY AND CONCLUSIONS

The ETL ground-based ozone lidar with a new 2D scanning system was deployed and tested at the former George Air Force Base near Victorville, CA, during early to mid August 1995. The scanning system worked well in terms of computer-controlled operation and the capability of showing whether or not there is any significant systematic errors of the system. Due to engineering problems, the scanner distorted the system in the morning and produced large errors from 600-1000 m AGL. However, the afternoon lidar scanning data showed better internal consistency.

During the experiment, the ozone lidar detected two layers of high ozone concentrations in the afternoon: one in the lower boundary layer, and one aloft. The layer aloft was usually located between 1000 to 1500 m AGL (1900-2400 m MSL), and a little lower in the evening. The two layers usually merged in 1400-1600 PDT when the layer in between reached a high lapse rate, as seen in the RASS data. The ozone layer aloft was detected every operational day of the lidar, which strongly indicated the chimney effect of the high mountains at the northeast boundary of the South Coast Air Basin when the sea breeze pushed against them.

Ozone advection fluxes were calculated as a product of ozone mixing ratio and horizontal wind. The results show that ozone flux in the layer aloft was usually higher due to the fact that winds were stronger. Except for a short time period when convection was active, the ozone flux from surface to 2 km was more or less uniform.

In conclusion, lidar measurements during the Victorville experiment demonstrated a new dimension of the capability of this remote sensing instrument. Hardware and software improvements of the system have been and will be carried out to provide higher accuracy of ozone concentration and ozone flux for future air quality monitoring and modeling.

REFERENCES

1. Yanzeng Zhao, R. M. Hardesty, J. E. Gaynor, " Demonstration of a New and Innovative Ozone Lidar's Capability to Measure Vertical Profiles of Ozone Concentration and Aerosol in the Lower Troposphere," Final Report to the California Air Resources Board, and the California Environmental Protection Agency, December 1994, 106 pages. This will also be published (with editorial revisions) as a NOAA's Technical Memorandum.

2. D. E. Wolfe, B. L. Weber, D. B. Wuerts, and K. P. Moran, "449-MHz Profiler/RASS: Meteorological support for the California Air Resource Board 1995 Mojave Desert Ozone Experiment," Final Report to the California Air Resource Board; NOAA Technical Memorandum ERL ETL-273, January 1997.

3. John J. Carroll and alan J. Dixon, *Aircraft Measurements in Support of the NOAA 2-D Lidar Demonstration*, Final Report to the California Air Resources Board, March 1997.

4. T. B. Smith *et al*, "The Impact of Transport from the South Coast Air Basin on Ozone Levels in the Southeast Desert Air Basin, Vol. 2 - Results and Discussion," Final Report to the California Air Resource Board, April 1983.

GLOSSARY OF TERMS, ABBREVIATIONS, AND SYMBOLS

LIDAR	**Li**ght **D**etection **a**nd **R**anging (Lidar is a system that transmits laser beam(s) and collects backscattered radiation through telescope(s). The received radiation is then transferred to electronic signals by optical detectors. Since the backscattered radiation from different distances has different time delays, the signal is range-resolved.)
DIAL	**Di**fferential **A**bsorption **L**idar
RASS	**R**adio **A**coustic **S**ounding **S**ystem
NOAA	**N**ational **O**ceanic and **A**tmospheric **A**dministration
ETL	**E**nvironmental **T**echnology **L**aboratory (former Wave Propagation Laboratory)
PDT	**P**acific **D**aylight **T**ime
AGL	**A**bove **G**round **L**evel
MSL	**M**ean **S**ea **L**evel

Appendix A: Eye Safety Check for YAG-Based Ozone Lidar

1. American National Standard for Safe Use of Lasers at 266, 289 and 355 nm (1993)

   C Exposure to Single Pulse

Wavelengths (μm)	Exposure Duration t(s)	MPE (J/cm^2)
0.180 - 0.302	10^{-9} to 3×10^{4}	3×10^{-3}
0.315 - 0.400	10 to 3×10^{4}	1.0

   C Repeated Exposures

Wavelengths (μm)	Exposure Duration	MPE (J/cm^2)
0.180 - 0.302	24 hours	1.2×10^{-3}
0.315 - 0.400	24 hours	0.4

2. Laser Energy Fluxes of the ETL ozone lidar

   The normal operating energy levels of the strongest output beams in YAG-based ETL ozone lidar are listed in the following table:

Wavelengths (μm)	Pulse Duration t(s)	Energy (J)	Beam Diameter (cm)
0.266	5×10^{-9}	0.016	3
0.289	5×10^{-9}	0.001	3
0.355	5×10^{-9}	0.008	1.8

   The scanning mirrors are coated with UV-enhanced aluminum. The reflectivity at each wavelength for one mirror is ~ 0.8, 0.9, 0.95 at 266, 289, and 355 nm, respectively, and 0.64, 0.81, and 0.90 for two mirrors. The above parameters are translated into laser fluxes at the second scanning mirror as follows:

Wavelengths (μm)	Pulse Duration t(s)	Energy Flux (J/cm^2)
0.266	5×10^{-9}	1.5×10^{-3}
0.289	5×10^{-9}	9.4×10^{-5}
0.355	5×10^{-9}	2.8×10^{-3}

   The energy fluxes are well below the MPE for single pulse exposure. Once the eyes are hit by a UV laser pulse, fluorescence can be seen. Thus it is almost impossible to get a second exposure. However, looking into the laser beams should be avoided in any case.

Appendix B:

1. Figure a and b demonstrate the systematic errors caused by mirror distortion. The scanning display on 8/08/95 show a very defined rainbow structure in the first scanning taken at 0752 PDT (Figure a). This distortion is much reduced at 8:58 PDT (Fig. b).

2. Fig. c to e are scanning displays from noon to late afternoon on the same day. The structure is more or less horizontally stratified.

3. A series of ozone profiles are plotted In Fig. f, which show a rapid systematic decrease at 600 m, the peak of the distorted ozone profiles, and a systematic increase at about 950 m, the artificial dip. At 845 PDT the profile looks more reasonable, and this is also demonstrated in the scanning display in Fig. b.

4. Fig. g and h show the difference of two calibrations taken at late afternoon and in the morning, and the equivalent error distribution in ozone concentration. The locations of the peak and dip of the error are in good agreement with the ozone profile taken in the morning (see Fig. f).

Figure A

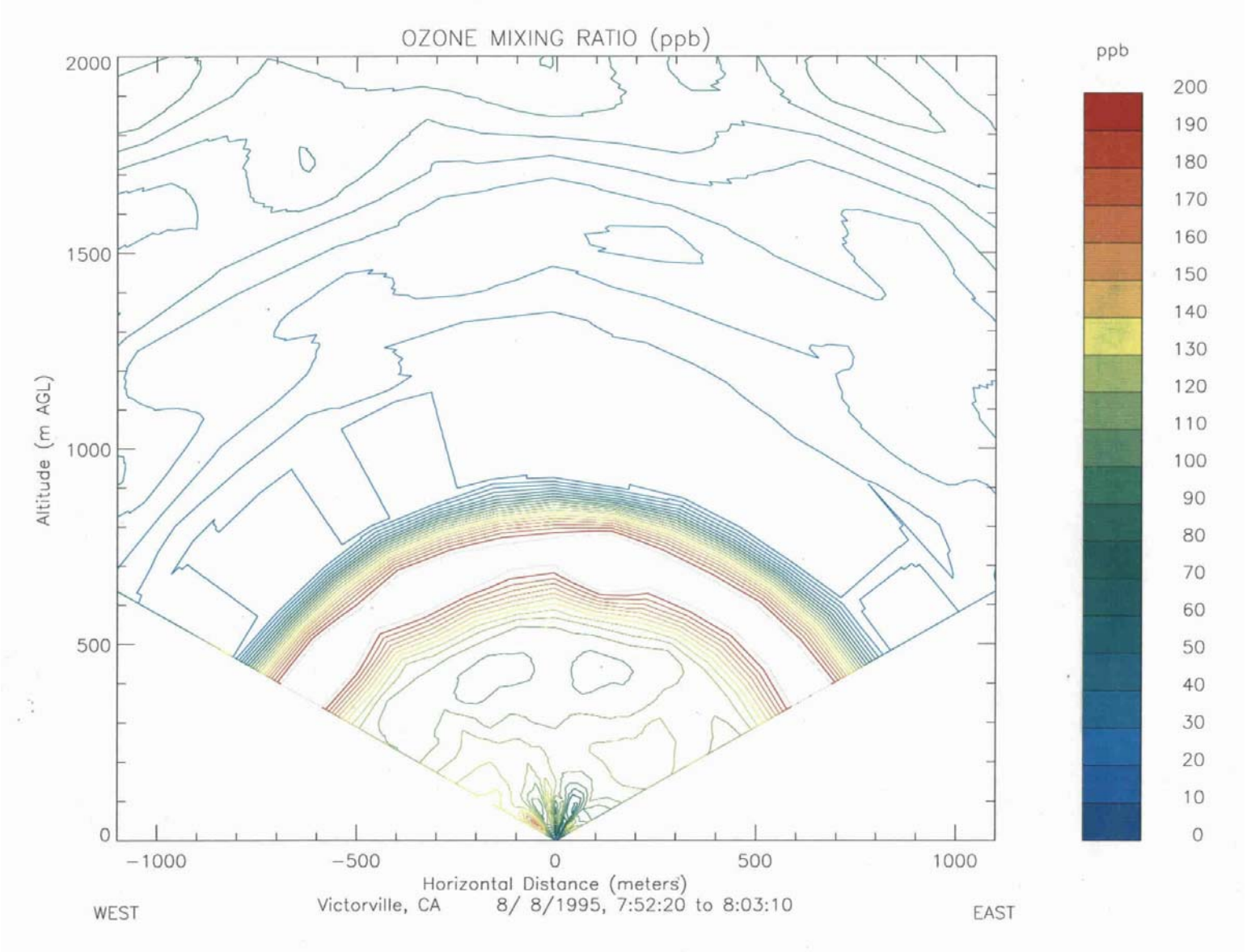
OZONE MIXING RATIO (ppb)
ppb
200
190
180
170
160
150
140
130
120
110
100
90
80
70
60
50
40
30
20
10
0
2000
1500
1000
500
0
Altitude (m AGL)
−1000
−500
0
500
1000
Horizontal Distance (meters)
WEST
Victorville, CA 8/ 8/1995, 7:52:20 to 8:03:10
EAST

Figure B

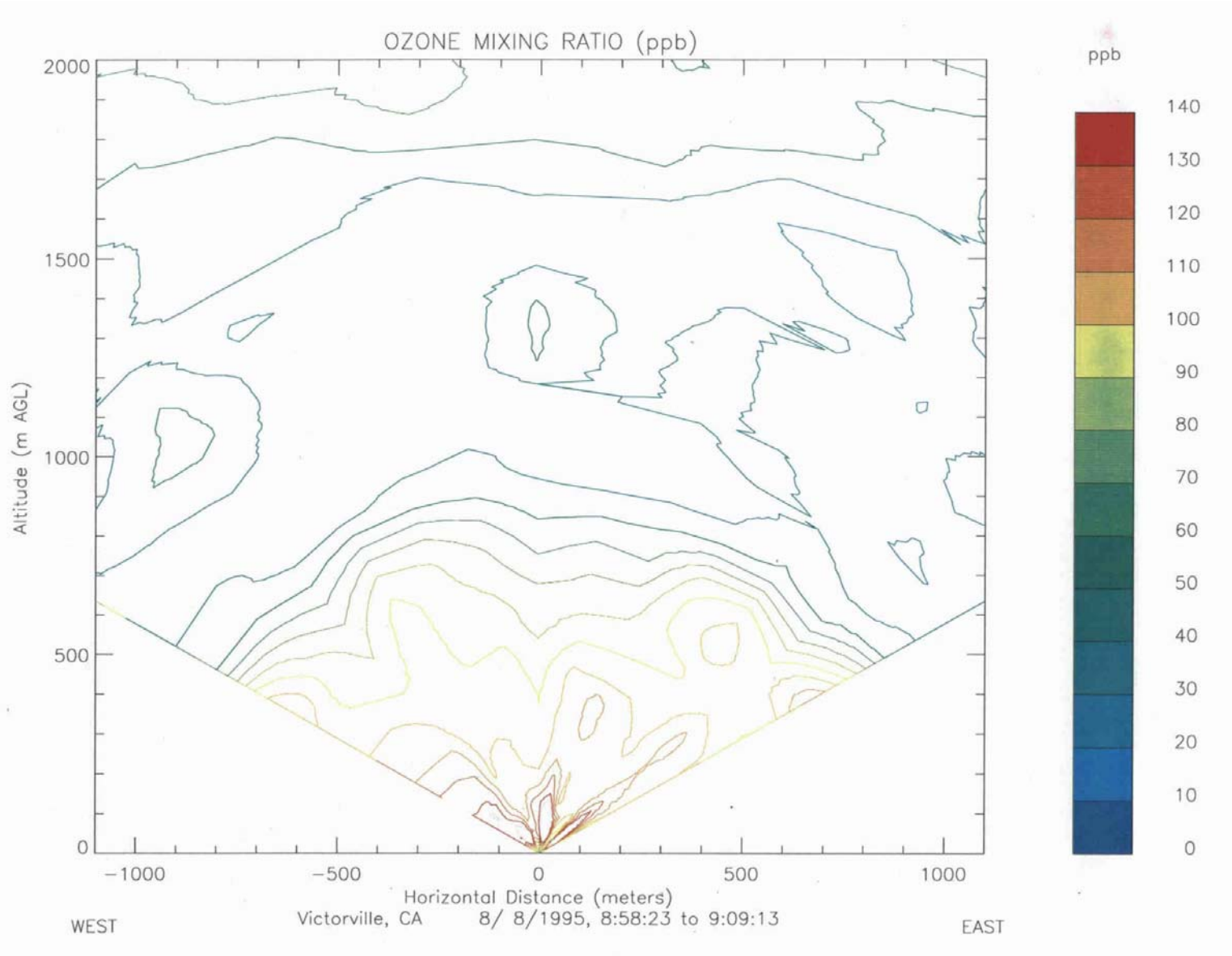
OZONE MIXING RATIO (ppb)
ppb
140
130
120
110
100
90
80
70
60
50
40
30
20
10
0
2000
1500
1000
500
0
Altitude (m AGL)
−1000
−500
0
500
1000
Horizontal Distance (meters)
WEST
Victorville, CA
8/ 8/1995, 8:58:23 to 9:09:13
EAST

Figure C

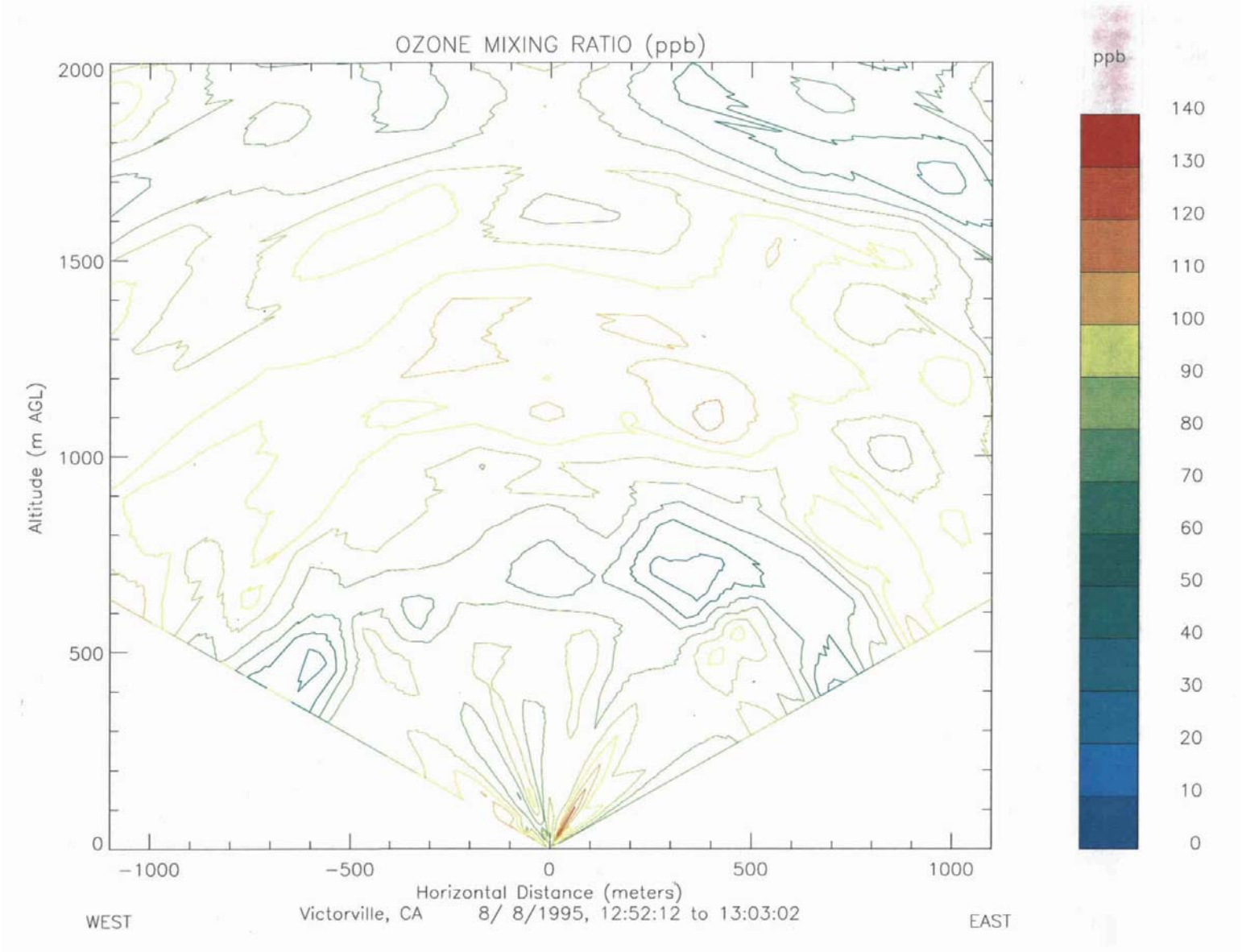
OZONE MIXING RATIO (ppb)
ppb
140
130
120
110
100
90
80
70
60
50
40
30
20
10
0
2000
1500
1000
500
0
Altitude (m AGL)
−1000
−500
0
500
1000
Horizontal Distance (meters)
WEST
Victorville, CA 8/ 8/1995, 12:52:12 to 13:03:02
EAST

Figure D

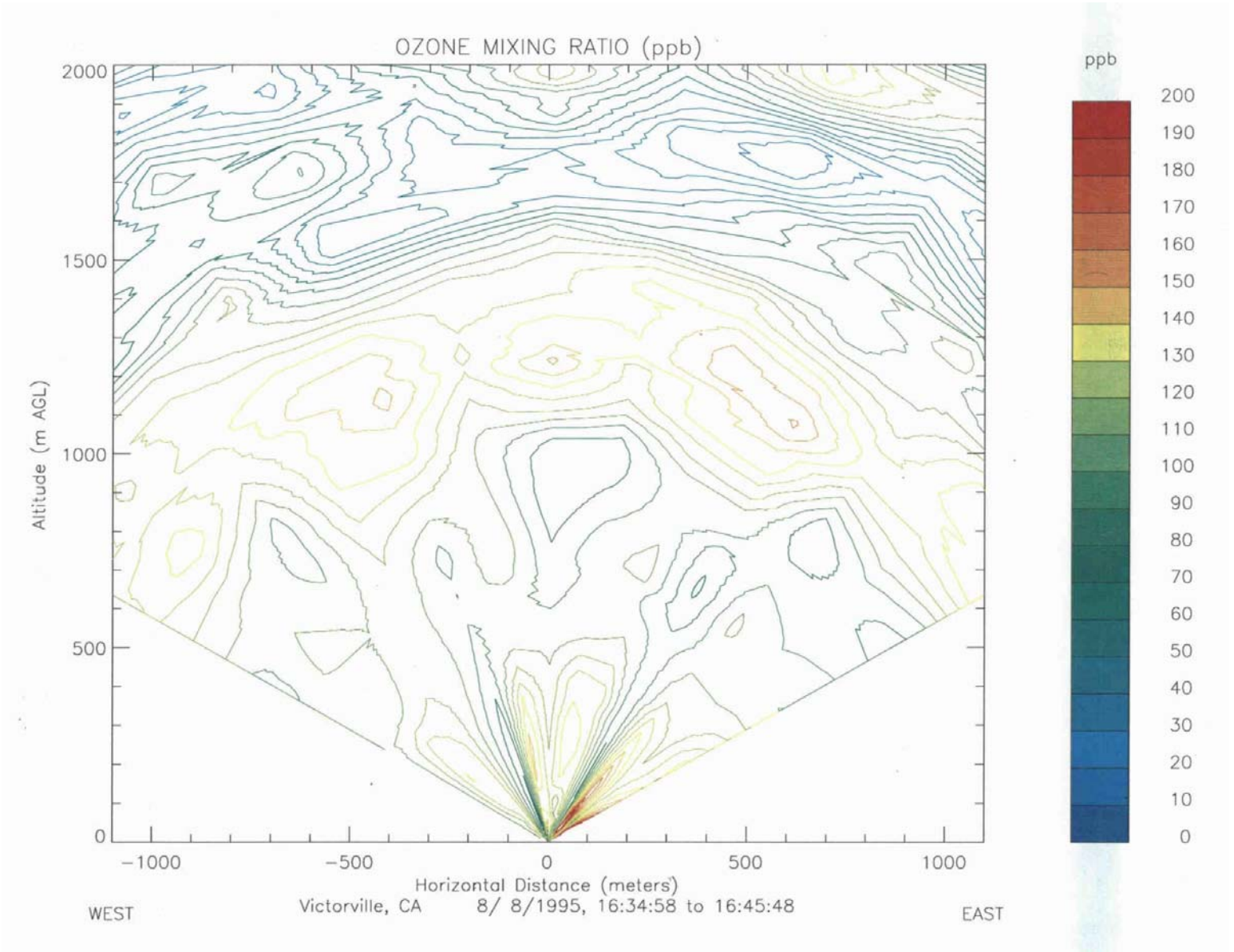
OZONE MIXING RATIO (ppb)
Altitude (m AGL)
2000
1500
1000
500
0
−1000
−500
0
500
1000
Horizontal Distance (meters)
WEST
Victorville, CA 8/ 8/1995, 16:34:58 to 16:45:48
EAST
ppb
200
190
180
170
160
150
140
130
120
110
100
90
80
70
60
50
40
30
20
10
0

Figure E

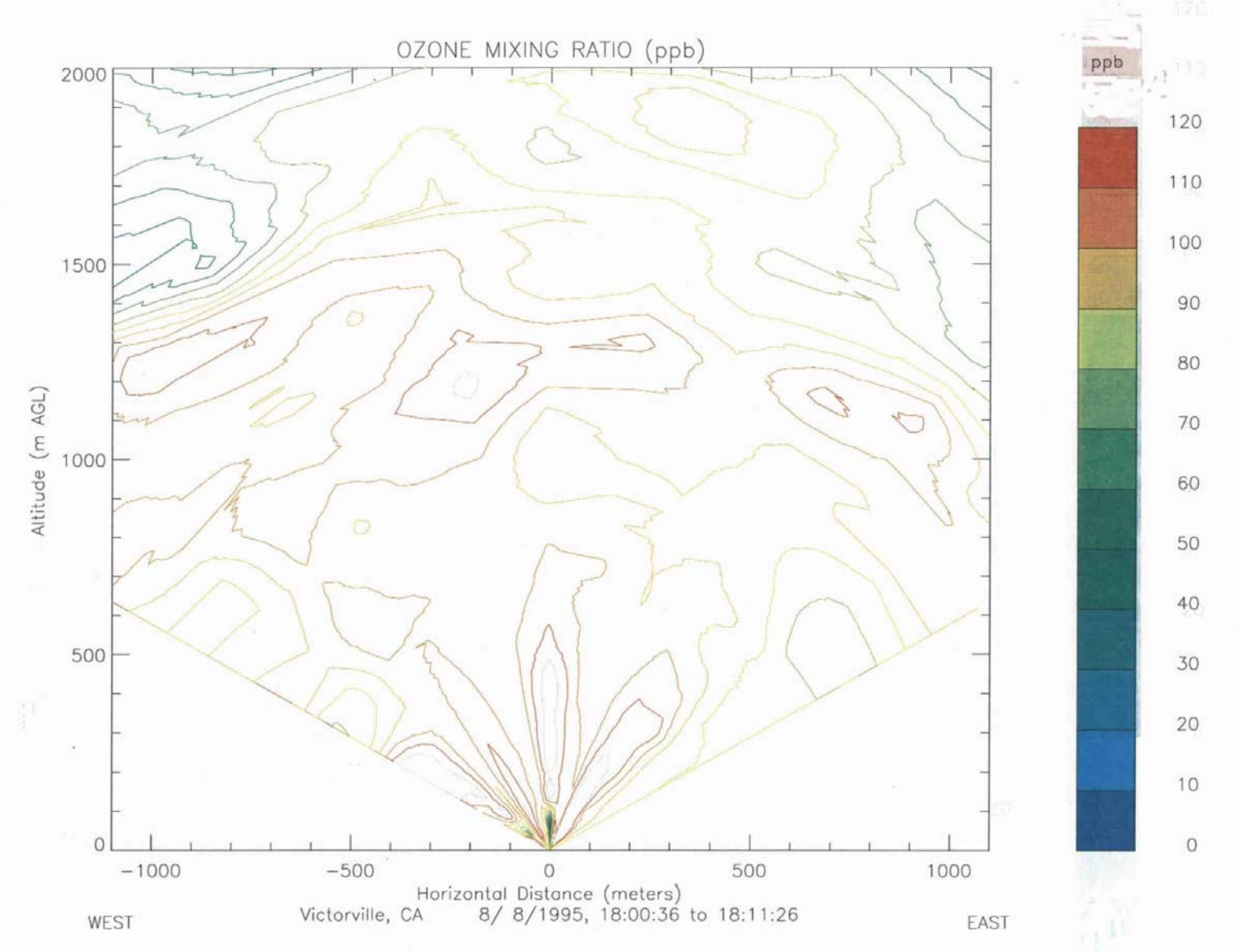
OZONE MIXING RATIO (ppb)
ppb
120
110
100
90
80
70
60
50
40
30
20
10
0
2000
1500
1000
500
0
Altitude (m AGL)
−1000
−500
0
500
1000
Horizontal Distance (meters)
WEST
Victorville, CA 8/ 8/1995, 18:00:36 to 18:11:26
EAST

Figure F

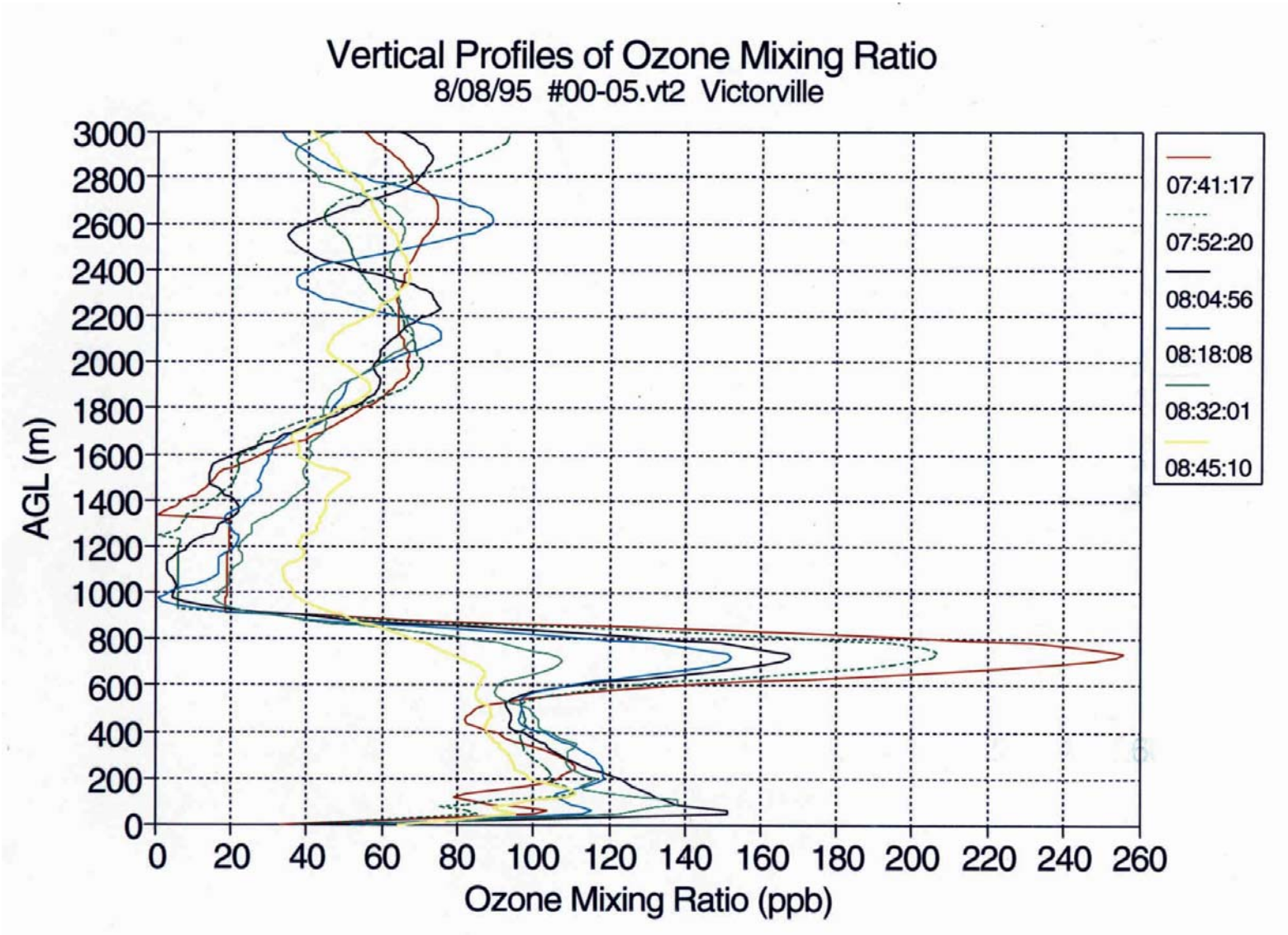
Vertical Profiles of Ozone Mixing Ratio
8/08/95 #00-05.vt2 Victorville
AGL (m)
3000
2800
2600
2400
2200
2000
1800
1600
1400
1200
1000
800
600
400
200
0
0 20 40 60 80 100 120 140 160 180 200 220 240 260
Ozone Mixing Ratio (ppb)
07:41:17
07:52:20
08:04:56
08:18:08
08:32:01
08:45:10

Figure G

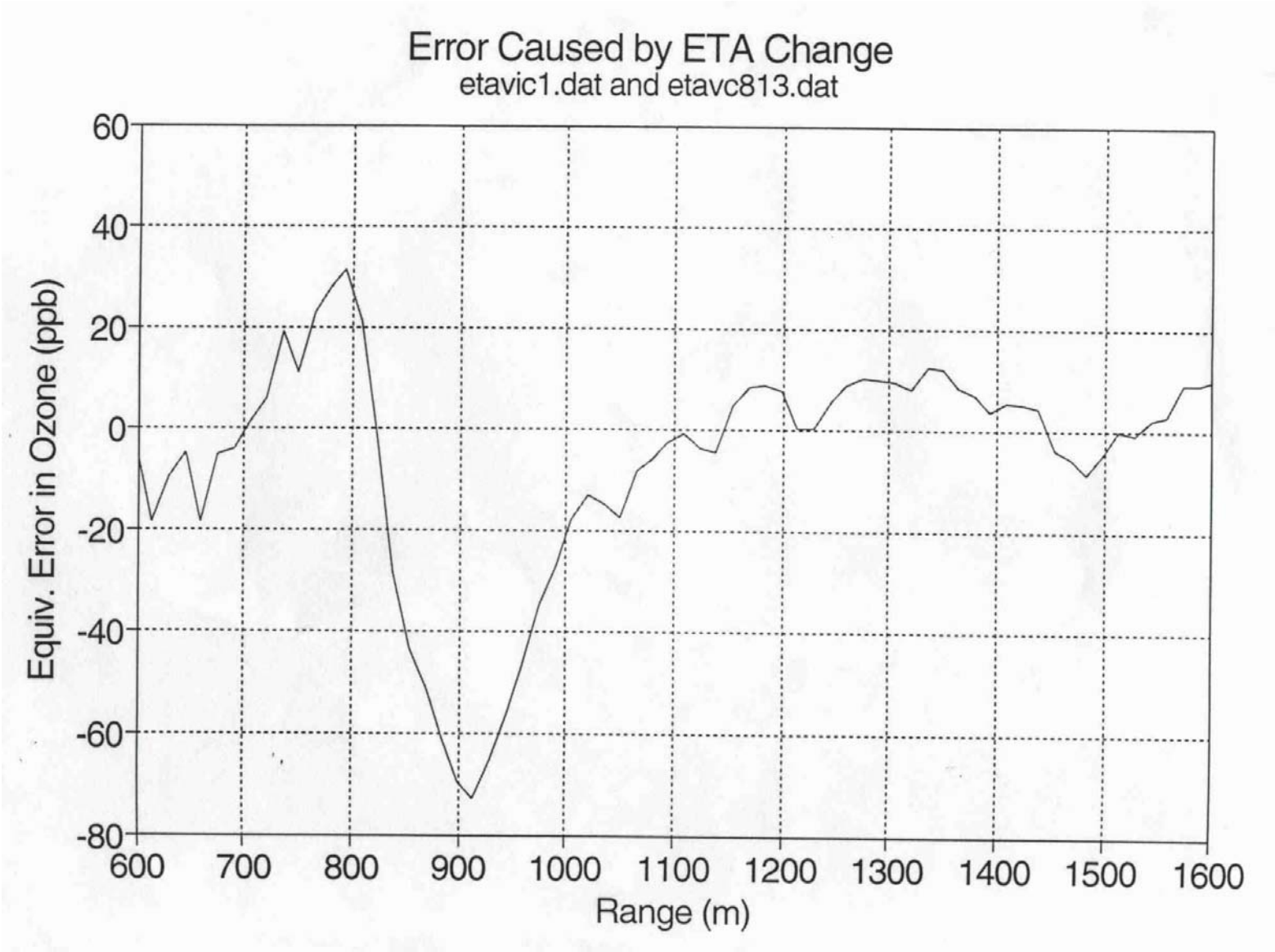
Error Caused by ETA Change
etavic1.dat and etavc813.dat
Equiv. Error in Ozone (ppb)
60
40
20
0
-20
-40
-60
-80
600
700
800
900
1000
1100
1200
1300
1400
1500
1600
Range (m)

Figure H

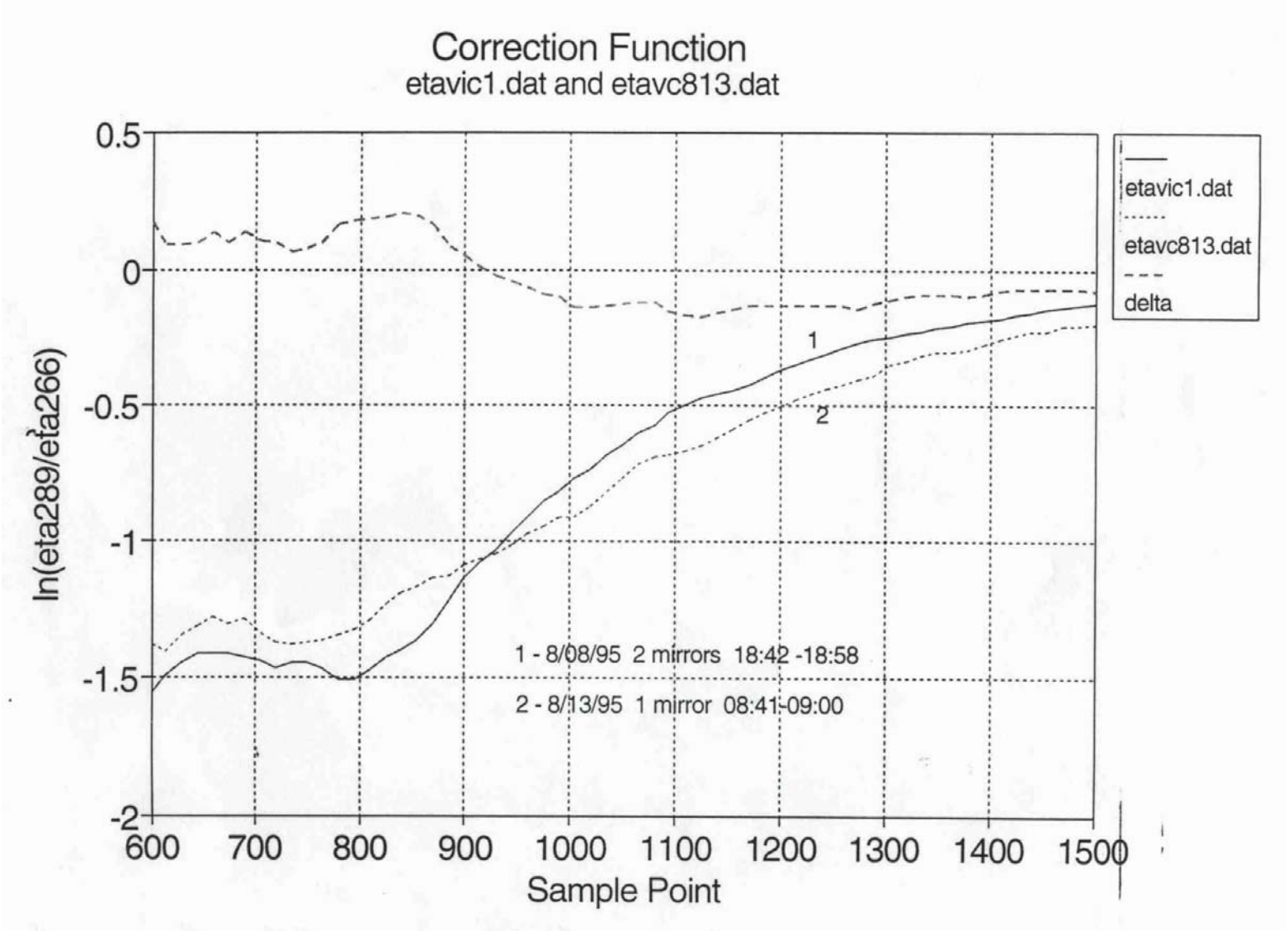
Correction Function
etavic1.dat and etavc813.dat
0.5
0
-0.5
-1
-1.5
-2
ln(eta289/eta266)
600
700
800
900
1000
1100
1200
1300
1400
1500
Sample Point
etavic1.dat
etavc813.dat
delta
1
2
1 - 8/08/95 2 mirrors 18:42 -18:58
2 - 8/13/95 1 mirror 08:41-09:00

Appendix C: REGIONAL MAP (from T&B System, Inc., Interim Report: Task 1, 1995)

Appendix C

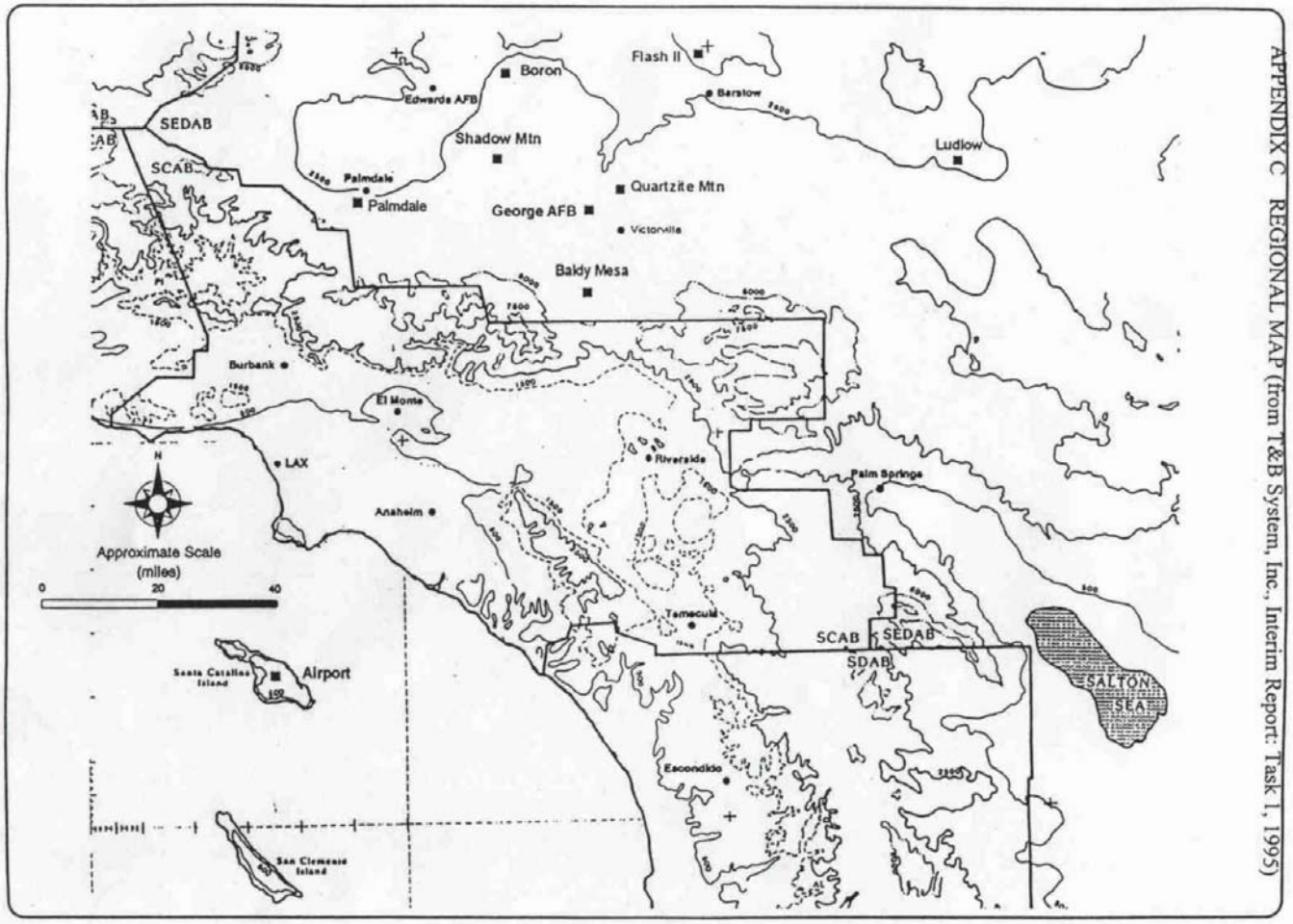

APPENDIX C REGIONAL MAP (from T&B System, Inc., Interim Report: Task 1, 1995)

(This page intentionally left blank.)

Appendix D: Tables and Figures to Supplement Prior Evaluations of the Inaugural Performance of NOAA's Two-Dimensional Scanning Ozone Lidar at Southern California International Airport During Early August 1995

Evaluation by UCD

The use of a single-engine aircraft owned and operated by the University of California, Davis, was contracted to aid in the evaluation of the performance of NOAA's refined ozone lidar system. The aircraft was flown three times per day to provide independent information to characterize the lidar's performance under different meteorological conditions (morning when a surface inversion is most likely to be present, afternoon when deep thermal mixing of the atmosphere is likely, and evening when transport is most likely to occur). Their analysis of the NOAA and UCD data sets, with and without consideration of time of day) led them to conclude that the revised configuration of the lidar was not ready from prime time and not capable of independently providing reliable data.

Evaluation by T&B Systems

Technical and Business Systems, Incorporated (T&B) operated several ground-based ozone monitoring sites during the Mojave Desert Ozone Study. One of the sites was on Quartzite Mountain which is located just a few kilometers northeast of the NOAA lidar site. A limited comparison of of the T&B data from Quartzite Mountain and NOAA lidar data from the old George Air Force Base led T&B to conclude that the lidar data were unreliable.

Evaluation by NOAA

NOAA also compared their lidar data with ozone data collected by T&B and UCD. They acknowledged problems with the lidar's scanning mirrors, particularly in the morning when rapidly rising temperatures caused distortions as the mirror supports expanded. Measurements in the scanning mode confirm that the system performance was much poorer in the morning than during the rest of the day. Although not trouble free, NOAA believed the lidar performance to be acceptable outside the period of rapid temperature change.

Evaluation by ARB

In response to requests by the contract manager, the original (T&B and UCD) analyses were expanded (UCD to compare by time of day and T&B to compare at beginning and end of field test) to accommodate some of the known and perceived problems with the lidar data. However, the results of these data comparisons did not improve significantly. Given the results of these comparisons and the some of the uncertainties in the "reference" platforms (e.g., aircraft vertical profile of ozone concentrations incorporating horizontal variations; airflow disturbance and deposition affects

influencing ozone concentrations on mountain top site), ARB staff focused on evaluating the reasonableness of the lidar data as opposed to redoing the earlier analyses and assessing the accuracy of the lidar data. In other words, do the lidar data portray a coherent story of the atmospheric processes in the region or are they obviously invalid, in addition to appearing inaccurate?

ARB staff looked at ozone concentrations and winds in the vicinity of the lidar site and at sites that could be associated with transport from the South Coast Air Basin into the area. Although complex atmospheric waves can form downwind of mountain ridges, the altitudes of the monitoring sites were of some use in interpreting the observed ozone concentrations.

The basic types of analyses conducted by ARB staff consisted of the following:

1) Assessment of the comparability of the ozone concentrations measured at Quartzite Mountain, Victorville, and the lidar site (at 495m AGL).
2) Assessment of the comparability of the ozone concentrations measured in the vicinity of Quartzite Mountain, in potential upwind source areas, and the maximum ozone concentrations reported with the lidar.
3) Assessment of the matched hourly vertical profiles of ozone concentrations by lidar in terms of maximum ozone concentrations and resultant winds observed that day and the day before in the area.
4) Assessment of the evolution of hourly vertical profiles of ozone concentrations by lidar during each day in terms of ozone concentrations and resultant winds observed that day and the day before in the area.

The analyses led ARB staff to conclude the the lidar results, although exhibiting some problems, were within reason given the context of ozone concentrations and winds in southern California. The peak ozone concentrations reported by the lidar were very consistent with peak ozone concentrations observed at ground-based monitoring sites on that day or the day before. The data for winds aloft are very limited and it is not possible to definitively determine how ozone concentrations might get from one location to above the lidar site but the lidar results were always consistent with peak concentrations observed with in the region. Thus, additional analysis of the atmospheric processes observed by the lidar and radar wind profiler as well as other data sources are warranted to characterize the validity of the lidar results. Some of the data tables and figures from the ARB analysis will be included in the "electronic" version of this report. If you desire this report on CD, please contact Mr. Dolislager at (916) 323-1533 or ldolisla@arb.ca.gov.

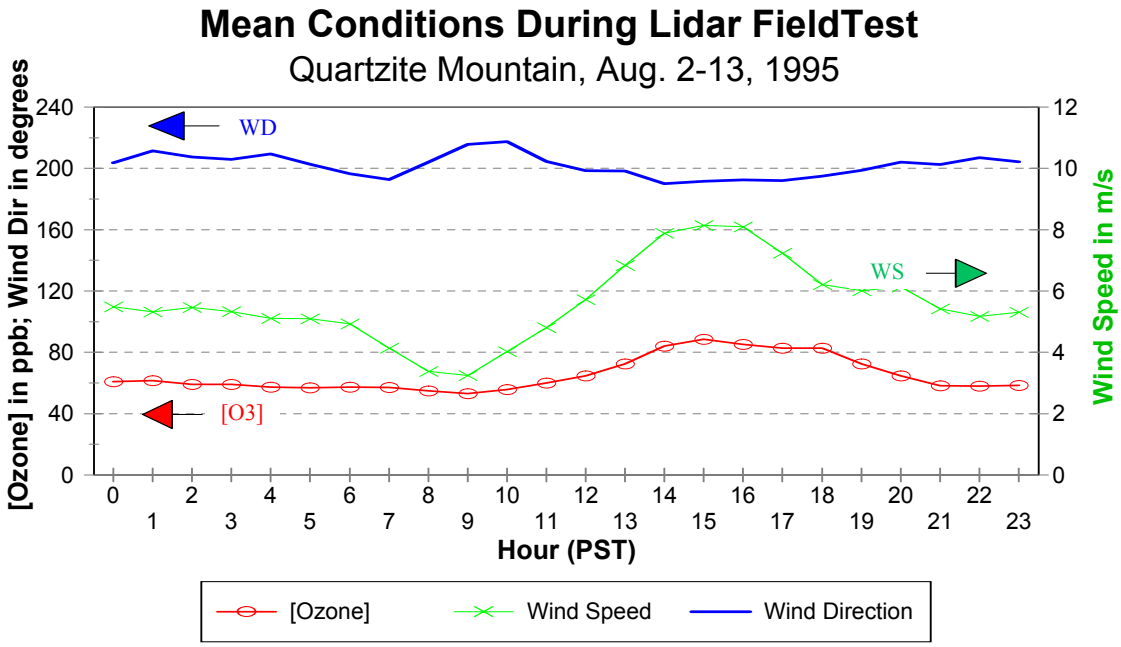

Figure D1-1. Mean diurnal ozone concentrations, wind speeds, and wind directions during the lidar field test (August 2-13, 1995).

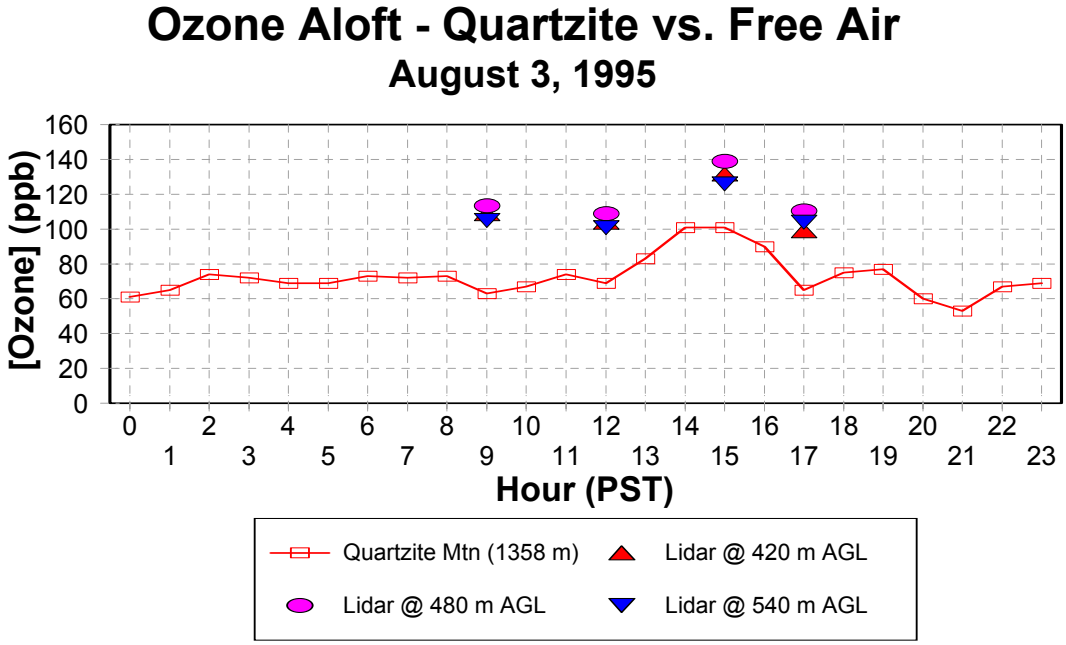

Figure D1-2. Hourly mean ozone concentrations on August 3, 1995 as detected by the continuous monitor on Quartzite Mountain and the lidar at altitudes approximating the altitude of the surface analyzer.

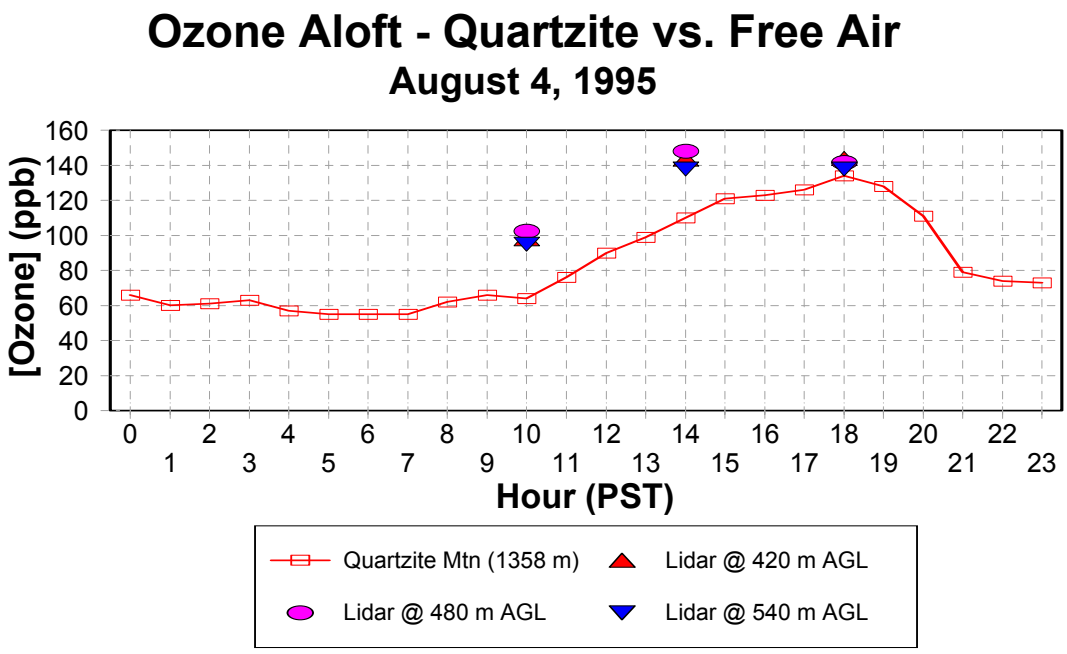

Figure D1-3. Hourly mean ozone concentrations on August 4, 1995 as detected by the continuous monitor on Quartzite Mountain and the lidar at altitudes approximating the altitude of the surface analyzer.

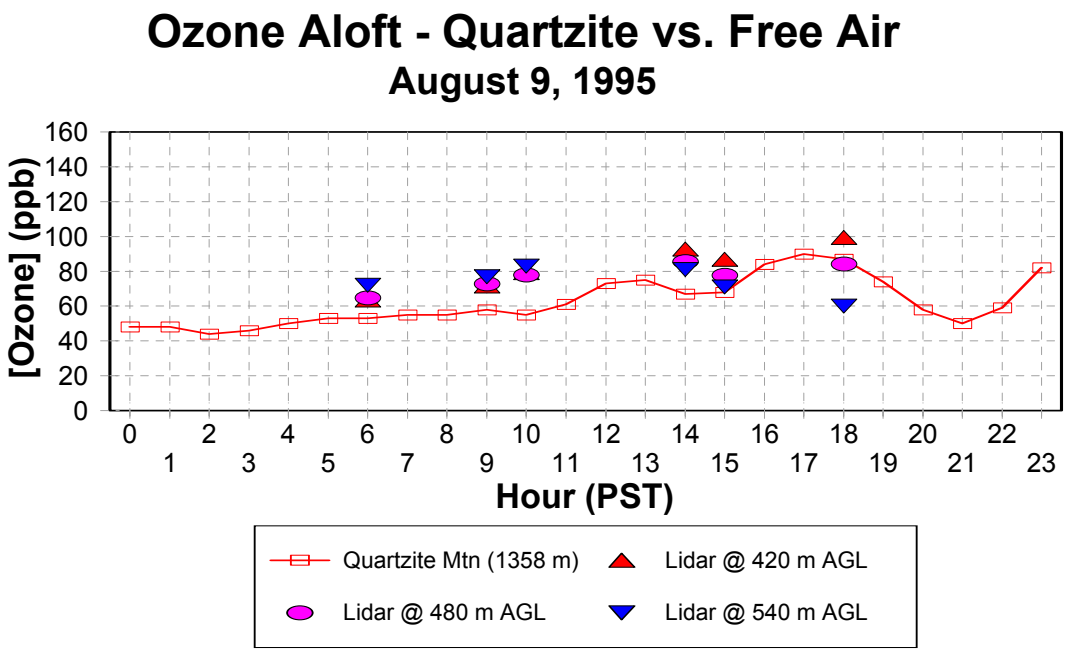

Figure D1-4. Hourly mean ozone concentrations on August 9, 1995 as detected by the continuous monitor on Quartzite Mountain and the lidar at altitudes approximating the altitude of the surface analyzer.

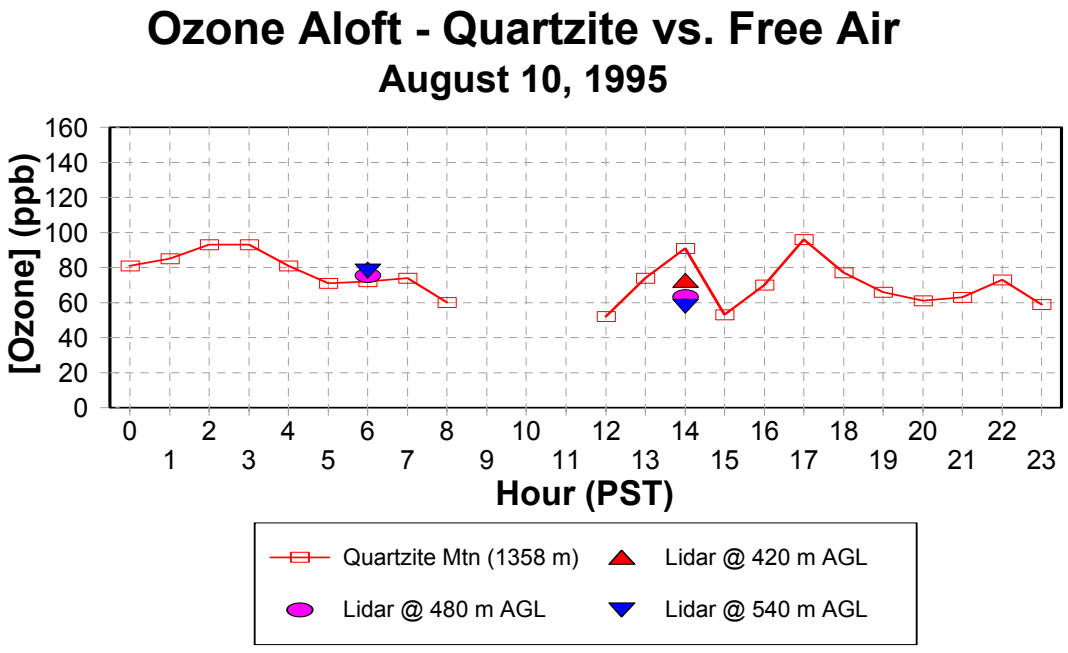

Figure D1-5. Hourly mean ozone concentrations on August 10, 1995 as detected by the continuous monitor on Quartzite Mountain and the lidar at altitudes approximating the altitude of the surface analyzer.

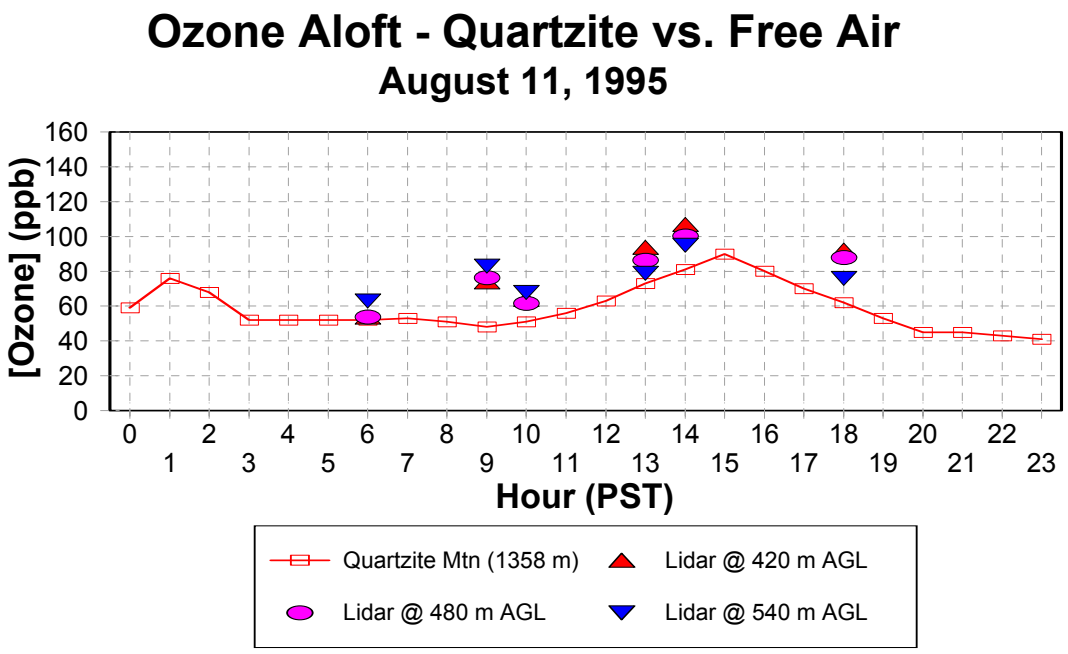

Figure D1-6. Hourly mean ozone concentrations on August 11, 1995 as detected by the continuous monitor on Quartzite Mountain and the lidar at altitudes approximating the altitude of the surface analyzer.

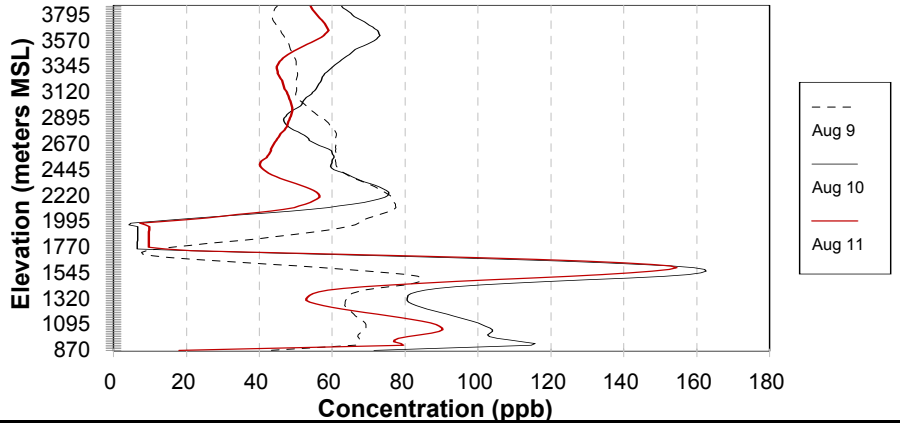

Figure D2-1. 6-7 a.m. PST vertical profiles of ozone concentrations as determined by NOAA's lidar during the August 1995 field test at Southern California International Airport near Victorville, CA.

Table D2-1. Maximum 1-hour ozone concentrations (ppb) observed at monitoring sites associated with potential transport through Cajon Pass. Dates shown in bold type correspond to days when the lidar system was in operation. Dates with normal type indicate maximum ozone concentrations on the day before lidar operation during the 6-7 a.m. PST hour.

Site	Aug. 8	**Aug. 9**	**Aug. 10**	**Aug. 11**
Shadow Mountain	110	99	92	74
Quartzite Mountain	103	90	96	90
Southern California Int'l AP	111	90	6	95
Victorville	104	87	101	58
Hesperia	80	112	86	70
Phelan	143	120	117	63
Baldy Mesa	133	96	115	101
Lake Gregory	111	165	121	108
San Gabriel Valley	153	207	99	167

Table D2-2. Six-hour resultant winds (RWS-resultant wind speed in mph, RWD-resultant wind direction in degrees, SF-steadiness factor is the ratio of the RWS divided by the arithmetic wind speed) observed at the monitoring sites associated with potential transport through Cajon Pass. Data are pertinent to vertical profiles of ozone concentrations as estimated by NOAA's lidar during the 6-7 a.m. PST hour.

Site	Type	Date 1995	Early PM Day B4			Late PM Day B4			Early AM		
			RWS	RWD	SF	RWS	RWD	SF	RWS	RWD	SF
Victorville	Instant	8/9	13.7	180	0.98	6.4	217	0.83	5.6	262	0.99
Victorville	Instant	8/10	17.6	184	1.00	8.9	193	0.99	4.1	229	0.98
Victorville	Instant	8/11	12.1	189	0.98	6.3	219	0.93	2.3	226	0.85
Hesperia	Instant	8/9	12.8	189	1.00	10.4	198	0.99	5.7	204	1.00
Hesperia	Instant	8/10	12.8	189	1.00	10.6	189	1.00	6.7	196	0.98
Hesperia	Instant	8/11	13.0	196	1.00	7.4	204	0.95	3.3	233	0.94
Phelan	Instant	8/9	11.1	153	0.98	6.7	184	0.93	5.4	208	0.98
Phelan	Instant	8/10	12.4	150	0.99	6.8	198	0.98	5.7	203	0.98
Phelan	Instant	8/11	10.2	176	0.98	5.1	212	0.93	4.3	219	0.88
L. Gregory	Vector	8/9	1.9	206	0.88	1.0	266	0.97	0.8	261	0.94
L. Gregory	Vector	8/10	1.9	211	0.89	2.4	167	0.91	2.4	178	0.94
L. Gregory	Vector	8/11	5.6	234	0.99	1.8	165	0.99	0.7	279	1.00
Fontana	Vector	8/9	6.6	243	0.99	2.1	214	0.99	0.0	0	calm
Fontana	Vector	8/10	6.6	246	0.99	2.7	236	1.00	0.0	0	calm
Fontana	Vector	8/11	5.8	240	0.99	2.4	241	0.97	0.8	12	0.99
Azusa	Vector	8/9	5.0	247	1.00	3.5	246	1.00	0.5	252	1.00
Azusa	Vector	8/10	4.5	248	1.00	1.8	248	1.00	0.3	250	1.00
Azusa	Vector	8/11	4.3	252	1.00	2.2	246	1.00	0.0	0	calm

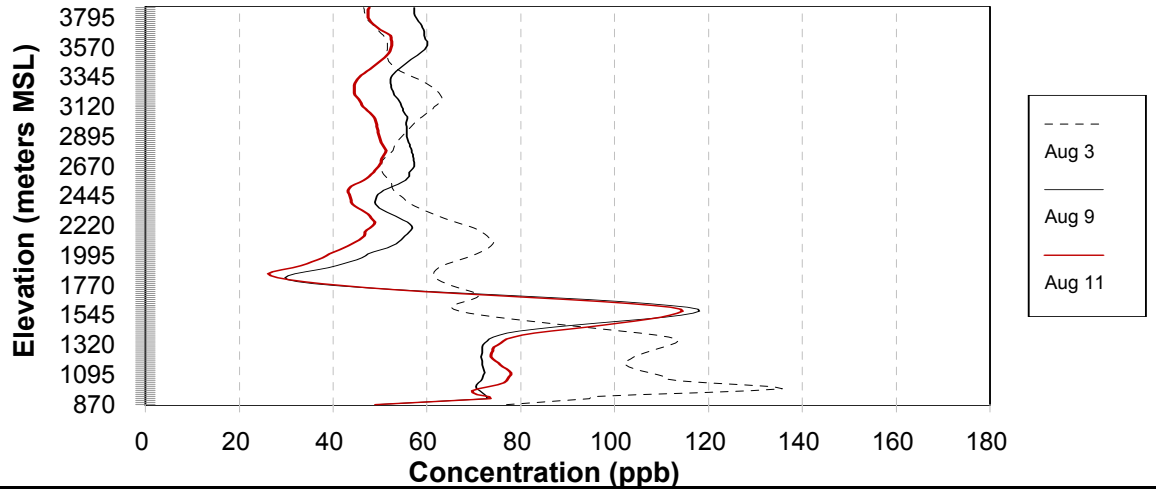

Figure D2-2. 9-10 a.m. PST vertical profiles of ozone concentrations as determined by NOAA's lidar during the August 1995 field test at Southern California International Airport near Victorville, CA.

Table D2-3. Maximum 1-hour ozone concentrations (ppb) observed at monitoring sites associated with potential transport through Cajon Pass. Dates shown in bold type correspond to days when the lidar system was in operation. Dates with normal type indicate concentrations on the day before lidar operation during the 9-10 a.m. PST hour.

Site	Aug. 2	**Aug. 3**	Aug. 8	**Aug. 9**	**Aug. 10**	**Aug. 11**
Shadow Mountain	81	108	10	99	92	74
Quartzite Mountain	110	101	103	90	96	90
Southern California Int'l AP	121	100	111	90	76	95
Victorville	72	79+	104	87	101	58
Hesperia	105	106	80	112	86	70
Phelan	196	95	143	120	117	63
Baldy Mesa	152	118	133	96	115	101
Lake Gregory	172	135	111	165	121	108
San Gabriel Valley	145	175	153	207	99	167

Table D2-4. Six-hour resultant winds (RWS-resultant wind speed in mph, RWD-resultant wind direction in degrees, SF-steadiness factor is the ratio of the RWS divided by the arithmetic wind speed) observed at the monitoring sites associated with potential transport through Cajon Pass. Data are pertinent to vertical profiles of ozone concentrations as estimated by NOAA's lidar during the 9-10 a.m. PST hour.

Site	Type	Date 1995	Early PM Day B4			Late PM Day B4			Early AM		
			RWS	RWD	SF	RWS	RWD	SF	RWS	RWD	SF
Victorville	Instant	8/3	16.4	184	0.99	6.6	195	0.99	3.2	190	0.76
Victorville	Instant	8/9	13.7	180	0.98	6.4	217	0.83	5.6	262	0.99
Victorville	Instant	8/11	12.1	189	0.98	6.3	219	0.93	2.3	226	0.85
Hesperia	Instant	8/3	14.8	193	1.00	6.8	200	0.95	6.7	223	1.00
Hesperia	Instant	8/9	12.8	189	1.00	10.4	198	0.99	5.7	204	1.00
Hesperia	Instant	8/11	13.0	196	1.00	7.4	204	0.95	3.3	233	0.94
Phelan	Instant	8/3	14.5	168	1.00	7.6	196	0.99	5.0	217	0.96
Phelan	Instant	8/9	11.1	153	0.98	6.7	184	0.93	5.4	208	0.98
Phelan	Instant	8/11	10.2	176	0.98	5.1	212	0.93	4.3	219	0.88
L. Gregory	Vector	8/3	3.8	187	0.94	2.6	156	0.98	1.3	169	1.00
L. Gregory	Vector	8/9	1.9	206	0.88	1.0	266	0.97	0.8	261	0.94
L. Gregory	Vector	8/11	5.6	234	0.99	1.8	165	0.99	0.7	279	1.00
Fontana	Vector	8/3	6.2	225	1.00	1.8	240	0.92	0.0	0	calm
Fontana	Vector	8/9	6.6	243	0.99	2.1	214	0.99	0.0	0	calm
Fontana	Vector	8/11	5.8	240	0.99	2.4	241	0.97	0.8	12	0.99
Azusa	Vector	8/3	4.2	250	1.00	2.2	246	1.00	0.3	251	1.00
Azusa	Vector	8/9	5.0	247	1.00	3.5	246	1.00	0.5	252	1.00
Azusa	Vector	8/11	4.3	252	1.00	2.2	246	1.00	0.0	0	calm

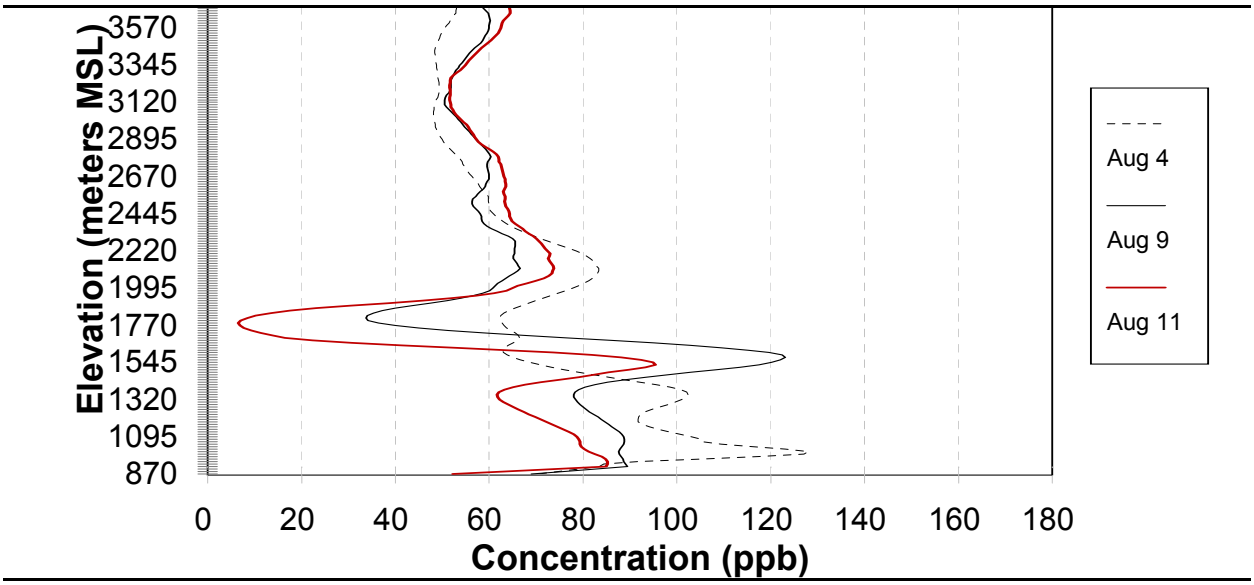

Figure D2-3. 10-11 a.m. PST vertical profiles of ozone concentrations as determined by NOAA's lidar during the August 1995 field test at Southern California International Airport near Victorville, CA.

Table D2-5. Maximum 1-hour ozone concentrations (ppb) observed at monitoring sites associated with potential transport through Cajon Pass. Dates shown in bold type correspond to days when the lidar system was in operation. Dates with normal type indicate concentrations on the day before lidar operation during the 10-11 a.m. PST hour.

Site	Aug. 3	**Aug. 4**	Aug. 8	**Aug. 9**	Aug. 10	**Aug. 11**
Shadow Mountain	109	96	110	99	92	74
Quartzite Mountain	101	134	103	90	96	90
Southern California Int'l AP	100	137	111	90	76	95
Victorville	79+	109	104	87	101	58
Hesperia	106	123	80	112	86	70
Phelan	95	136	143	120	117	63
Baldy Mesa	118	140	133	96	115	101
Lake Gregory	135	158	111	165	121	108
San Gabriel Valley	175	150	153	207	99	167

Table D2-6. Six-hour resultant winds (RWS-resultant wind speed in mph, RWD-resultant wind direction in degrees, SF-steadiness factor is the ratio of the RWS divided by the arithmetic wind speed) observed at the monitoring sites associated with potential transport through Cajon Pass. Data are pertinent to vertical profiles of ozone concentrations as estimated by NOAA's lidar during the 10-11 a.m. PST hour.

Site	Type	Date 1995	Early PM Day B4			Late PM Day B4			Early AM		
			RWS	RWD	SF	RWS	RWD	SF	RWS	RWD	SF
Victorville	Instant	8/4	19.6	187	1.00	8.3	200	0.84	2.1	292	0.85
Victorville	Instant	8/9	13.7	180	0.98	6.4	217	0.83	5.6	262	0.99
Victorville	Instant	8/11	12.1	189	0.98	6.3	219	0.93	2.3	226	0.85
Hesperia	Instant	8/4	16.1	187	1.00	12.8	194	1.00	11.6	206	1.00
Hesperia	Instant	8/9	12.8	189	1.00	10.4	198	0.99	5.7	204	1.00
Hesperia	Instant	8/11	13.0	196	1.00	7.4	204	0.95	3.3	233	0.94
Phelan	Instant	8/4	13.4	209	0.97	11.4	188	0.99	6.6	205	0.97
Phelan	Instant	8/9	11.1	153	0.98	6.7	184	0.93	5.4	208	0.98
Phelan	Instant	8/11	10.2	176	0.98	5.1	212	0.93	4.3	219	0.88
L. Gregory	Vector	8/4	0.6	201	0.40	0.9	124	0.94	3.7	130	0.97
L. Gregory	Vector	8/9	1.9	206	0.88	1.0	266	0.97	0.8	261	0.94
L. Gregory	Vector	8/11	5.6	234	0.99	1.8	165	0.99	0.7	279	1.00
Fontana	Vector	8/4	7.5	236	0.99	1.6	234	0.99	0.3	8	1.00
Fontana	Vector	8/9	6.6	243	0.99	2.1	214	0.99	0.0	0	calm
Fontana	Vector	8/11	5.8	240	0.99	2.4	241	0.97	0.8	12	0.99
Azusa	Vector	8/4	4.8	247	1.00	2.7	246	1.00	1.2	249	0.99
Azusa	Vector	8/9	5.0	247	1.00	3.5	246	1.00	0.5	252	1.00
Azusa	Vector	8/11	4.3	252	1.00	2.2	246	1.00	0.0	0	calm

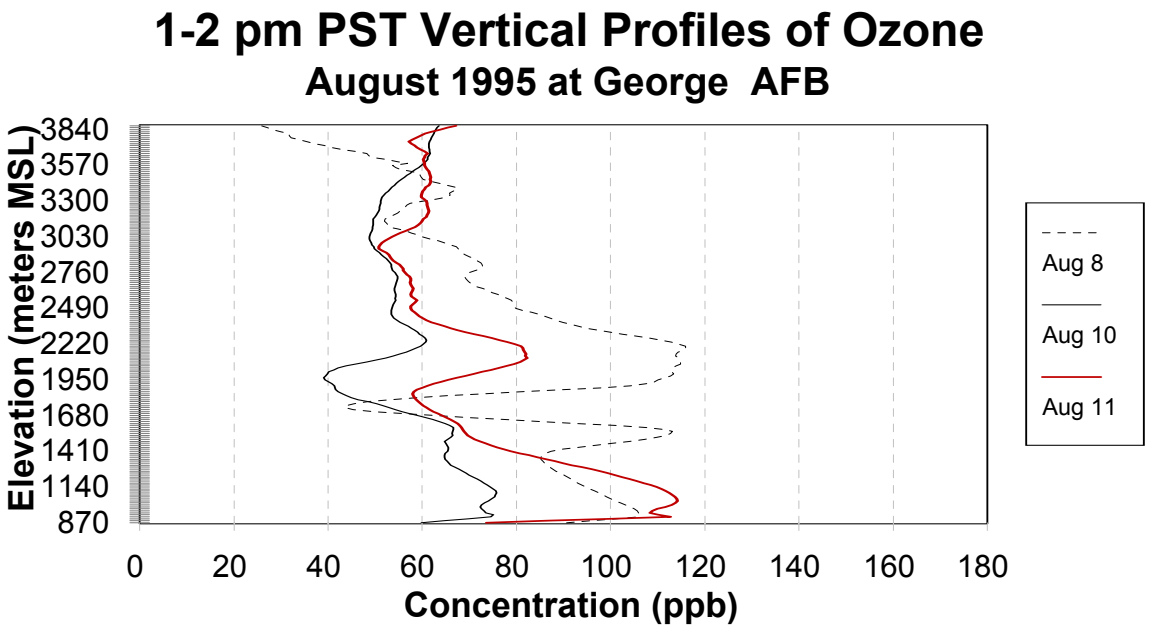

Figure D2-4. 1-2 p.m. PST vertical profiles of ozone concentrations as determined by NOAA's lidar during the August 1995 field test at Southern California International Airport near Victorville, CA.

Table D2-7. Maximum 1-hour ozone concentrations (ppb) observed at monitoring sites associated with potential transport through Cajon Pass. Dates shown in bold type correspond to days when the lidar system was in operation. Dates with normal type indicate concentrations on the day before lidar operation during the 1-2 p.m. PST hour.

Site	Aug. 7	**Aug. 8**	Aug. 9	**Aug. 10**	**Aug. 11**
Shadow Mountain	81	110	99	92	74
Quartzite Mountain	88	103	90	96	90
Southern California Int'l AP	82	111	90	76	95
Victorville	109	104	87	101	58
Hesperia	94	80	112	86	70
Phelan	140	143	120	117	63
Baldy Mesa	157	133	96	115	101
Lake Gregory	137	111	165	121	108
San Gabriel Valley	154	153	207	99	167

Table D2-8. Six-hour resultant winds (RWS-resultant wind speed in mph, RWD-resultant wind direction in degrees, SF-steadiness factor is the ratio of the RWS divided by the arithmetic wind speed) observed at the monitoring sites associated with potential transport through Cajon Pass. Data are pertinent to vertical profiles of ozone concentrations as estimated by NOAA's lidar during the 1-2 p.m. PST hour.

Site	Type	Date 1995	Late PM Day B4			Early AM			Late AM		
			RWS	RWD	SF	RWS	RWD	SF	RWS	RWD	SF
Victorville	Instant	8/8	5.1	257	0.83	2.1	215	0.70	2.4	21	0.90
Victorville	Instant	8/10	8.9	193	0.99	4.1	229	0.98	2.6	204	0.58
Victorville	Instant	8/11	6.3	219	0.93	2.3	226	0.85	7.2	170	0.83
Hesperia	Instant	8/8	4.0	228	0.88	3.7	216	0.89	1.2	153	0.35
Hesperia	Instant	8/10	10.6	189	1.00	6.7	196	0.98	6.9	214	0.96
Hesperia	Instant	8/11	7.4	204	0.95	3.3	233	0.94	9.1	186	0.89
Phelan	Instant	8/8	3.7	217	0.77	5.1	216	0.95	2.5	27	0.76
Phelan	Instant	8/10	6.8	198	0.98	5.7	203	0.98	2.1	81	0.49
Phelan	Instant	8/11	5.1	212	0.93	4.3	219	0.88	9.0	228	0.96
L. Gregory	Vector	8/8	0.9	185	0.76	0.3	182	0.54	1.2	210	0.93
L. Gregory	Vector	8/10	2.4	167	0.91	2.4	178	0.94	3.8	180	0.91
L. Gregory	Vector	8/11	1.8	165	0.99	0.7	279	1.00	1.8	125	0.98
Fontana	Vector	8/8	2.7	226	0.99	0.8	4	1.00	1.7	219	0.94
Fontana	Vector	8/10	2.7	236	1.00	0.0	0	calm	2.0	220	0.99
Fontana	Vector	8/11	2.4	241	0.97	0.8	12	0.99	0.8	205	0.66
Azusa	Vector	8/8	0.8	248	1.00	0.3	247	1.00	1.5	249	0.99
Azusa	Vector	8/10	1.8	248	1.00	0.3	250	1.00	1.1	245	0.94
Azusa	Vector	8/11	2.2	246	1.00	0.0	0	calm	0.6	217	0.94

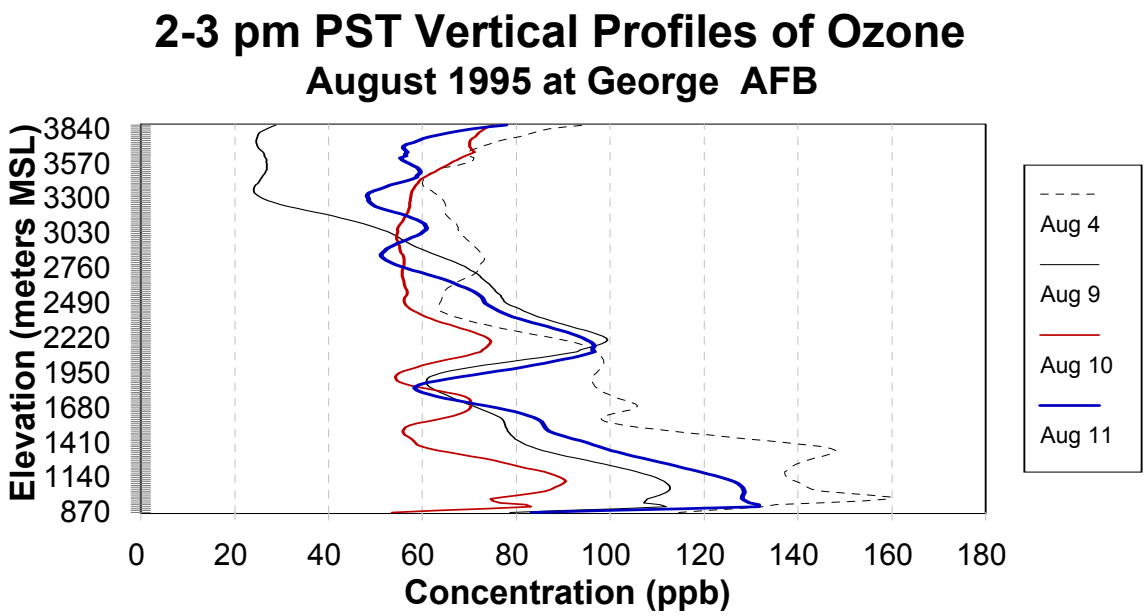

Figure D2-5. 2-3 p.m. PST vertical profiles of ozone concentrations as determined by NOAA's lidar during the August 1995 field test at Southern California International Airport near Victorville, CA.

Table D2-9. Maximum 1-hour ozone concentrations (ppb) observed at monitoring sites associated with potential transport through Cajon Pass. Dates shown in bold type correspond to days when the lidar system was in operation. Dates with normal type indicate concentrations on the day before lidar operation during the 2-3 p.m. PST hour.

Site	Aug. 3	**Aug. 4**	Aug. 8	**Aug. 9**	**Aug. 10**	**Aug. 11**
Shadow Mountain	108	96	110	99	92	74
Quartzite Mountain	101	134	103	90	96	90
Southern California Int'l AP	100	137	111	90	76	95
Victorville	79+	109	104	87	101	58
Hesperia	106	123	80	112	86	70
Phelan	95	136	143	120	117	63
Baldy Mesa	118	140	133	96	115	101
Lake Gregory	135	158	111	165	121	108
San Gabriel Valley	175	150	153	207	99	167

Table D2-10. Six-hour resultant winds (RWS-resultant wind speed in mph, RWD-resultant wind direction in degrees, SF-steadiness factor is the ratio of the RWS divided by the arithmetic wind speed) observed at the monitoring sites associated with potential transport through Cajon Pass. Data are pertinent to vertical profiles of ozone concentrations as estimated by NOAA's lidar during the 2-3 p.m. PST hour.

Site	Type	Date 1995	Late PM Day B4			Early AM			Late AM		
			RWS	RWD	SF	RWS	RWD	SF	RWS	RWD	SF
Victorville	Instant	8/4	8.3	200	0.84	2.1	292	0.85	11.8	192	0.96
Victorville	Instant	8/9	6.4	217	0.83	5.6	262	0.99	6.3	176	0.80
Victorville	Instant	8/10	8.9	193	0.99	4.1	229	0.98	2.6	204	0.58
Victorville	Instant	8/11	6.3	219	0.93	2.3	226	0.85	7.2	170	0.83
Hesperia	Instant	8/4	12.8	194	1.00	11.6	206	1.00	11.6	203	0.99
Hesperia	Instant	8/9	10.4	198	0.99	5.7	204	1.00	7.1	181	0.90
Hesperia	Instant	8/10	10.6	189	1.00	6.7	196	0.98	6.9	214	0.96
Hesperia	Instant	8/11	7.4	204	0.95	3.3	233	0.94	9.1	186	0.89
Phelan	Instant	8/4	11.4	188	1.00	6.6	205	0.97	2.5	134	0.60
Phelan	Instant	8/9	6.7	184	0.93	5.4	208	0.98	3.6	173	0.72
Phelan	Instant	8/10	6.8	198	0.98	5.7	203	0.98	2.1	81	0.49
Phelan	Instant	8/11	5.1	212	0.93	4.3	219	0.88	9.0	228	0.96
L. Gregory	Vector	8/4	0.9	124	0.94	3.7	130	0.97	2.8	169	0.94
L. Gregory	Vector	8/9	1.0	266	0.97	0.8	261	0.94	1.4	197	0.70
L. Gregory	Vector	8/10	2.4	167	0.91	2.4	178	0.94	3.8	180	0.91
L. Gregory	Vector	8/11	1.8	165	0.99	0.7	279	1.00	1.8	125	0.98
Fontana	Vector	8/4	1.6	234	0.99	0.3	8	1.00	2.1	224	0.98
Fontana	Vector	8/9	2.1	214	0.99	0.0	0	calm	2.1	220	0.89
Fontana	Vector	8/10	2.7	236	1.00	0.0	0	calm	2.0	220	0.99
Fontana	Vector	8/11	2.4	241	0.97	0.8	12	0.99	0.8	205	0.66
Azusa	Vector	8/4	2.7	246	1.00	1.2	249	0.99	0.8	238	0.99
Azusa	Vector	8/9	3.5	246	1.00	0.5	252	1.00	1.0	245	0.99
Azusa	Vector	8/10	1.8	248	1.00	0.3	250	1.00	1.1	245	0.94
Azusa	Vector	8/11	2.2	246	1.00	0.0	0	calm	0.6	217	0.94

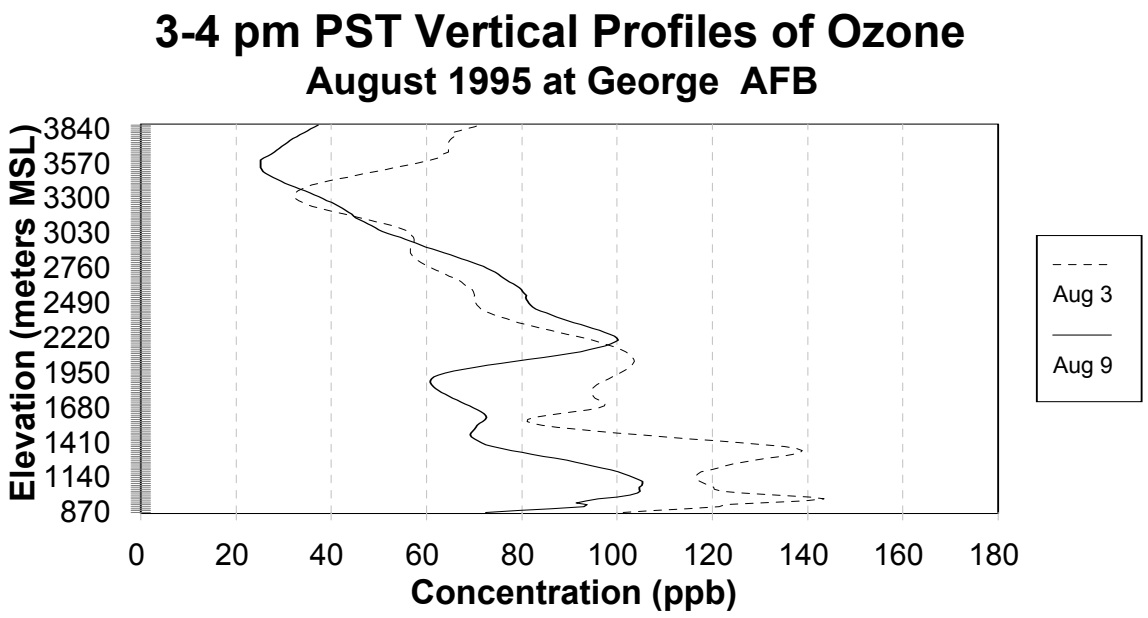

Figure D2-6. 3-4 p.m. PST vertical profiles of ozone concentrations as determined by NOAA's lidar during the August 1995 field test at Southern California International Airport near Victorville, CA.

Table D2-11. Maximum 1-hour ozone concentrations (ppb) observed at monitoring sites associated with potential transport through Cajon Pass. Dates shown in bold type correspond to days when the lidar system was in operation. Dates with normal type indicate concentrations on the day before lidar operation during the 3-4 p.m. PST hour.

Site	Aug. 2	**Aug. 3**	Aug. 8	**Aug. 9**
Shadow Mountain	81	108	110	99
Quartzite Mountain	110	101	103	90
Southern California Int'l AP	121	100	111	90
Victorville	72	79+	104	87
Hesperia	105	106	80	112
Phelan	196	95	143	120
Baldy Mesa	152	118	133	96
Lake Gregory	172	135	111	165
San Gabriel Valley	145	175	153	207

Table D2-12. Six-hour resultant winds (RWS-resultant wind speed in mph, RWD-resultant wind direction in degrees, SF-steadiness factor is the ratio of the RWS divided by the arithmetic wind speed) observed at the monitoring sites associated with potential transport through Cajon Pass. Data are pertinent to vertical profiles of ozone concentrations as estimated by NOAA's lidar during the 3-4 p.m. PST hour.

Site	Type	Date 1995	Early AM			Late AM			Early PM		
			RWS	RWD	SF	RWS	RWD	SF	RWS	RWD	SF
Victorville	Instant	8/3	3.2	190	0.76	4.2	170	0.77	19.6	187	1.00
Victorville	Instant	8/9	5.6	262	0.99	6.3	176	0.80	17.6	184	1.00
Hesperia	Instant	8/3	6.7	223	1.00	8.3	196	0.99	16.1	189	1.00
Hesperia	Instant	8/9	5.7	204	1.00	7.1	181	0.90	12.8	189	1.00
Phelan	Instant	8/3	5.0	217	0.96	5.6	201	0.73	13.4	209	0.97
Phelan	Instant	8/9	5.4	208	0.98	3.6	173	0.72	12.4	150	0.99
L. Gregory	Vector	8/3	1.3	169	1.00	2.8	137	0.99	0.6	201	0.40
L. Gregory	Vector	8/9	0.8	261	0.94	1.4	197	0.70	1.9	211	0.89
Fontana	Vector	8/3	0.0	0	calm	0.9	207	0.53	7.5	236	0.99
Fontana	Vector	8/9	0.0	0	calm	2.1	220	0.89	6.6	246	0.99
Azusa	Vector	8/3	0.3	251	1.00	1.2	255	1.00	4.8	247	1.00
Azusa	Vector	8/9	0.5	252	1.00	1.0	245	0.99	4.5	248	1.00

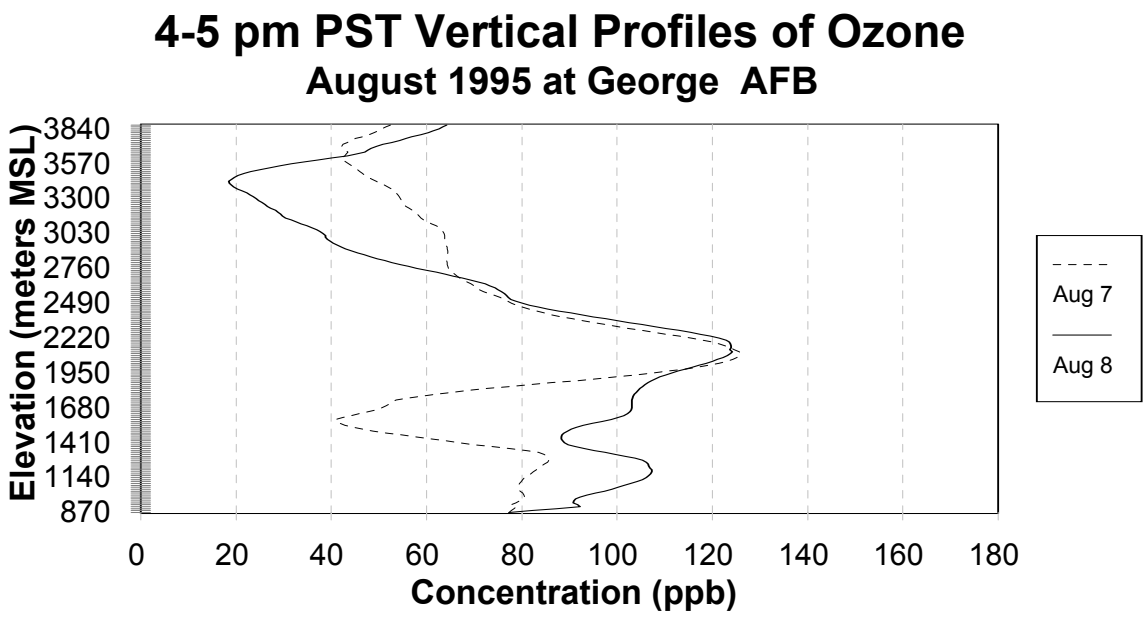

Figure D2-7. 4-5 p.m. PST vertical profiles of ozone concentrations as determined by NOAA's lidar during the August 1995 field test at Southern California International Airport near Victorville, CA.

Table D2-13. Maximum 1-hour ozone concentrations (ppb) observed at monitoring sites associated with potential transport through Cajon Pass. Dates shown in bold type correspond to days when the lidar system was in operation. Dates with normal type indicate concentrations on the day before lidar operation during the 4-5 p.m. PST hour.

Site	Aug. 6	**Aug. 7**	**Aug. 8**
Shadow Mountain	65	81	110
Quartzite Mountain	81	88	103
Southern California Int'l AP	99	82	111
Victorville	75	109	104
Hesperia	82	94	80
Phelan	120	140	143
Baldy Mesa	154	157	133
Lake Gregory	127	137	111
San Gabriel Valley	186	154	153

Table D2-14. Six-hour resultant winds (RWS-resultant wind speed in mph, RWD-resultant wind direction in degrees, SF-steadiness factor is the ratio of the RWS divided by the arithmetic wind speed) observed at the monitoring sites associated with potential transport through Cajon Pass. Data are pertinent to vertical profiles of ozone concentrations as estimated by NOAA's lidar during the 4-5 p.m. PST hour.

Site	Type	Date 1995	Early AM			Late AM			Early PM		
			RWS	RWD	SF	RWS	RWD	SF	RWS	RWD	SF
Victorville	Instant	8/7	1.5	207	0.84	2.4	94	0.81	11.6	190	0.94
Victorville	Instant	8/8	2.1	215	0.70	2.4	21	0.90	13.7	180	0.98
Hesperia	Instant	8/7	5.3	202	0.99	5.4	185	0.99	12.8	189	1.00
Hesperia	Instant	8/8	3.7	216	0.89	1.2	153	0.35	12.8	189	1.00
Phelan	Instant	8/7	4.5	213	0.96	3.4	116	0.94	6.0	211	0.72
Phelan	Instant	8/8	5.1	216	0.95	2.5	27	0.76	11.1	153	0.98
L. Gregory	Vector	8/7	0.0	0	calm	1.5	175	0.84	3.0	216	0.94
L. Gregory	Vector	8/8	0.3	182	0.54	1.2	210	0.93	1.9	206	0.88
Fontana	Vector	8/7	0.5	11	0.98	1.8	217	1.00	5.6	229	0.99
Fontana	Vector	8/8	0.8	4	1.00	1.7	219	0.94	6.6	243	0.99
Azusa	Vector	8/7	0.2	269	1.00	1.6	241	0.99	3.8	243	0.99
Azusa	Vector	8/8	0.3	247	1.00	1.5	249	0.99	5.0	247	1.00

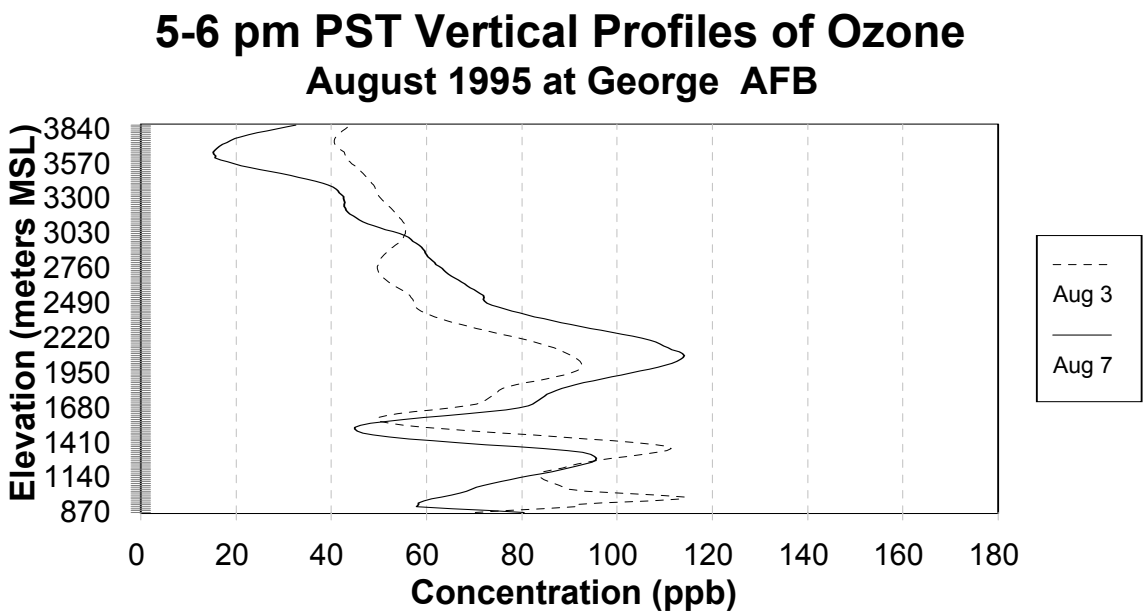

Figure D2-8. 5-6 p.m. PST vertical profiles of ozone concentrations as determined by NOAA's lidar during the August 1995 field test at Southern California International Airport near Victorville, CA.

Table D2-15. Maximum 1-hour ozone concentrations (ppb) observed at monitoring sites associated with potential transport through Cajon Pass. Dates shown in bold type correspond to days when the lidar system was in operation. Dates with normal type indicate concentrations on the day before lidar operation during the 5-6 p.m. PST hour.

Site	Aug. 2	**Aug. 3**	Aug. 6	**Aug. 7**
Shadow Mountain	81	108	65	81
Quartzite Mountain	110	101	81	88
Southern California Int'l AP	121	100	99	82
Victorville	72	79+	75	109
Hesperia	105	106	82	94
Phelan	196	95	120	140
Baldy Mesa	152	118	154	157
Lake Gregory	172	135	127	137
San Gabriel Valley	145	175	186	154

Table D2-16. Six-hour resultant winds (RWS-resultant wind speed in mph, RWD-resultant wind direction in degrees, SF-steadiness factor is the ratio of the RWS divided by the arithmetic wind speed) observed at the monitoring sites associated with potential transport through Cajon Pass. Data are pertinent to vertical profiles of ozone concentrations as estimated by NOAA's lidar during the 5-6 p.m. PST hour.

Site	Type	Date 1995	Early AM			Late AM			Early PM		
			RWS	RWD	SF	RWS	RWD	SF	RWS	RWD	SF
Victorville	Instant	8/3	3.2	190	0.76	4.2	170	0.77	19.6	187	1.00
Victorville	Instant	8/7	1.5	207	0.84	2.4	94	0.81	11.6	190	0.94
Hesperia	Instant	8/3	6.7	223	1.00	8.3	196	0.99	16.1	189	1.00
Hesperia	Instant	8/7	5.3	202	0.99	5.4	185	0.99	12.8	189	1.00
Phelan	Instant	8/3	5.0	217	0.96	5.6	201	0.73	13.4	209	0.97
Phelan	Instant	8/7	4.5	213	0.96	3.4	116	0.94	6.0	211	0.72
L. Gregory	Vector	8/3	1.3	169	1.00	2.8	137	0.99	0.6	201	0.40
L. Gregory	Vector	8/7	0.0	0	calm	1.5	175	0.84	3.0	216	0.94
Fontana	Vector	8/3	0.0	0	calm	0.9	207	0.53	7.5	236	0.99
Fontana	Vector	8/7	0.5	11	0.98	1.8	217	1.00	5.6	229	0.99
Azusa	Vector	8/3	0.3	251	1.00	1.2	255	1.00	4.8	247	1.00
Azusa	Vector	8/7	0.2	269	1.00	1.6	241	0.99	3.8	243	0.99

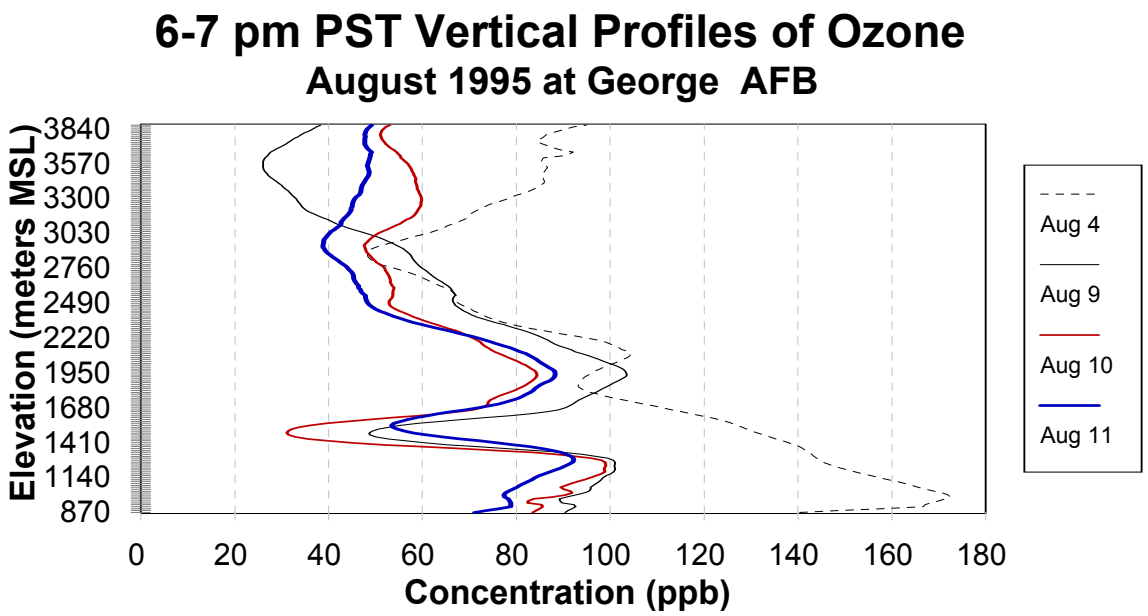

Figure D2-9. 6-7 p.m. PST vertical profiles of ozone concentrations as determined by NOAA's lidar during the August 1995 field test at Southern California International Airport near Victorville, CA.

Table D2-17. Maximum 1-hour ozone concentrations (ppb) observed at monitoring sites associated with potential transport through Cajon Pass. Dates shown in bold type correspond to days when the lidar system was in operation. Dates with normal type indicate concentrations on the day before lidar operation during the 6-7 p.m. PST hour.

Site	Aug. 3	**Aug. 4**	Aug. 8	**Aug. 9**	**Aug. 10**	**Aug. 11**
Shadow Mountain	108	96	110	99	92	74
Quartzite Mountain	101	134	103	90	96	90
Southern California Int'l AP	100	137	111	90	76	95
Victorville	79+	109	104	87	101	58
Hesperia	106	123	80	112	86	70
Phelan	95	136	143	120	117	63
Baldy Mesa	118	140	133	96	115	101
Lake Gregory	135	158	111	165	121	108
San Gabriel Valley	175	150	153	207	99	167

Table D2-18. Six-hour resultant winds (RWS-resultant wind speed in mph, RWD-resultant wind direction in degrees, SF-steadiness factor is the ratio of the RWS divided by the arithmetic wind speed) observed at the monitoring sites associated with potential transport through Cajon Pass. Data are pertinent to vertical profiles of ozone concentrations as estimated by NOAA's lidar during the 6-7 p.m. PST hour.

Site	Type	Date 1995	Early AM			Late AM			Early PM		
			RWS	RWD	SF	RWS	RWD	SF	RWS	RWD	SF
Victorville	Instant	8/4	2.1	292	0.85	11.8	192	0.96	18.1	190	1.00
Victorville	Instant	8/9	5.6	262	0.99	6.3	176	0.80	17.6	184	1.00
Victorville	Instant	8/10	4.1	229	0.98	2.6	204	0.58	12.1	189	0.98
Victorville	Instant	8/11	2.3	226	0.85	7.2	170	0.83	14.6	184	1.00
Hesperia	Instant	8/4	11.6	206	1.00	11.6	203	0.99	14.7	191	1.00
Hesperia	Instant	8/9	5.7	204	1.00	7.1	181	0.90	12.8	189	1.00
Hesperia	Instant	8/10	6.7	196	0.98	6.9	214	0.96	13.0	196	1.00
Hesperia	Instant	8/11	3.3	233	0.94	9.1	186	0.89	12.8	185	0.99
Phelan	Instant	8/4	6.6	205	0.97	2.5	134	0.60	16.0	157	1.00
Phelan	Instant	8/9	5.4	208	0.98	3.6	173	0.72	12.4	150	0.99
Phelan	Instant	8/10	5.7	203	0.98	2.1	81	0.49	10.2	176	0.98
Phelan	Instant	8/11	4.3	219	0.88	9.0	228	0.96	11.8	237	0.99
L. Gregory	Vector	8/4	3.7	130	0.97	2.8	169	0.94	3.1	219	0.77
L. Gregory	Vector	8/9	0.8	261	0.94	1.4	197	0.70	1.9	211	0.89
L. Gregory	Vector	8/10	2.4	178	0.94	3.8	180	0.91	5.6	234	0.99
L. Gregory	Vector	8/11	0.7	279	1.00	1.8	125	0.98	0.8	241	0.84
Fontana	Vector	8/4	0.3	8	1.00	2.1	224	0.98	7.5	239	0.99
Fontana	Vector	8/9	0.0	0	calm	2.1	220	0.89	6.6	246	0.99
Fontana	Vector	8/10	0.0	0	calm	2.0	220	0.99	5.8	240	0.99
Fontana	Vector	8/11	0.8	12	0.99	0.8	205	0.66	6.5	237	0.99
Azusa	Vector	8/4	1.2	249	0.99	0.8	238	0.99	4.5	251	1.00
Azusa	Vector	8/9	0.5	252	1.00	1.0	245	0.99	4.5	248	1.00
Azusa	Vector	8/10	0.3	250	1.00	1.1	245	0.94	4.3	252	1.00
Azusa	Vector	8/11	0.0	0	calm	0.6	217	0.94	4.8	247	0.99